



NTNU – Trondheim
Norwegian University of
Science and Technology

Electric Heating of Subsea Pipelines

*Design and Testing of an Applicable Ring Core
Transformer*

Kristian Thinn Solheim

Master of Energy and Environmental Engineering

Submission date: June 2013

Supervisor: Arne Nysveen, ELKRAFT

Co-supervisor: Atle Pedersen, SINTEF Energi

Norwegian University of Science and Technology
Department of Electric Power Engineering

NORWEGIAN UNIVERSITY OF SCIENCE AND TECHNOLOGY
FACULTY OF INFORMATION TECHNOLOGY, MATHEMATICS AND ELECTRICAL
ENGINEERING

Department of Electric Power Engineering



MASTER'S THESIS

Student's name: Kristian Thinn Solheim

Area: Electric Power Engineering

Title: **Electric Heating of Subsea Pipeline**
Design and Testing of an Applicable Ring Core Transformer

Description:

SINTEF and NTNU have together with Statoil developed a system for electric heating of subsea pipelines, DEH (Direct Electric Heating). Several systems are in operation in the North Sea. Their energy supply is customized since the load is a one phase load with low power factor. In the project work carried out in autumn 2012, a feasibility study of different t-off configurations was examined. In order to design and build a system with t-offs, a transformer connected to the existing energy supply («piggy-back») is needed. The thesis aims at specify, design and test a suitable transformer.

More specifically the work shall focus on:

- Perform a literature survey and establish a theoretical foundation for transformer design with low turn numbers
- Evaluate different solutions and describe a suitable transformer
- Manufacture and test a prototype.


Details in the work and selection of transformer type clarified with the supervisors.

Start date: 16.01.2013

Deadline: 12.06.2013

Co-supervisor: Atle Pedersen, SINTEF Energy Research

Trondheim, 11.01.2013


Arne Nysveen
Professor

PREFACE

This thesis concludes my Master of Science within Energy and Environmental Engineering at The Norwegian University of Science and Technology (NTNU) in Trondheim. The thesis was performed through my 10th semester, spring 2013, at the Department of Electric Power Engineering, in collaboration with SINTEF Energy Research.

I would like to thank Professor Arne Nysveen at NTNU and my co-supervisor Atle Pedersen at SINTEF Energy Research for valuable ideas and comments throughout the work period. I am truly delighted to announce their survival of every frustration outburst taking place from mid-January to mid-March.

Trondheim, 06 June 2013

Kristian Thinn Solheim

ABSTRACT

As it becomes profitable to extract oil and gas from smaller and smaller reservoirs, jumpers (t-offs) connected to the main pipelines become necessary. This master's thesis has investigated a simple transformer design which makes it possible to heat these t-offs using electrical energy. Two prototypes have been designed and tested. Based on these prototypes, electrical parameters and physical dimensions of a full-scale transformer supplying a 500 meter long eight inches thick t-off have been approximated. In addition, numerical and analytical approaches have been proposed to find the theoretical minimum series reactance of this transformer design.

Based on transformer design theory and the special application requirements, a ring core transformer consisting of multiple stabled toroidal cores build up from magnetic tape is found to be suitable. This construction design provides the maximum utilization of magnetic flux with the minimum of magnetic force. Two main reasons distinguish themselves regarding the application requirements. The first is absence of termination points. This enables the use of a piggy-back cable as primary winding, increasing the overall system reliability compared to a system consisting of joints. The other main design benefit is the possibility to connect appropriate winding ratio in an unproblematic manner.

Open-circuit and short-circuit tests were performed in order to find parameters for an electrical equivalent circuit. The iron cores were produced by ThyssenKrupp Electrical Steel, but the prototypes were assembled by the author. The finite element analyse software COMSOL Multiphysics 4.3a has been used when creating computer models of the prototypes.

The two prototypes have ratings of 918 VA (small) and 7,200 VA (large) at 50 Hz. Their dimensions (*inner radius x outer radius x length*) are 2.5 cm x 4.5 cm x 48 cm and 5.0 cm x 9.0 cm x 56 cm. The small transformer has a rated voltage and current of 3.4 V and 270 A while the corresponding values of the large transformer are 8.0 V and 900 A. An appurtenant datasheet is attached in Appendix A. Other electrical properties of the prototypes were also extracted from these tests. No unusual electrical characteristics were found, compared with iron core theory and regular power transformers.

The t-off could be heated either by use of direct electric heating (DEH) or induction heating (IH). If the transformer is to supply a DEH-system, it must deliver 192 V and have a winding ratio of 1:1. Correspondingly, an IH-system needs 282 V and a secondary winding consisting of two parallel conductor pairs, of two turns each. The transformer core dimensions are 7.2 cm x 34 cm x 2 m for a DEH-system while 10.9 cm x 50 cm x 2 m for an IH-system. Their weights are around 5.2 and 11.2 metric tons. Corresponding efficiencies are found to be 97 % and 96 %. All values are calculated based on the prototype tests.

Based on the calculations and considerations performed in this thesis, this transformer type is found to be suitable for this kind of application. Since this proposed design avoids any need for splices in the conductors, the overall system reliability is enhanced in relation to a regular power transformer. In addition, the full-scale transformer size is manageable for installation.

SAMANDRAG

Det er naudsynt med små fordelingsrør koplå til det eksisterande undervassrørleidningsnettå etter kvart som lønsemda ved å produsera olje og gass frå mindre og mindre reservoar aukar. Denne hovudoppgåva ser på ei enkel transformatorutforming og to prototypar er utforma og testa. Basert på desse målaingane er dei elektriske verdiar og fysiske dimensjonar til ein fullskala transformator funne. Den fullskala transformatoren skal forsyne ein 500 meter lang og eit åtte tommar tjukt fordelingsrør. I tillegg til dette er det gjort framlegg til numeriske og analytiske måtar å finne ein minimum teoretisk verdi for seriereaktans, for denne transformator typen.

Ein ringkjernetransformator beståande av stabla toroidar bygd opp av magnetisk teip er funne høveleg, basert på transformatorutformingsteori og dei spesielle krava for dette bruksområdet. Denne konstruksjonsutforminga gjev maksimal utnytting av den magnetiske fluksen ved bruk av minimal magnetisk kraft. To hovudgrunnar skil seg ut med tanke på bruksområdet. Den første er fråvere av koplingspunkt. Dette gjer det mogleg å bruke den eksisterande straumforsyningskabelen «piggy-back» som primærvikling, noko som aukar pålitelegheita samanlikna med eit system som inneheld samanføyingar. Den andre hovudgrunnen er at det på ein lett måte er mogeleg å kople opp passande viklingsforhold.

Testar som omfattar open-krins og kortslutta-krins vart utført for å finne verdiar til ein elektrisk krinsekvivalent. Jarnkjernane er produsert av ThyssenKrupp Electrical Steel, men prototypane vart sett saman av underskrivaren. Uendelelementmetode-programvaren COMSOL Multiphysics 4.3a er brukt for å lage datamaskinmodellar av prototypane.

Dei to prototypane har merkedata på 918 VA (liten) og 7.200 VA (stor) ved 50 Hz. Dimensjonane er (*indre radius x ytre radius x lengd*) 2,5 cm x 4,5 cm x 48 cm og 5,0 cm x 9,0 cm x 56 cm. Den vetle transformatoren har merkespenning og -straum på 3,4 V og 270 A, medan den store på 8,0 V og 900 A. Eit tilhøyrande datablad er funne i Appendiks A. Også andre elektriske verdiar frå desse prototypane vart funne frå desse testane. Ved å samanlikne med jarnkjernet teori og typiske krafttransformatorar er det ikkje funne nokre uvanlege elektriske karakteristikkar.

Fordelingsrøret kan anten bli varma ved hjelp av direkte elektrisk oppvarming (DEH) eller induksjonsoppvarming (IH). Om transformatoren forsyner eit DEH-system må sekundærsida levere 192 V og ha vindingsforholdet 1:1. For eit tilsvarande IH-system er det naudsynt med 282 V, og ei sekundærvikling beståande av to parallelle straumleidningspar, kvar med to vindingar. Transformator kjernedimensjonane er 7.2 cm x 34 cm x 2 m for eit DEH-system, mot 10.9 cm x 50 cm x 2 m for eit IH-system. Ved desse dimensjonane veg dei omlag 5.2 og 11.2 tonn. Tilhøyrande effektivitet er funne til 97 % og 96 %. Alle verdiane er kalkulert med bakgrunn i dei testa prototypane.

Denne transformator typen er funne passande for den bruken som er skildra, med bakgrunn i berekningane og argumenta som er brukt i denne hovudoppgåve. Sidan denne transformatorutforminga unngår bruk av samanføyingar er det mindre sjanse for at noko går galt. Dette er ein fordel framfor tradisjonelle transformatorutformingar brukt i kraftsystemet. I tillegg er den fullskala transformator storleiken medgjærleg for installasjon.

TABLE OF CONTENTS

1	Introduction.....	1
2	Background and theory.....	3
2.1	DEH – an alternative to chemical treatments	3
2.2	Magnetic circuits	4
2.2.1	Ampere’s law.....	4
2.2.2	Flux density.....	4
2.2.3	Magnetic reluctance.....	4
2.3	Magnetic components.....	5
2.3.1	Magnetic core materials.....	5
2.3.2	Hysteresis loss	5
2.3.3	Saturation	6
2.3.4	Skin effect limitations.....	7
2.3.5	Copper windings.....	8
2.3.6	Winding loss due to DC resistance of windings.....	8
2.3.7	Skin effect in copper windings.....	9
2.3.8	Proximity effect	10
2.4	Transformer and inductor design.....	10
2.4.1	Material permeability.....	10
2.4.2	Air gaps	11
2.4.3	Exciting current.....	11
2.4.4	Tap wound C, EE, and toroidal cores.....	12
2.5	Engineering aspects of transformer analysis	13
2.5.1	Short-circuit test.....	14
2.5.2	Open-circuit test.....	16
2.5.3	No-load conditions	17
2.6	Support routine CONVERT.....	19
2.7	Find series reactance using FEM-analysis	20
2.8	Calculation of resistance and reactance in subsea cable systems	21
2.8.1	Introduction.....	21
2.8.2	Single-phase loop with circular conductors	21
3	Transformer design and calculations	23

3.1	System overview	23
3.2	Transformer design	23
3.3	Prototype dimensions	24
3.4	The core.....	24
3.5	Rated voltage.....	25
3.6	Rated current.....	25
4	Laboratory setup	27
4.1	Introduction.....	27
4.2	Laboratory setup	27
4.3	Short-circuit and open-circuit tests.....	27
4.4	Conductor coupling	28
4.5	The windings.....	28
4.6	Elucidation.....	29
4.7	Equipment and measurements	29
4.7.1	Detailed measurement instructions of the small transformer	29
4.7.2	Detailed measurement instructions of the large transformer.....	30
4.7.3	DC-tests	31
4.8	Long secondary winding.....	31
4.8.1	Laboratory setup	31
4.8.2	Long conductor length.....	32
5	Laboratory results	33
5.1	Part I: Transformer only	33
5.1.1	Introduction.....	33
5.1.2	Short-circuit tests	34
5.1.3	Open circuit tests.....	35
5.1.4	Datasheet	40
5.2	Part II: Long secondary winding	40
5.2.1	Introduction.....	40
5.2.2	Equivalent series reactance.....	41
5.2.3	Equivalent series resistance	41
5.2.4	Equivalent series impedance.....	42
6	Discussion.....	43
6.1	Instrument inaccuracy.....	43
6.1.1	Current clamps; Fluke 80i-500 and Fluke i1000s.....	43

6.1.2	Power quality analyser, Fluke 43.....	43
6.1.3	Power quality analyser, Norma 5000	44
6.2	Voltage probe placement, twisting and external influence	44
6.3	Formula simplifications	45
6.3.1	Short-circuit formula simplifications	45
6.3.2	Open-circuit formula simplifications	46
6.4	Transformer only short-circuit tests.....	46
6.4.1	Equivalent series resistance	46
6.4.2	Equivalent series reactance.....	48
6.5	Transformer only open-circuit tests.....	49
6.5.1	Magnetic field strength and loss as function of magnetic flux density.....	49
6.5.2	Impact of having long secondary conductors connected to the secondary winding during open-circuit tests	52
6.6	Short-circuit tests when long conductor are connected to the transformers' secondary winding	53
6.6.1	Introduction.....	53
6.6.2	Series reactance deviation	53
6.6.3	Series resistance deviation	53
6.6.4	Analytical and numerical analyses of the series reactance and resistance deviation ..	54
7	Addendum I: Numerical and analytical approach of series reactance calculations.....	59
7.1	Elucidation	59
7.2	Numerical model	60
7.3	Analytic model.....	60
7.3.1	Introduction.....	60
7.3.2	Formulas – magnetic field strength and magnetic energy as function of radius.....	61
7.3.3	Notations and credibility	62
7.4	Results from the numerical and analytical models	63
8	Addendum II: A full-scale model	65
8.1	Introduction.....	65
8.2	Physical dimensions of pipelines and appurtenant electrical conductors	66
8.3	Electrical and thermal material values	67
8.4	Electrical and thermal calculations of a t-off system	68
8.5	Physical dimensions of a full-scale transformer	69
8.6	Electrical parameters and physical dimensions of a defined full-scale model.....	70
9	Conclusions.....	73

10	Further work.....	75
11	Bibliography.....	77
12	Appendix.....	79
12.1	Appendix A: Prototype datasheet and dimensions.....	79
12.2	Appendix B: Full-scale model datasheet and dimensions.....	80
12.3	Appendix C – analytical formula development	81
12.3.1	Introduction.....	81
12.3.2	Magnetic field strength as function of radial direction out from origin	82
12.3.3	Magnetic energy as function of radial direction out from origin.....	82
12.3.4	$r \in \mathbf{0}, \mathbf{a}]$	83
12.3.5	$r \in \mathbf{a}, \mathbf{a} + \mathbf{b}]$	84
12.3.6	$r \in \mathbf{a} + \mathbf{b}, \mathbf{a} + \mathbf{b} + \mathbf{c}]$	85
12.3.7	$r \in \mathbf{d}, \mathbf{d} + \mathbf{e}]$	86
12.3.8	$r \in \mathbf{d} + \mathbf{e}, \mathbf{d} + \mathbf{e} + \mathbf{f}]$	87
12.3.9	$r \in \mathbf{d} + \mathbf{e} + \mathbf{f}, \mathbf{d} + \mathbf{e} + \mathbf{f} + \mathbf{g}]$	88
13	Attachments.....	i
13.1	Tables.....	i
13.2	Photos.....	x
13.3	Graphs	xiii
13.4	Illustrations.....	xvii
13.5	MATLAB-scripts	xix

1 INTRODUCTION

Formation of hydrates is a well-known problem in subsea production systems for oil and gas. As the unprocessed well-stream cools down, hydrates are formed at temperatures up to 25°C depending on the water cut and pressure inside the pipeline. Several options are available to solve this problem. One way is to send electricity through the pipeline which generates heat due to the pipeline resistance, leading to a temperature increase of the pipeline content. This method is called direct electric heating (DEH). [1]

As it becomes profitable to extract oil and gas from smaller and smaller reservoirs, t-offs connected to the main pipelines become necessary. In order to avoid installation of separate heating systems for the t-offs, research work of two promising systems are currently being developed. One is to heat the t-off and main pipeline as a mutual system, with the difficulties of achieving desirable current distribution between them. The other is to install a subsea transformer, using the main pipeline's piggy-back cable as primary winding. Doing this, the secondary windings may be used to heat up a t-off as a separate system, either using DEH or the principle of induction heating (IH).

No research work of the specific transformer type described here is been found. Therefore, laboratory tests of two prototype ring core transformers of different sizes are performed. The results help understanding if this transformer design is applicable for its application, focusing on losses and physical dimensions. In addition, how the overall impedance changes depending of the secondary conductor's placement outside the transformer is tested and discussed.

This thesis is divided in the following way. First, background information of the necessary area of knowledge is presented, including DEH together with basic electromagnetism and transformer theory. Secondly, the specific transformer design is described. Thirdly, results from the laboratory work are presented, subsequently followed by a discussion chapter. At last, two addendum chapters are included. The first develops simplified analytical formulas and numerical models of the transformers' equivalent series reactance, while the last uses previous calculations and results to find electrical and physical parameters of a full-scale model.

2 BACKGROUND AND THEORY

2.1 DEH – AN ALTERNATIVE TO CHEMICAL TREATMENTS

When a hydrocarbon production line is shut down for a given period of time, the fluid in the line cools to an extent that may cause flow in the line to be impeded or even blocked due to the formation of hydrates or wax plugs. The traditional method for preventing wax or hydrate deposits in the pipelines is by use of chemical treatments. In continuous operation this method has considerable operation costs and presents a risk to the environment if a leak occurs. [2]

There are a few methods based on electric heating which may be used to prevent hydrates or wax plugs. In all methods, electricity is used to raise the pipe temperature above a critical value for hydrates (typically 15-25°C) and wax formation (typically 20-40°C). [2]

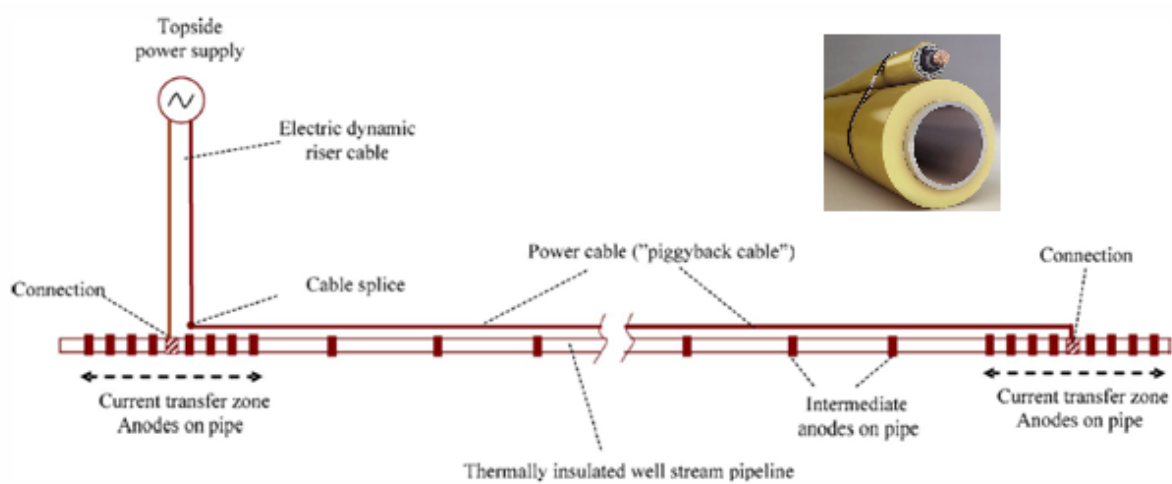


Figure 2-1: Outline drawing of the DEH system [3]

The direct heating system is based on the fact that an electric altering current in a metallic conductor (i.e. cable/pipe etc.) generates heat. In the direct pipe heating system, the pipe to be heated is an active conductor in a single-phase electric circuit, together with a single core power cable as the forward conductor, located in parallel and close to the heated pipe. This is called a piggy-back, as from Figure 2-1. For safety and reliability reasons, the heating system is electrically connected to surrounding seawater through several sacrificial anodes for a length of approximately 50 meters at both ends where the cables are connected [3].

The consequence of applying the open system is that seawater acts as an electric conductor in parallel to the pipe by the direct electric contact between pipe and seawater at both ends of the heated pipe. The current is divided between pipe and seawater, and typically 40 % of the current flows in the sea water. [2]

2.2 MAGNETIC CIRCUITS

2.2.1 AMPERE'S LAW

A current-carrying conductor produces a magnetic field of intensity H whose SI unit is amperes per meter (A/m). According to Ampere's law, the line integral of the magnetic field intensity H equals the total (enclosed current):

$$\oint H dl = \sum i \tag{Eq. (2-1) [4]}$$

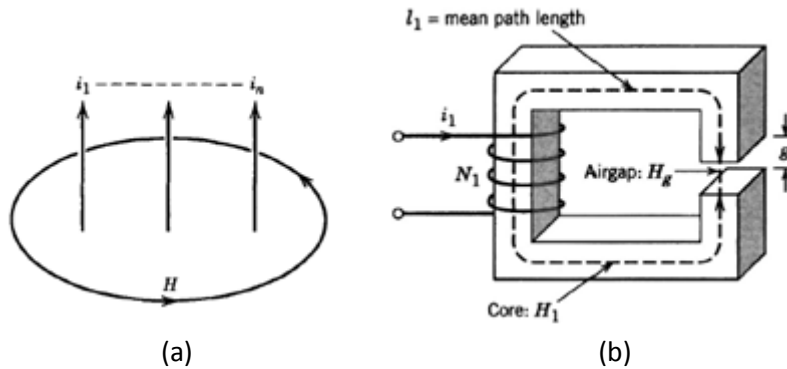


Figure 2-2: General formulation of Ampere's law [4]

For most practical circuits, Eq. (2-1) can be written as

$$\sum_k H_k l_k = \sum_m N_m i_m \tag{Eq. (2-2) [4]}$$

2.2.2 FLUX DENSITY

The H -field is related to the flux density B (B-field) by the property of the medium in which these fields exist:

$$B = \mu H \tag{Eq. (2-3) [4]}$$

B is in SI units of Wb/m^2 and μ is called the permeability of the medium in SI units of (H/m). The permeability μ of a medium is defined in terms of the permeability of free space or air, μ_0 , and the relative permeability μ_r :

$$\mu = \mu_0 \mu_r \tag{Eq. (2-4) [4]}$$

μ_0 equals $4\pi \cdot 10^{-7}$ H/m and μ_r may range from 1.0 for air or a nonmagnetic medium to several thousand for iron.

2.2.3 MAGNETIC RELUCTANCE

Ampere's law in the form of Eq. (2-2) and continuity of flux can be combined to define the reluctance of a magnetic circuit. In general, for a magnetic circuit of the type shown in Figure 2-2b,

$$\sum_k H_k l_k = \sum_k H_k (\mu_k A_k) \cdot \frac{l_k}{\mu_k A_k} = \sum_k (B_k A_k) \cdot \frac{l_k}{\mu_k A_k} = \sum_k \phi_k \frac{l_k}{\mu_k A_k} = \phi \sum_k \frac{l_k}{\mu_k A_k} \quad \text{Eq. (2-5) [4]}$$

Where $\phi_k = \phi$ for each k by applying the continuity-of-flux. Therefore, from Eq. (2-2) Eq. (2-5)

$$\phi \sum_k \frac{l_k}{\mu_k A_k} = \sum_m N_m i_m \quad \text{Eq. (2-6) [4]}$$

For each section k, the term in the summation on the left-hand side of Eq. (2-6) is defined as the magnetic reluctance in the path of the magnetic flux lines:

$$R_k = \sum_k \frac{l_k}{\mu_k A_k} \quad \text{Eq. (2-7) [4]}$$

$$NI = \phi R = (BA) \cdot \frac{l}{\mu A} = \frac{B \cdot l}{\mu_0 \mu_r} \quad \text{Eq. (2-8) [4]}$$

2.3 MAGNETIC COMPONENTS

The assumptions that magnetic circuits and devices are made of loss-free magnetic materials are not satisfied in real materials, and the loss that occurs in them has a significant effect on the design and fabrication of inductors and transformer. Any inductor or transformer design procedure must take these losses into account, and the designer must have a good understanding of the material properties. This section discusses these material properties. [4]

2.3.1 MAGNETIC CORE MATERIALS

One broad class of materials are comprised of alloys principally of iron and small amounts of other elements including chrome and silicon. These alloys have large electrical conductivity compared with ferrites and large values of saturation flux density, near 1.8 T. Two types of loss are found in iron alloy materials, hysteresis loss and eddy current loss. Iron alloy core materials (often termed magnetic steels) are usually used only in low-frequency (2 kHz or less for transformers) applications because of eddy current losses. Iron alloy magnetic materials must be laminated to reduce eddy current loss even at modest frequencies such as 60 Hz. [4]

2.3.2 HYSTERESIS LOSS

All magnetic core exhibit some degree of hysteresis in their B-H characteristic. A typically B-H characteristic (B-H loop) is shown in Figure 2-3. The area inside the B-H loop represents work done on the material by the applied field. The work (energy) is dissipated in the material, and the heat caused by the dissipation raises the temperature of the material. [4]

As magnetic parts are being heated, such as those made from carbon steel, by induction, the alternating magnetic flux field causes the magnetic dipoles of the material to oscillate as the magnetic poles change their polar orientation every cycle. This oscillation is called hysteresis, and a minor amount of heat is produced due to the friction produced when the dipoles oscillate. [5]

The hysteresis loss increases in all core materials with increases in ac flux density, B_{ac} , and operating or switching frequency, f . The general form of the loss per unit volume, $P_{m,sp}$, is

$$P_{m,sp} = kf^a(\hat{B}_{ac})^d \tag{Eq. (2-9)}$$

Where k , a , and d are constants that vary from one material to another. This equation applies over a limited range of frequencies and flux density with the range of validity being dependent on the specific material. [4]

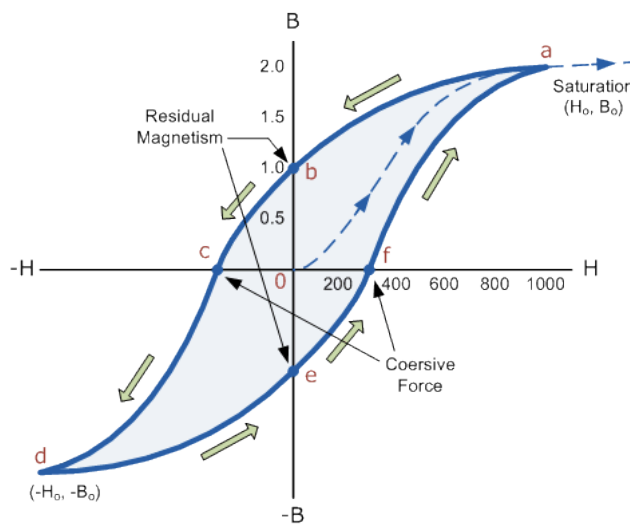


Figure 2-3: Non-linear magnetic hysteresis loop [6]

2.3.3 SATURATION

When a high magnetizing force is encountered, a point is reached where further increase in H , does not cause useful increase in B . This point is known as the saturation point of that material as shown in Figure 2-3. [7]

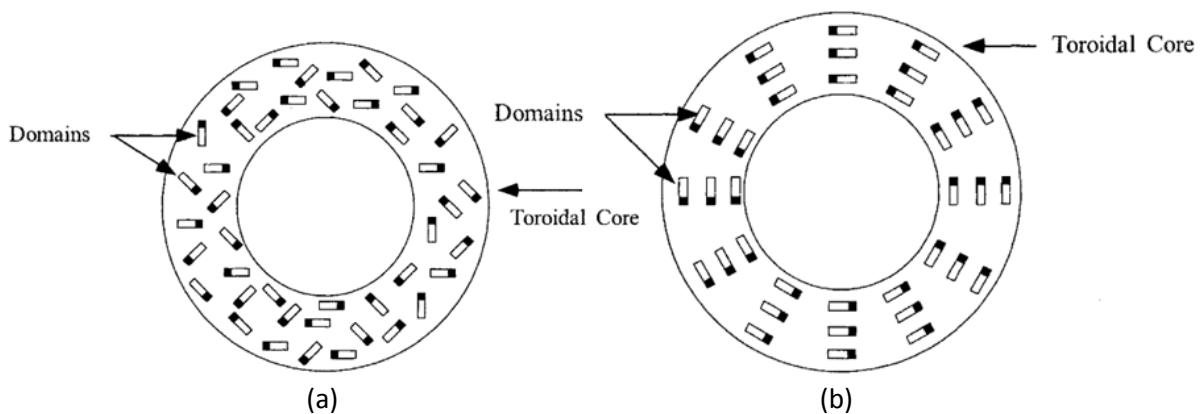


Figure 2-4: (a) Magnetic domains; (a) arranged in a random manner, (b) aligned in a definite direction [7].

The domain theory of the nature of magnetism is based on the assumption that all magnetic materials consist of individual molecular magnets. These minute magnets are capable of movement within the material. When a magnetic material is in its unmagnetized state, the individual magnetic particles are arranged at random, and effectively neutralize each other. An example of this is shown in Figure 2-4a, where the tiny magnetic particles are arranged in a disorganized manner. The north poles are represented by the darkened ends of the magnetic particles. When a material is magnetized, the individual particles are aligned or oriented in a definite directed, as shown in Figure 2-4b. [7]

The degree of magnetization of a material depends on the degree of alignment of the particles. The external magnetizing force can continue to affect the material up to the point of saturation, the point at which essentially all of the domains are lined up in the same direction.

2.3.4 SKIN EFFECT LIMITATIONS

When a magnetic core is made from conducting materials such as magnetic steels, time-varying magnetic fields applied to the core will generate circulating currents as is diagrammed in Figure 2-5a. Using the right-hand rule, it can be seen that these currents, generically termed eddy currents, flow in the direction such that secondary magnetic fields are produced that oppose the applied (primary) magnetic field. These opposing fields tend to screen the interior of the core from the applied field, and the total magnetic field in the core decays exponentially with distance into the core as shown in Figure 2-5b. [4]

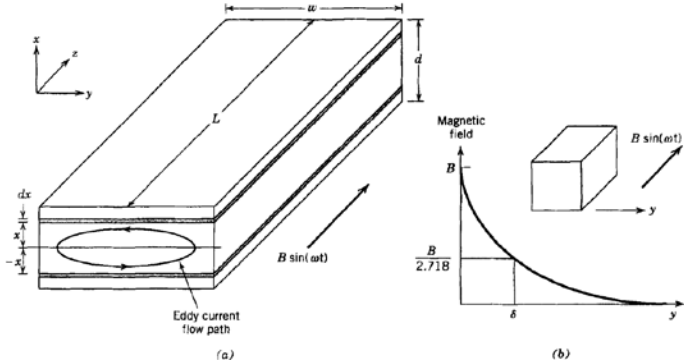


Figure 2-5(a) Eddy currents generated in a thin transformer lamination by an applied time-varying magnetic field and (b) decay of the magnetic field versus depth y into the interior of a thick bar of magnetic material [4]

The characteristic decay length in the exponential is termed the skin depth and is given by

$$\delta = \sqrt{\frac{2}{\omega\mu\sigma}} \tag{Eq. (2-10) [8]}$$

$f = \omega/2\pi$ is the frequency (in hertz) of the applied magnetic field, μ is the magnetic permeability of the core material, and σ is the conductivity of the magnetic material. If the cross-sectional dimensions of the core are large compared to the skin depth, then the interior of the core carries little or none of the applied magnetic flux as is diagrammed in Figure 2-5b and the core is ineffective in its intended role of providing a low reluctance return path for the applied magnetic field. Typical values of the skin depth are quite small even at low frequencies (typically 1 mm at 60 Hz) because of the large

permeability of the materials. The skin depth becomes more of a problem as the applied frequency increases. [4]

Thus magnetic cores for inductors and transformers that utilize conducting magnetic materials are made from stacks of many thin laminations as is shown in Figure 2-6. Each lamination is electrically isolated from the other by means of a thin insulating coating on each lamination. The core stacking factor is defined as the ratio of the cross sectional area of the magnetic material to the total cross-sectional area of the core. The stacking factor will be less than 1 (typical values are 0.9 to 0.95) because part of the total area of the core is occupied by the insulation layers. [4]

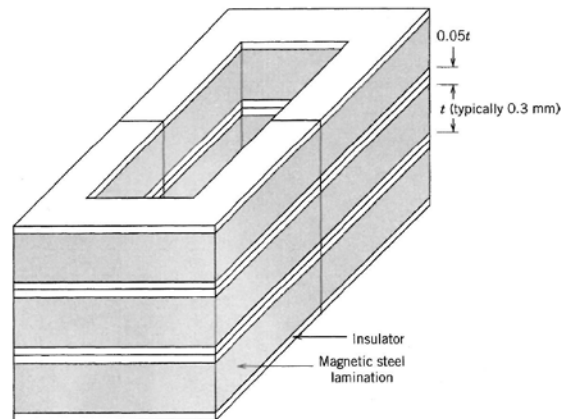


Figure 2-6: Magnetic core for a transformer or inductor made from a stack of magnetic steel laminations separated by insulators [4]

Most magnetic steels have a small percentage of silicon added to the iron to increase the resistivity of the material and thus increase the skin depth. Addition of more than a few percent, however, reduces the magnetic properties such as saturation flux density more than it increases the resistivity. Hence a reasonable compromise for transformers for 50/60 Hz applications is an iron alloy of 97% iron – 3% silicon and a lamination thickness approximately of 0.3 mm. [4]

2.3.5 COPPER WINDINGS

The conductor windings in an inductor or transformer are made from copper because of its high conductivity. The high ductility of the copper makes it easy to bend the conductors into tight windings around a magnetic core and thus minimize the amount of copper and volume needed for the windings. High conductivity contributes to minimizing the amount of copper needed for the windings and thus to the volume and weight of the windings. At the current densities used in inductors and transformers, electrical loss is a significant source of heat even though the conductivity of copper is large. The heat generated raises the temperature of both the windings and the magnetic core. The amount of dissipation allowable in the windings will be limited by maximum temperature considerations. [4]

2.3.6 WINDING LOSS DUE TO DC RESISTANCE OF WINDINGS

The power $P_{Cu,sp}$ is dissipated per unit of copper volume in a copper winding due to its DC resistance is given by

$$P_{Cu,sp} = \rho_{Cu} \left(\frac{I_{rms}}{A_{Cu}} \right)^2 \tag{Eq. (2-11) [4]}$$

I_{rms} is the rms current in the windings.

2.3.7 SKIN EFFECT IN COPPER WINDINGS

The skin effect occurs in the copper conductor used in inductor and transformer windings in exactly the same manner as described for the magnetic core. Consider the single copper conductor shown in Figure 2-7a, which is carrying a time-varying current $i(t)$. This current generates the magnetic field shown in Figure 2-7, and they in turn generate the eddy currents illustrated in Figure 2-7b. These eddy currents flow in the opposite direction to the applied current in the interior of the wire and thus tend to shield the interior of the conductor from the applied current and resulting magnetic field. As a result the total current density is largest at the surface of the conductor, and it decays exponentially with distance into the interior of the conductor as shown in Figure 2-7c. The characteristic decay length is the skin depth given by Eq. (2-10). [4]

If the cross-sectional dimensions of the conductor used in the winding are significantly larger than the skin depth, most of the current carried by the conductor will be constricted to a relatively thin layer at the surface approximately one skin depth in thickness as is illustrated in Figure 2-7c. The net result of this is that the effective resistance of the conductor will be far larger than the DC resistance because the effective cross-sectional area for current flow is small compared to the geometric cross section of the conductor. This will cause the winding losses to be much larger than if it were a DC current. [4]

The solution to this problem is to use conductors with cross-sectional dimensions on the order of the skin depth in size. If d is the diameter of a round conductor or the thickness of a rectangular conductor, calculations have shown that if $d \leq 2\delta$ the consequences of the skin effect can be neglected.

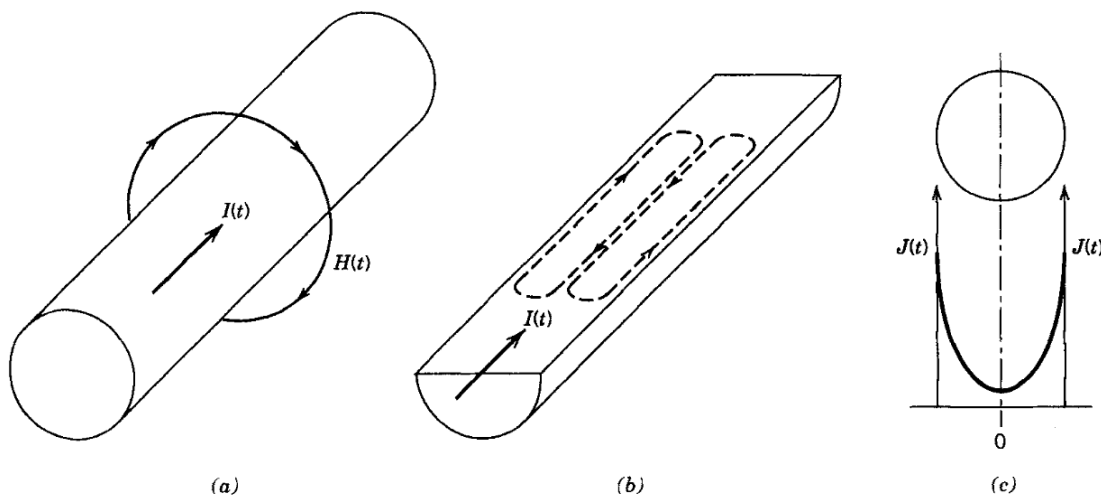


Figure 2-7: Isolated copper conductor carrying (a) a current $i(t)$, (b) eddy currents generated by the resulting magnetic field, and (c) the consequences of the skin effect on the current distribution [4]

2.3.8 PROXIMITY EFFECT

The operating frequency for power supplies is in the range of 50 Hz to 500 kHz. With it came along new tasks for the engineer to address skin effects and proximity effects. They are quite similar in that they both generate eddy currents in the magnet wire. The eddy currents produced by these effects have the same solution, keeping the ratio of the AC resistance, R_{AC} , to the DC resistance, R_{DC} , down:

$$R_R = \frac{R_{AC}}{R_{DC}} \quad \text{Eq. (2-12) [7]}$$

Proximity effect is caused by eddy currents induced in a wire due to the altering magnetic field of other conductors in the vicinity. The flux generated by the magnet wire is shown in Figure 2-8. The eddy currents cause a distortion of the current density. This distortion is the result of magnetic flux lines that generate eddy currents in the magnet wire, therefore enhancing the main current, I , on one side and subtracting from the main current on the other side, as shown in Figure 2-7b. [7]

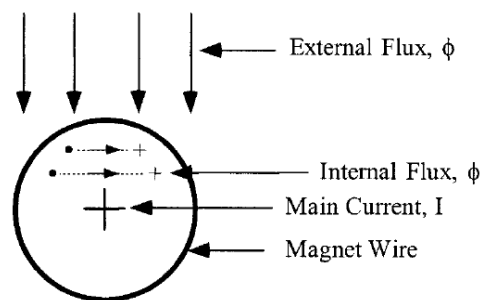


Figure 2-8: Flux distribution in a magnet wire [7]

Proximity effect has a minimum impact on a transformer with a single layer secondary. Keeping the proximity effect to a minimum requires the transformer to be designed with a minimum of layers.

2.4 TRANSFORMER AND INDUCTOR DESIGN

2.4.1 MATERIAL PERMEABILITY

The B-H loops that are normally seen in the manufacturer's catalogues are usually taken from a toroidal sample of the magnetic material. The toroidal core, without air gap, is the ideal shape to view the B-H loop of a given material. The material permeability, μ_m , will be seen at its highest in the toroidal shape, as shown in Figure 2-9. [7]

A small amount of air gap, less than 25 microns, has a powerful effect by shearing over the B-H loop. This shearing over of the B-H loop reduces the permeability. High permeability ferrites that are cut, like E cores, have only about 80 per cent of the permeability, than that of a toroid of the same material. This is because of the induced gap, even though the mating surfaces are highly polished [7].

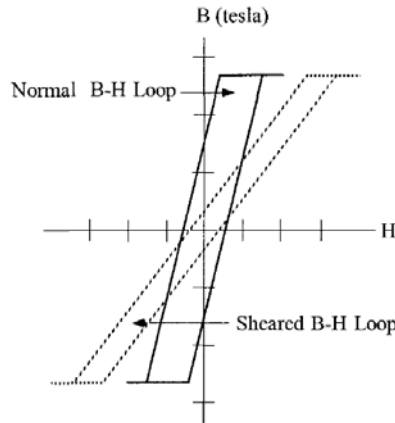


Figure 2-9: The shearing of an idealized B-H loop due to an air gap [7]

2.4.2 AIR GAPS

Air gaps are introduced into magnetic cores for a variety of reasons. In a transformer design a small air gap, l_g , inserted into the magnetic path, will lower and stabilize the effective permeability, μ_e . This will result in a tighter control of the permeability change with temperature, and exciting voltage. Whenever an air gap is inserted into the magnetic path, as shown in Figure 2-10, there is an induced, fringing flux at the gap. [7]

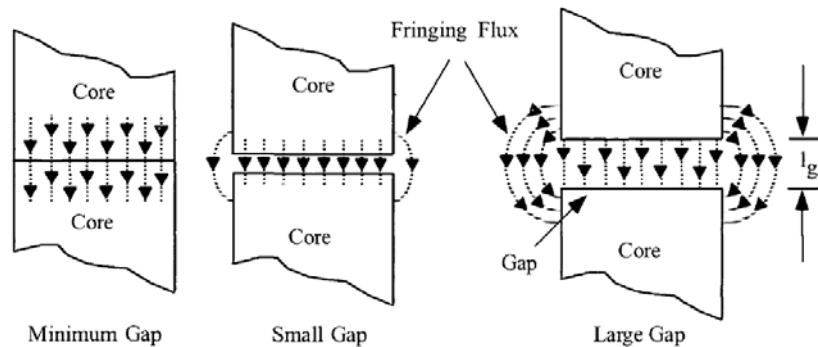


Figure 2-10: Fringing flux at the gap [7]

The fringing flux effect is a function of gap dimensions, the shape of the pole faces, and the shape, size and location of the windings. Fringing flux decreases the total reluctance of the magnetic path and, therefore, increases the inductance by a factor, F , to a value greater than the one calculated. Fringing flux can reduce the overall efficiency of, by generating eddy currents that cause localized heating in the windings and/or the brackets. When designing inductors, fringing flux must be taken into consideration. If the fringing flux is not handled correctly, there will be premature core saturation. [7]

2.4.3 EXCITING CURRENT

The flux will skirt the low permeability air gap and migrate into the adjacent lamination, causing flux crowding in that lamination. Eventually, this crowding will cause saturation in that portion of the lamination, and the excitation current will rise. After that portion of the lamination has been

saturated, the flux will migrate back to the lower permeability segment of the lamination from where it left. This effect can be viewed by observing the B-H loops at low and high flux densities, and comparing them with a toroidal core of the same material, with a minimum air gap as shown in Figure 2-11. The B-H loop, along with the magnetizing current, I_{ϕ} , of a toroidal core, is shown in Figure 2-11A. The toroidal core, with its inherent minimum air gap, will have almost a square of current. Using the same material in lamination form will exhibit a B-H loop, and a magnetizing current similar to Figure 2-11B operating at low flux densities. Increasing the excitation will cause premature saturation of the lamination, as seen by the non-linear exciting current, as shown in Figure 2-11C. [7]

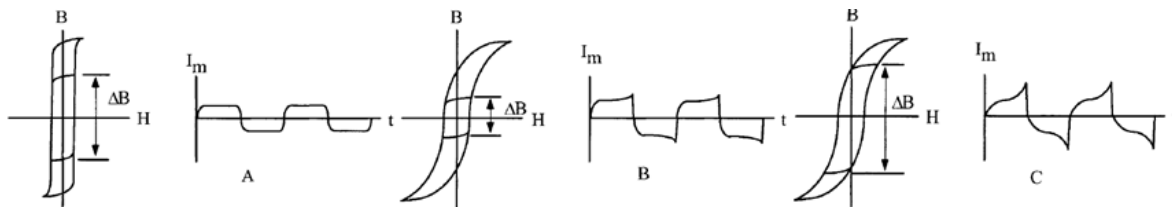


Figure 2-11: Comparing the exciting currents and three B-H loops

2.4.4 TAP WOUND C, EE, AND TOROIDAL CORES

Tape wound cores are constructed by winding a magnetic material in the form of a preslit tape, as shown in Figure 2-12a, around a mandrel. This tape material comes in all of the iron alloys, plus the amorphous materials. The tape thickness varies from 0.0127 mm to 0.305 mm. The advantage of this type of construction is that the flux is parallel with the direction of rolling of the magnetic material. This provides the maximum utilization of flux with the minimum of magnetic force. There are two disadvantages in this type of construction. When the core is cut in half, as shown in Figure 2-12b, the mating surface has to be ground, lapped, and then, acid etched. This is done to provide a smooth mating surface with minimum of air gap and the maximum of permeability. The other disadvantage is when the cores are reassembled, the method used is normally done with a band and buckle, and this procedure requires a little skill to provide the right alignment and correct tension. The C cores are impregnated for strength, prior to being cut. The cut C core can be used in many configurations in the design of a magnetic component. [7]

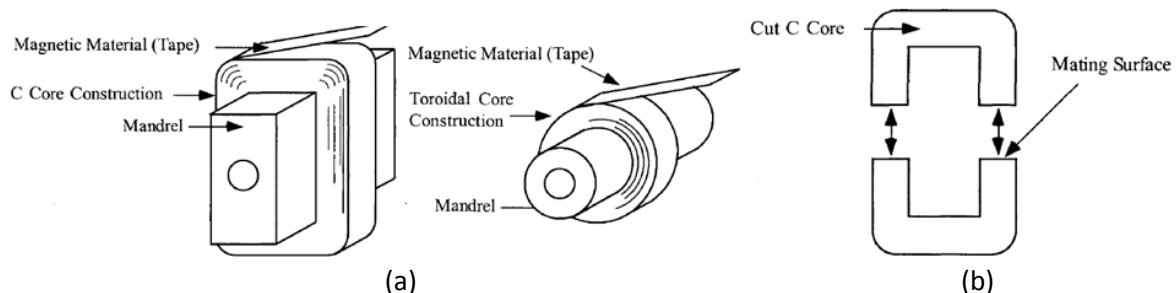


Figure 2-12: (a) Tape cores being wound on a mandrel. (b) Two halves of a cut C core [7]

Tape toroidal cores are constructed in the same way as tape C cores, by winding the magnetic material around a mandrel, in the form of a preslit tape. This tape material comes in all of the iron alloys, plus the amorphous materials. The tape thickness varies from 0.00318 mm to 0.305 mm. The

tape toroid is normally offered in two configurations, cased and encapsulated. The cased toroid offers superior electrical properties and stress protection against winding. The encapsulated cores are used when not all of the fine magnetic properties are important to the design, such as in power transformers. [7]

2.5 ENGINEERING ASPECTS OF TRANSFORMER ANALYSIS

In engineering analyses involving the transformer as a circuit element, it is customary to adopt one of several approximate forms of the equivalent circuit of Figure 2-14 rather than the full circuit. The approximations chosen in a particular case depend largely on physical reasoning based on orders of magnitude of the neglected quantities. The more common approximations are presented in this section. In addition, test methods are given for determining the transformer constants. [9]

The approximate equivalent circuits commonly used for constant-frequency power transformer analyses are summarized for comparison in Figure 2-13. All quantities in these circuits are referred to either the primary or the secondary, and the ideal transformer is not shown. [9]

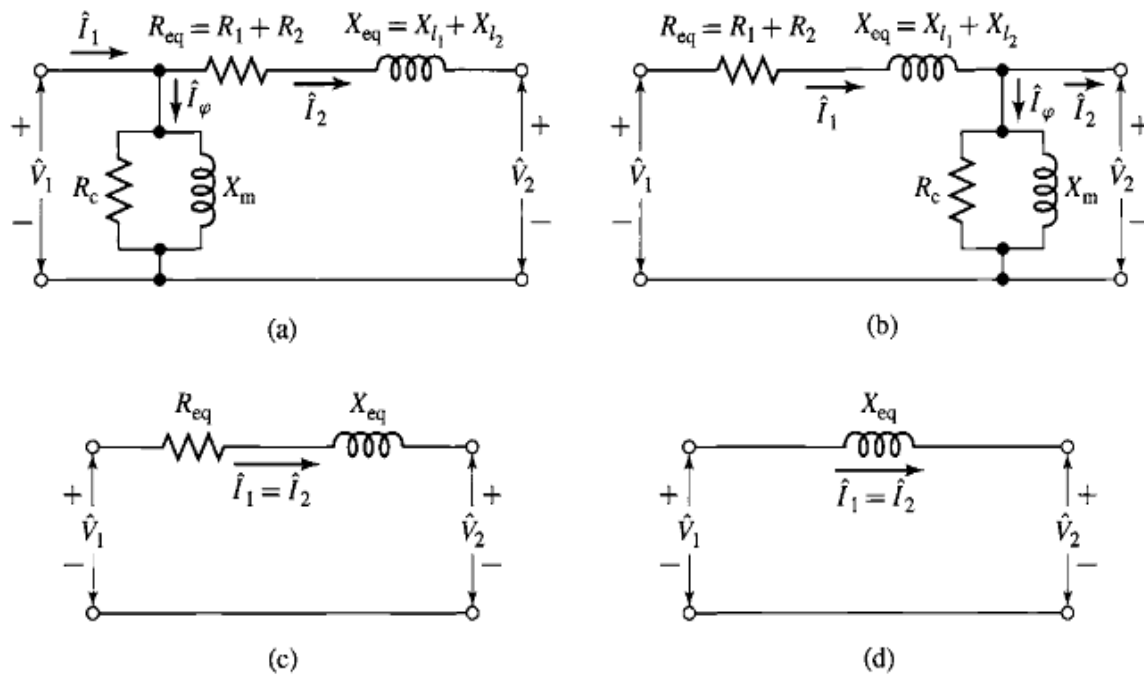


Figure 2-13: Approximate transformer equivalent circuits [9]

Computations can often be greatly simplified by moving the shunt branch representing the exciting current out from the middle of the T circuit to either the primary or the secondary terminals, as in Figure 2-13a and b. These forms of the equivalent circuit are referred to as *cantilever circuits*. The series branch is the combined resistance and leakage reactance of the primary and secondary, referred to the same side. This impedance is sometimes called the equivalent series impedance and its components, the equivalent series resistance R_{eq} and equivalent series reactance X_{eq} , are shown in Figure 2-13a and b. [9]

As compared to the equivalent-T circuit of Figure 2-14, the cantilever circuit is in error in that it neglects the voltage drop in the primary or secondary leakage impedance caused by the exciting current. Because the impedance of the exciting branch is typically quite large in large power transformers, the corresponding exciting current is quite small. This error is insignificant in most situations involving large transformers. [9]

Further analytical simplification results from neglecting the exciting current entirely, as in Figure 2-13c, in which the transformer is represented as equivalent series impedance. If the transformer is large (several hundred kilovoltamperes or more), the equivalent resistance R_{eq} is small compared with the equivalent reactance X_{eq} and can frequently be neglected, giving the equivalent circuit of Figure 2-13d. The circuits of Figure 2-13c and d are sufficiently accurate for most ordinary power system problems and are used in all but the most detailed analyses. Finally, in situations where the currents and voltages are determined almost wholly by the circuits external to the transformer or when a high degree of accuracy is not required, the entire transformer impedance can be neglected and the transformer considered being ideal. [9]

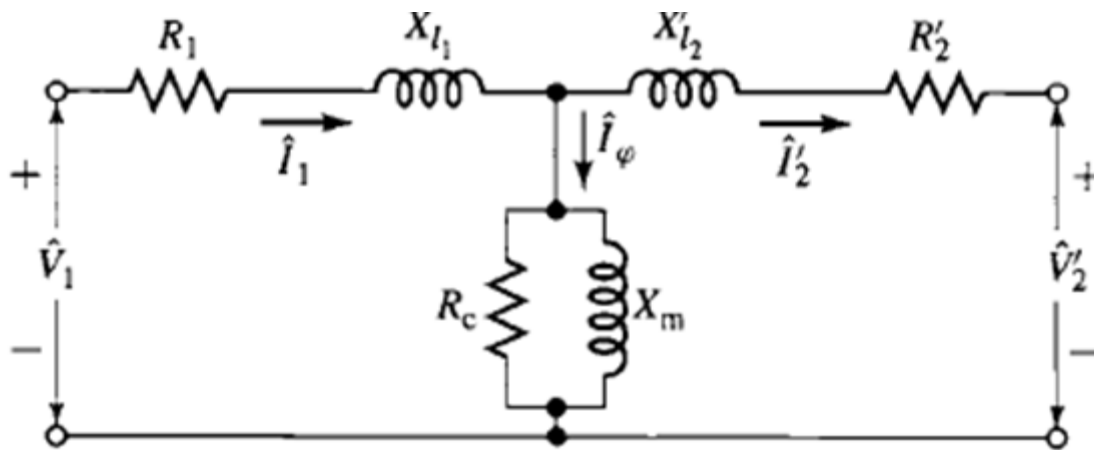


Figure 2-14: Transformer equivalent circuit [9]

The circuits of Figure 2-13 has the additional advantage that the total equivalent resistance and equivalent reactance can be found from a very simple test in which one terminal is short-circuited. On the other hand, the process of determination of the individual leakage reactances X_{l1} and X_{l2} and a complete set of parameters for the equivalent T-circuit Figure 2-13c is more difficult. In fact, without some a priori knowledge of the turns ratio (based for example upon knowledge of the internal construction of the transformer), it is not possible to make a set of measurements which uniquely determine the turns ratio, the magnetizing inductance, and the individual leakage impedances. [9]

2.5.1 SHORT-CIRCUIT TEST

The short-circuit test can be used to find the equivalent series impedance $R_{eq} + jX_{eq}$. Although the choice of winding to short-circuit is arbitrary, for the sake of this discussion we will consider the short circuit to be applied to the transformer secondary and voltage applied to primary. For convenience, the high-voltage side is usually taken as the primary in this test. Because the equivalent series impedance in a typical transformer is relatively small, typically an applied primary voltage on the order of 10 to 15 per cent or less of the rated value will result in rated current. [9]

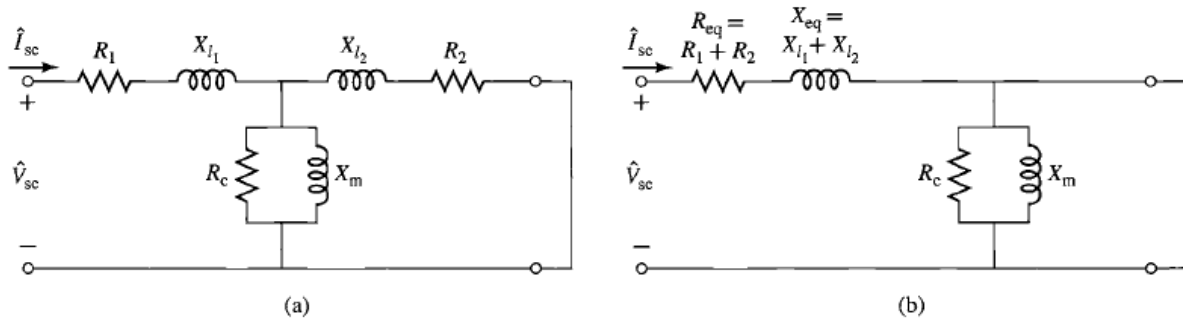


Figure 2-15: Equivalent circuit with short-circuited secondary. (a) Complete equivalent circuit. (b) Cantilever equivalent circuit with the exciting branch at the transformer secondary [9]

Figure 2-15a shows the equivalent circuit with transformer secondary impedance referred to the primary side and a short circuit applied to the secondary. The short-circuit impedance Z_{sc} looking into the primary under these conditions is

$$Z_{sc} = R_1 + jX_{l1} + \frac{Z_\phi(R_2 + jX_{l2})}{Z_\phi + R_2 + jX_{l2}} \tag{Eq. (2-13) [9]}$$

Because the impedance Z_ϕ of the exciting branch is much larger than that of the secondary leakage impedance (which will be true unless the core is heavily saturated by excessive voltage applied to the primary; certainly not the case here), the short-circuit impedance can be approximated as

$$Z_{sc} \approx R_1 + jX_{l1} + R_2 + jX_{l2} = R_{eq} + jX_{eq} \tag{Eq. (2-14) [9]}$$

Note that the approximation made here is equivalent to the approximation made in reducing the equivalent-T circuit to the cantilever equivalent. This can be seen from Figure 2-15b; the impedances seen at the input of this equivalent circuit is clearly $Z_{sc} = Z_{eq} = R_{eq} + jX_{eq}$ since the exciting branch is directly shorted out by the short on the secondary. [9]

Typically the instrumentation used for this test will measure the rms magnitude of the applied voltage V_{sc} , the short-circuit current I_{sc} , and the power P_{sc} . Based upon these three measurements, the equivalent resistance and reactance (referred to the primary) can be found from

$$|Z_{eq}| = |Z_{sc}| = \frac{V_{sc}}{I_{sc}} \tag{Eq. (2-15) [9]}$$

$$R_{eq} = R_{sc} = R_{sc}/I_{sc}^2 \tag{Eq. (2-16) [9]}$$

$$X_{eq} = X_{sc} = \sqrt{|Z_{sc}|^2 - R_{sc}^2} \tag{Eq. (2-17) [9]}$$

where the symbols $||$ indicates the magnitude of the enclosed complex quantity. [9]

The equivalent impedance can, of course, be referred from one side to the other in the usual manner. On the rare occasions when the equivalent-T circuit in Figure 2-14 must be resorted to, approximate values of the individual primary and secondary resistances and leakage reactances can

be obtained by assuming that $R_1=R_2=0.5R_{eq}$ and $X_{l1}=X_{l2}=0.5X_{eq}$ when all impedances are referred to the same side. Strictly speaking, of course, it is possible to measure R_1 and R_2 directly by a DC resistance measurement on each winding (and then referring one or the other to the other side of the idea transformer). No such simple test exists for the leakage reactances X_{l1} and X_{l2} . [9]

2.5.2 OPEN-CIRCUIT TEST

The open-circuit test is performed with the secondary open circuited and rated voltage impressed on the primary. Under this condition an exciting current of a few per cent of full-load current (less on large transformers and more on smaller ones) is obtained. Rated voltage is chosen to insure that the magnetizing reactance will be operating at a flux level close to that which will exist under normal operating conditions. If the transformer is to be used at other than its rated voltage, the test should be done at that voltage. For convenience, the low-voltage side is usually taken as the primary in this test. If the primary in this test is chosen to be the opposite winding from that of the short-circuit test, one must of course be careful to refer the various measured impedances to the same side of the transformer in order to obtain a self-consistent set of parameter values. [9]

Figure 2.16a shows the equivalent circuit with the transformer secondary impedance referred to the primary side and the secondary open-circuited. The open-circuit impedance Z_{oc} looking into the primary under these conditions is

$$Z_{OC} = R_1 + jX_{l1} + Z_{\phi} = R_1 + jX_{l1} + \frac{R_c \cdot jX_m}{R_c + jX_m} \quad \text{Eq. (2-18) [9]}$$

Because the impedance of the exciting branch is quite large, the voltage drop in the primary leakage impedance caused by the exciting current is typically negligible, and the primary impressed voltage \hat{V}_{OC} very nearly equals the emf \hat{E}_{oc} induced by the resultant core flux. Similarly, the primary $I_{OC}^2 R_1$ loss caused by the exciting current is negligible, so that the power input P_{OC} very nearly equals the core loss P_{OC}^2/R_c . As a result, it is common to ignore the primary leakage impedance and to approximate the open-circuit impedance as being equal to the magnetizing impedance

$$Z_{OC} \approx Z_{\phi} = \frac{R_c \cdot jX_m}{R_c + jX_m} \quad \text{Eq. (2-19) [9]}$$

Note that the approximation made here is equivalent to the approximation made in reducing the equivalent-T circuit to the cantilever equivalent circuit of Figure 2-16b; the impedance seen at the input of this equivalent circuit is clearly Z_{ϕ} since no current will flow in the open-circuited secondary. [9]

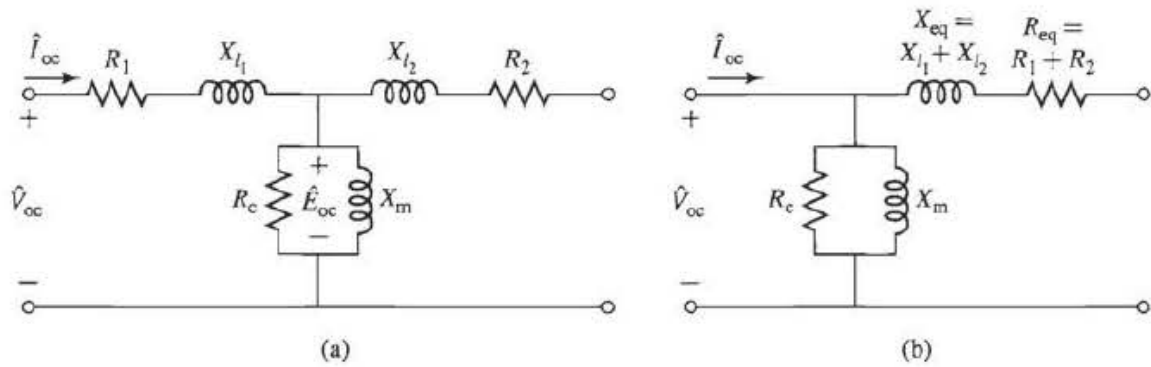


Figure 2-16: Equivalent circuit with open-circuited secondary. (a) Complete equivalent circuit. (b) Cantilever equivalent circuit with the existing branch at the transformer primary. [9]

As with the short-circuit test, typically the instrumentation used for this test will measure the rms magnitude of the applied voltage, V_{oc} , the open-circuit current I_{oc} and the power P_{oc} . Neglecting the primary leakage impedance and based upon these three measurements, the magnetizing resistance and reactance (referred to the primary) can be found from

$$R_c = \frac{V_{oc}^2}{P_{oc}} \tag{Eq. (2-20) [9]}$$

$$|Z_\varphi| = \frac{V_{oc}}{I_{oc}} \tag{Eq. (2-21) [9]}$$

$$X_m = \frac{1}{\sqrt{(1/|Z_\varphi|)^2 - (1/R_c)^2}} \tag{Eq. (2-22) [9]}$$

The open-circuit test can be used to obtain the core loss for efficiency computations and to check the magnitude of the exciting current. Sometimes the voltage at the terminals of the open-circuited secondary is measured as a check on the turns ratio. [9]

Note that, if desired, a slightly more accurate calculation of X_m and R_c by retaining the measurements of R_1 and X_{l1} obtained from the short-circuit test (referred to the proper side of the transformer) and basing the derivation on Eq. (2-18). However, such additional effort is rarely necessary for the purposes of engineering accuracy. [9]

2.5.3 NO-LOAD CONDITIONS

Figure 2-17 shows in schematic form a ring core. Suppose that a voltage, v_1 is applied to its primary terminals. A small exciting current, i_φ , flows in the primary and establishes an altering flux in the magnetic circuit. This flux induces an emf in the primary equal to:

$$e_p = \frac{d}{dt} \lambda_1 = N_1 \cdot \frac{d\varphi}{dt} \tag{Eq. (2-23) [9]}$$

λ_1 is the flunk linkage of the primary windings, φ is flux in the core linking both windings, while N_1 is the number of turns in the primary winding. [9]

The voltage e_1 is in volts when ϕ is in webers. This emf, together with the voltage drop in the primary resistance R_1 , must balance the applied voltage v_1 , thus

$$v_1 = R_1 i_\phi + e_1 \tag{Eq. (2-24) [9]}$$

Note that for the purposes of the current discussion, we are neglecting the effects of primary leakage flux, which will add an additional induced-emf term in Eq. (2-24). In typical transformers, this flux is a small percentage of the core flux, and it is quite justifiable to neglect it for our current purposes. It does however play an important role in the behaviour of transformers.

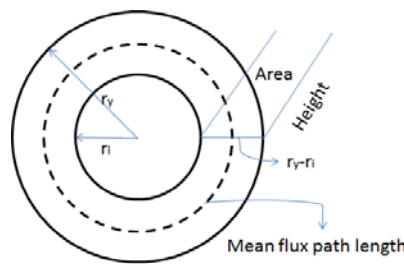


Figure 2-17: Ring core transformer

In most large transformers, the no-load resistance drop is very small indeed, and the induced emf, e_1 very nearly equals the applied voltage v_1 . Furthermore, the waveforms of voltage and flux are very nearly sinusoidal. The analysis can then be greatly simplified. This, if the instantaneous flux is

$$\phi = \phi_{max} \cdot \sin(\omega t) \tag{Eq. (2-25) [9]}$$

the induced voltage is

$$e_p = N_p \cdot \frac{d\phi}{dt} = N_p \omega \phi_{max} \cos(\omega t) \tag{Eq. (2-26) [9]}$$

where ϕ_{max} is the maximum value of the flux and $\omega=2\pi f$, the frequency being in Hz. For the current and voltage, the induced emf leads the flux by 90° . The rms value of the induced emf e_1 is

$$E_p = N_p \omega \phi_{max} \tag{Eq. (2-27) [9]}$$

If the resistive voltage drop is negligible, the counter emf equals the applied voltage. Under these conditions, if a sinusoidal voltage is applied to a winding, a sinusoidal varying core flux must be established whose maximum value $\hat{\phi} = \phi_{max}$

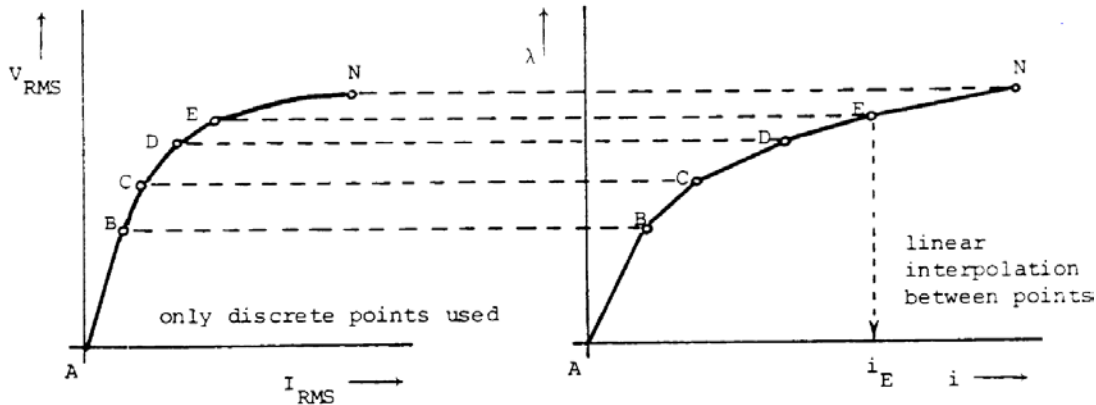
$$\hat{\phi} = \frac{\sqrt{2}U_p}{N_p \omega} \tag{Eq. (2-28) [9]}$$

$$\hat{B} = \frac{\sqrt{2}U_p}{N_p \omega A_p} \tag{Eq. (2-29) [9]}$$

2.6 SUPPORT ROUTINE CONVERT

Often, saturation curves supplied by manufacturers give rms voltages as a function of rms current. The support routine CONVERT changes V_{rms}/I_{rms} -curves into flux/current-curves $\lambda=f(i)$ with the following simplifying assumptions [10]:

1. Hysteresis and eddy current losses in the iron-core are ignored
2. Resistance in the winding is ignored
3. The λ/i -curve is to be generated point by point at such distances that linear interpolation is acceptable in between points



4. Figure 2-18: Recursive conversion of a V_{rms}/I_{rms} -curve into a λ - i curve [10]

For the conversion it is necessary to assume that the flux varies sinusoidal at the fundamentally frequency as a function of time, because it is most likely that the V_{rms}/I_{rms} -curve has been measured with a sinusoidal terminal voltage. With assumption 2, $v=d\lambda/dt$, the voltage will also be sinusoidal and the conversion of V_{rms} values to flux values becomes a simple re-scaling [10]:

$$\lambda = \frac{V_{RMS}\sqrt{2}}{\omega} \tag{Eq. (2-30) [10]}$$

The re-scaling of currents is more complicated, except for point i_B at the end of the linear region A-B, from Figure 2-18:

$$i_B = I_{RMS-B}\sqrt{2} \tag{Eq. (2-31) [10]}$$

The following points i_C, i_D, \dots are found recursively: assume that i_E is the next value to be found. Assume further that the sinusoidal flux just reaches the value λ_E at its maximum,

$$\lambda = \lambda_E \sin(\omega t) \tag{Eq. (2-32) [10]}$$

Within each segment of the curve already defined by its end points, in this case A-B and B-C and C-D, i is known as a function of λ (named piecewise linear), and with Eq. (2-32) is then also known as a function of time. Only the last segment is undefined inasmuch as i_E is still unknown. Therefore, $i=f(t, i_E)$ in the last segment. If the integral needed for rms-values,

$$F = \frac{2}{\pi} \int_0^{2/\pi} i^2 d(\omega t) \tag{Eq. (2-33) [10]}$$

is evaluated segment by segment, the result will contain i_E as an unknown variable. With the trapezoidal rule of integration (reasonable step size = 1°), F has the form

$$F = a + bi_E + ci_E^2 \tag{Eq. (2-34) [10]}$$

with a, b and c known. Since F must be equal to i_{rms-E}^2 by definition, Eq. (2-34) can be solved for the unknown value i_E . This process is repeated recursively until the last point i_N has been found. [10]

2.7 FIND SERIES REACTANCE USING FEM-ANALYSIS

In a transformer, the leakage reactance and inductance can be calculated with an energy method. First, a simple system with two coils with self-inductances L_1 and L_2 is investigated. Between the two coils is a magnetic coupling described by the mutual inductance M. When currents flow in the windings, the resulting magnetic energy is:

$$W = \frac{1}{2}L_1I_1^2 + \frac{1}{2}L_2I_2^2 + MI_1I_2 \tag{Eq. (2-35) [11]}$$

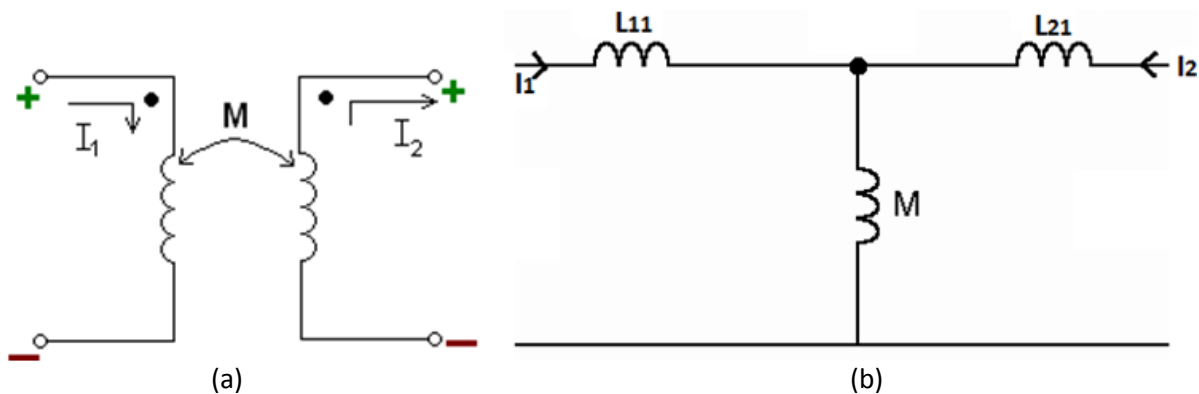


Figure 2-19: Model of (a) two coils with mutual inductance M and (b) traditional equivalent transformer circuit [10]

Figure 2-19a can be changed into the well-known equivalent scheme, b, for a transformer by setting

$$L_{11} = L_1 - M \tag{Eq. (2-36) [11]}$$

$$L_{21} = L_2 - M \tag{Eq. (2-37) [11]}$$

For this system the magnetic energy is given by:

$$W = \frac{1}{2}L_{11}I_1^2 + \frac{1}{2}L_{21}I_2^2 + \frac{1}{2}M(I_1 + I_2)^2 \tag{Eq. (2-38) [11]}$$

Be aware of the definition of the current directions. As one can see that the magnetization inductance is the same as the mutual inductance between the primary and secondary winding.

During a short circuit, the core flux is close to zero and hence the magnetization current is zero. Thus $I_1+I_2=0$. The magnetic energy can then be calculated by:

$$W = \frac{1}{2}L_{11}I_1^2 + \frac{1}{2}L_{21}I_2^2 = \frac{1}{2}(L_{11} + L_{21})I_k^2 \tag{Eq. (2-39) [11]}$$

$$I_1 = -I_2 = I_k \tag{Eq. (2-40) [11]}$$

If $L_k=L_{11}+L_{21}$ is set, the following equation is obtained:

$$L_k = \frac{2W}{I_k^2}, \quad Z_k = \frac{2W}{I_k^2}\omega \tag{Eq. (2-41) [11]}$$

2.8 CALCULATION OF RESISTANCE AND REACTANCE IN SUBSEA CABLE SYSTEMS

2.8.1 INTRODUCTION

In order to achieve an impedance estimate of long conductors, the Carson’s formulas are used. The formulas comply with the following assumptions [12]:

1. The inducing line is a horizontal straight conductor of infinite length in which flows a constant, evenly distributed current.
2. The lines, between which the mutual impedance is to be calculated, are parallel to each other.
3. The earth is homogeneous of finite resistivity.
4. The materials have no magnetic properties, meaning that their relative permeability equals 1.

2.8.2 SINGLE-PHASE LOOP WITH CIRCULAR CONDUCTORS

Figure 2-20 shows a single-phase loop with circular conductors both having radius r and mean centre-to-centre distance D . The object is now to calculate the reactance for the loop.

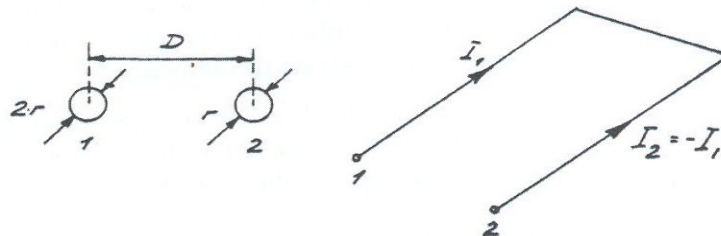


Figure 2-20: A single-phase loop with two massive conductors [8]

$$\Delta U_1 = R_1I_1 + js\mu f \cdot \ln\left(\frac{1}{g_{11}}\right)I_1 + js\mu f \ln\left(\frac{1}{g_{12}}\right)I_2 \tag{Eq. (2-42) [8]}$$

$$\Delta U_2 = R_2I_2 + js\mu f \cdot \ln\left(\frac{1}{g_{21}}\right)I_1 + js\mu f \ln\left(\frac{1}{g_{22}}\right)I_2 \tag{Eq. (2-43) [8]}$$

Since the total current is zero, $I_1 = -I_2$

$$\Delta U_1 = R_1 I_1 + js\mu f \ln\left(\frac{g_{12}}{g_{11}}\right) I_1 \quad \text{Eq. (2-44) [8]}$$

$$\Delta U_2 = R_2 I_2 + js\mu f \ln\left(\frac{g_{21}}{g_{22}}\right) I_2 \quad \text{Eq. (2-45) [8]}$$

The two conductors are equal in size and have the same resistance, hence $g_{11} = g_{22} = 0.78r$, $R_1 = R_2$ and $g_{12} = g_{21} = D$

$$\Delta U_{12} = \Delta U_1 - \Delta U_2 = 2R_1 I_1 + 2js\mu f \ln\left(\frac{D}{0.78r}\right) \cdot I_1 \quad \text{Eq. (2-46) [8]}$$

And finally, the reactance becomes

$$X = 2js\mu f \ln\left(\frac{D}{0.78r}\right) \quad \text{Eq. (2-47) [8]}$$

3 TRANSFORMER DESIGN AND CALCULATIONS

3.1 SYSTEM OVERVIEW

The transformer is to be set into a system where a long main pipeline is to be heated using DEH. An electric current carrying conductor, piggy-back cable, supplies the DEH system and is used as current source for this transformer. The electricity from the secondary side of the transformer is subsequently used to heat a t-off, connected to the primary pipeline. An example of a t-off system heated using IH-system is illustrated in Figure 3-1. The t-off could also be heated using the same principle as for the main pipeline, DEH.

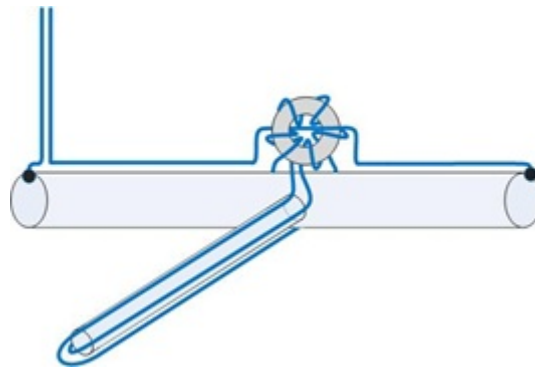


Figure 3-1: Sketch of a main pipeline headed using DEH, and a t-off heated by induction heating

How the secondary winding placement impacts on the overall impedance is also of interest to examine. Three different approaches are tested; a no-loop, half-loop and full-loop configuration, as seen in Figure 3-2. The grey conductor represents a piggy-back cable, while the black are supposed to heat a jumper by the concept of IH.

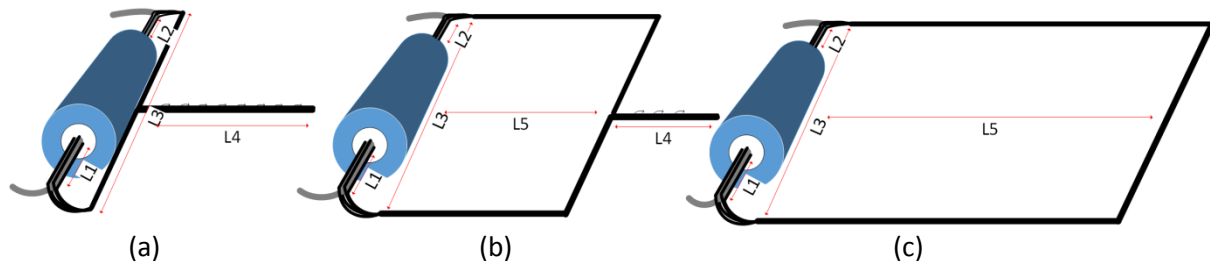


Figure 3-2: Transformer with long secondary winding. Left: no loop. Middle: half-loop. Right: Full loop

3.2 TRANSFORMER DESIGN

In order to create a transformer, some design criteria have to be met. In contrast to a regular power transformer, large current is needed in both primary and secondary windings. The primary winding current is usually around 1200 ampere, depending on pipeline size and insulation type. The current needed in the secondary winding(s) depends on the chosen heating method. From the feasibility study performed previous autumn, it was found that the winding ratio in most cases will be less than four.

Another important factor is the possibility to connect a transformer, but avoid the use of termination points. Since joints are said to be the weakest link in a conductor system, termination free

transformers increases the overall system reliability. Due to this, the transformer's primary winding only consist of one single turn, and is therefore quite similar to a current transformer mode of operation.



Figure 3-3: Transformer short-circuit test. Grey: primary winding (piggy-back cable). Black: secondary winding

This design type does also prevent fringing flux produced by air gaps as there are none in the magnetic flux direction. Fringing flux can reduce the overall efficiency, due to eddy currents that cause localized heating in the windings and/or in the brackets, meaning than an air gap absence might be advantageous. This design does also give maximum utilization of flux with the minimum of magnetic force, as quoted form chapter 2.4.4.

Based on the mentioned requirements a ring-core transformer is found to be suitable in this kind of application. Figure 3-3 indicates how a transformer of this design might look like. The blue cylinder consists of multiple stabled round wounded iron cores. The grey line is the piggy-back cable, while the black are short circuited secondary windings.

3.3 PROTOTYPE DIMENSIONS

Two different transformers are tested in the laboratory, termed small and large. Their construction is identical; multiple stabled toroidal cores build up from magnetic tape. Table 3-1 indicates their physical dimensions.

Table 3-1: Prototype dimensions

Transformer type	Inner radius [mm]	Outer radius [mm]	Total height [mm]	Volume [dm ³]	Weight [kg]
Small	25	45	480	2.111	15.81
Large	50	90	560	9.852	71.76

3.4 THE CORE

The tape wound toroidal cores are bought from the manufacturer ThyssenKrupp Electrical Steel. The grain oriented electrical steel Power Core[®] C 140-30 type is used, named M 140-30 S5 in the IEC 60404-8-7 standard. Some typical physical properties obtained from the manufacturer are listed in Table 3-2. Comparing with the theory chapter, the stacking factor and lamination thickness are within the regular range of this iron core class.

Table 3-2: Typical physical properties of the magnetic tape wound toroidal core [13]

Description	Value	Unit
Saturation polarisation (J_s)	2.03	T
Coercive field strength (H_c)	5	A/m
Density (P_m)	7.65	kg/dm ³
Electrical resistivity (P_e)	0.48	$\mu\Omega\text{m}$
Stacking factor (0.30mm)	96.5	%
Coating thickness	2-5	μm

3.5 RATED VOLTAGE

In order to find the rated voltage of this transformer, formulas developed earlier are used. A rule of thumb is to set the average magnetic field density capability to a maximum of 1.6 T, assuming a 50 Hz power system. From this, it is possible to calculate an approximate voltage which may be supplied across the transformer terminals. Supplying larger voltage results in extensive saturation, increasing the transformer losses.

From Figure 2-17, the flux area and mean flux path length are developed:

$$A = (r_y - r_i) \cdot h \quad \text{Eq. (3-1)}$$

$$l = 2\pi \cdot \frac{r_y + r_i}{2} = \pi(r_y + r_i) \quad \text{Eq. (3-2)}$$

Using the two preceding equations together with Eq. (2-29), Table 3-3 is created.

Table 3-3: Prototype transformer dimensions and voltage

Transformer type	Inner radius [mm]	Outer radius [mm]	Total height [mm]	Area [m ²]	Mean path length [m]	Reference voltage [V]
Small	25	45	480	$9.6 \cdot 10^{-3}$	$0.070\pi \approx 0.22$	3.41
Large	50	90	560	$22.4 \cdot 10^{-3}$	$0.140\pi \approx 0.44$	7.96

This means that the theoretical reference voltage of the small and large transformers are 3.41 V and 7.96 V, respectively.

3.6 RATED CURRENT

The rated current of the transformer is based upon the NEK-standard 400-5-52:2010. From table 52B-4, the current-carrying capacities are found, assuming that the conductors are multi-conductor cables. It is common to specify the rated values both for operational condition, subsea, in addition to onshore. For the onshore circumstance, an ambient temperature of 30 °C is chosen. At subsea, an ambient temperature of 10°C is selected, giving a correlation factor of 1.22 found from table 52B-14. In contrast, a correction factor <1 should also be used due to the high number of conductors inside the transformer, but since ambient temperature of water is around 5°C, and the thermal conductivity of water in motion is much higher than air, these two factors are set to cancel each other.

Table 3-4: Rated current based on NEK-standard 400-5-52:2010

Application		Area [mm²]	Insulation type	Subsea [A]	Onshore [A]
Small transformer	Secondary winding	4·16	PVC	371	304
	Primary winding	95	PVC	272	223
Large transformer	Secondary winding	4·70	PVC	898	736
	Primary winding	3·185	PVC	1248	1023

Based on the calculated values from Table 3-4, the rated current is set to 270 A and 900 A for the small and large transformer, respectively, when operating at subsea. The analogous values onshore are set to 220 A and 735 A.

4 LABORATORY SETUP

4.1 INTRODUCTION

This chapter presents the performed laboratory work, including detailed description of the experiments and utilized instruments and equipment. All following tests are executed for both the small and large transformer. An illustration of the short-circuit test is shown in Figure 3-3. The ambient temperature is measured to be 18°C.

4.2 LABORATORY SETUP

A variable autotransformer is connected to a 230V 1-phase 50 Hz supply. The output claps are next connected to a regular transformer. Finally, the test object transformer's primary winding is supplied from the regular transformer. A photography of the short-circuit setup of the small transformer is attached as Figure 13-1. All setups are created in accordance with theory from chapter 2.5.

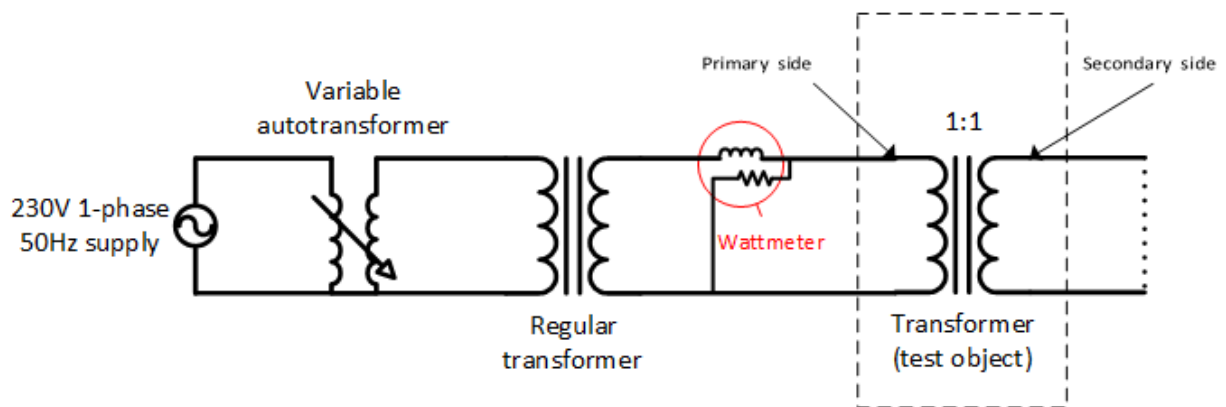


Figure 4-1: Single line diagram of the laboratory setup

4.3 SHORT-CIRCUIT AND OPEN-CIRCUIT TESTS

The connection diagram for the open-circuit and short-circuit tests is shown in Figure 4-1. A wattmeter is connected at the primary side of the test object. By help of the variac, voltage is slowly increased to a set of predefined values at which results from the wattmeter are registered.

When performing open-circuit measurements, wattmeter readings are performed at predefined voltages. These readings are carried out at every half-volt from 0.5-4.5 V, in addition to 2.225 V, 2.750 V and 3.250 V for the small transformer. The analogous large transformer values are every integer volt from 1 V to 10 V, together with 4.5 V, 5.5 V and 5.75 V. The predefined short-circuit values are 50 ampere intervals from 50-300 A for the small transformer, and every 100 A for the large, from 100-1100 A.

4.4 CONDUCTOR COUPLING

The conductor placement inside the core is implemented with emphasis of achieve good symmetry, within feasible practical limits, see Figure 4-2. The inside of the small transformer core consists of one single primary winding and four secondary conductors, all coupled in parallel. This differs from the large transformer, where the primary winding consists of three conductors. Unavailability of a large primary conductor is the reason for choosing a three-conductor replacement. The orange rectangle within the large transformer core is a small piece of wood which keeps the conductor profile as desired. Pictures from the laboratory are found in Figure 13-2 and Figure 13-3. The dots and crosses inside the conductors in Figure 4-2 indicate the current direction at one specific time instant based on regular notation.

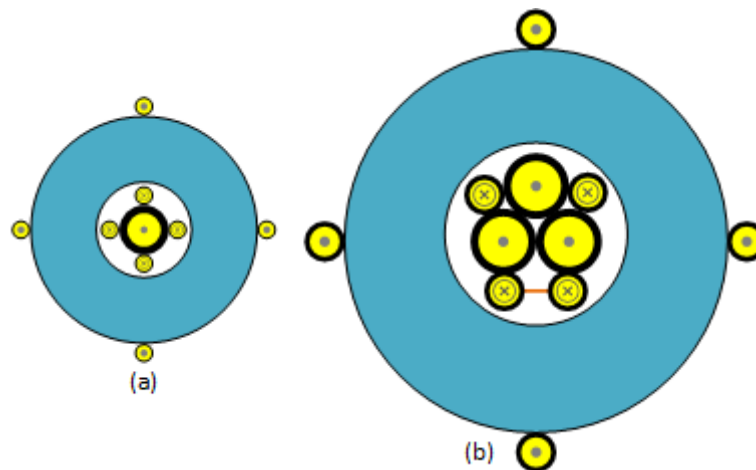


Figure 4-2: Conductor placement inside and around the transformer core of (a) small transformer and (b) Large transformer

4.5 THE WINDINGS

The winding dimensions are presented in Table 4-1. They are circular and surrounded by insulation, as regular power conductors. As can be seen, the primary winding lengths of the small and large transformers are equal, even though the small transformer is shorter than the large transformer. This is because the supports holding both transformers are of equal length, 64 cm. For more correct results of the transformer parameters, the primary length of the transformers should have been somewhat shorter, ideally the same length as the core height. Analogous, the secondary windings could also have been somewhat shorter.

Table 4-1: Winding dimensions

	Core dimensions ($r_i \times r_o \times h$)[mm ³]	Primary winding		Secondary winding	
		Area [mm ²]	Length [m]	Area [mm ²]	Length [m]
Small transformer	45x25x480	95	0.64	4·70	1.36
Large transformer	90x50x560	3·185	0.64	4·70	1.38

4.6 ELUCIDATION

The open-circuit tests are performed when long conductors are connected to the secondary side of the transformer. The results are though presented together with the short-circuit tests of the transformer only. Since the current traveling in the secondary windings is assumed to be negligible and independent of the secondary conductor's length, this could be done without significant error.

4.7 EQUIPMENT AND MEASUREMENTS

Table 4-2 summarises the most important apparatus which are used during the laboratorial work. An important issue to read from the table is that the short-circuit tests of both transformer are all measured using the power analyser tool Fluke Norma 5000, which is a high-precision analyser. The open-circuit tests are performed using the power quality analyser instrument Fluke 43. The reason for not using Norma 5000 on all measurements was availability; it was only available in the periods when the short-circuit tests were performed. Regarding the measurements including long secondary conductors, Fluke 43 was used as power quality analyser.

Table 4-2: Equipment summary

Equipment type	Producer/ model/rating	NTNU number	Transformer test			
			Small SC	Small OC	Large SC	Large OC
Variable autotransformers	0-260V, 10A	B01-426	x	x		
	0-250V, 100A	B01-144			x	x
Transformers	5V, 1000A	B01-0613	x	x		
	25V, 1000A	B01-0354			x	x
Power quality analyser	Norma 5000	H02-0122	x		x	
Power quality analyser	Fluke 43	H02-0110 -01		x		x
rms multimeter	Fluke 175	I04-481, I04-0409	x	x	x	x
rms multimeter	Fluke 177	NA	x	x	x	x
Electric current pincer	Fluke i1000s	I04-481, I04-0409			x	x
Electric current pincer	Fluke 80i-500	H02-0110 -03	x	x		
rms clamp meter	Fluke 336	I04-0486	x	x	x	x
Digital low resistance ohmmeter	Megger DLRO® 10X	H01-0101				

4.7.1 DETAILED MEASUREMENT INSTRUCTIONS OF THE SMALL TRANSFORMER

During the *open-circuit* tests, an electric current pincer, Fluke 80i-500, was connected to the power quality analyser Fluke 43. In addition, two voltage measurement conductors were connected from

the transformer terminals to the same apparatus. From the analyser tool; actual voltage, current and power quantities were obtained. Current and voltage waveforms were also extracted. During *short-circuit* tests, the power quality analyser Fluke 43 was replaced with Norma 5000.



Figure 4-3: Illustration of twisted voltage measurement conductors, small transformer

In order to extract correct results, the voltage measurement conductors were twisted from the power analyser to the middle of the transformer, where they were mounted outside the transformer core. Each conductor was subsequently mounted along the transformer to the termination point. This was done to avoid electrical noise going into the cables, contaminating the low measured voltages.

4.7.2 DETAILED MEASUREMENT INSTRUCTIONS OF THE LARGE TRANSFORMER

For the large transformer, this was a bit trickier. In contrast to the primary winding of the small transformer, the primary winding of the large transformer consists of three conductors. Due to variations in conductor and transition resistance, the voltage drops across the three different conductors are not identical. To compensate for this, the voltage drop of each conductor was recorded to see the significance of the prospective differences.

The multimeters Fluke 175 (2 pcs) and Fluke 177 measured the voltage drops across the primary conductor winding during *open-circuit* tests, and the values were noted at each measuring point. Fluke i1000s was used to measure the total current in the three conductors, connected to Fluke 43. Fluke 43 calculates the power loss based on the total current of the three primary conductors together with the voltage drop across *one* of the primary conductors. An image of how the voltage measurement conductors were placed is seen in Figure 4-4.

For the *short-circuit* measurements, Fluke Norma 5000 was used. The instrument has capability to measure all three voltage drops. Still, the current pincer terminal is only connected to one of the input terminals on the apparatus.

The large transformer's primary winding were much longer than the transformer length itself. To extract the voltage loss across the transformer, connection points had to be made. The easiest way to establish these terminal points was puncturing the cables by screw screws into the copper of the conductors.

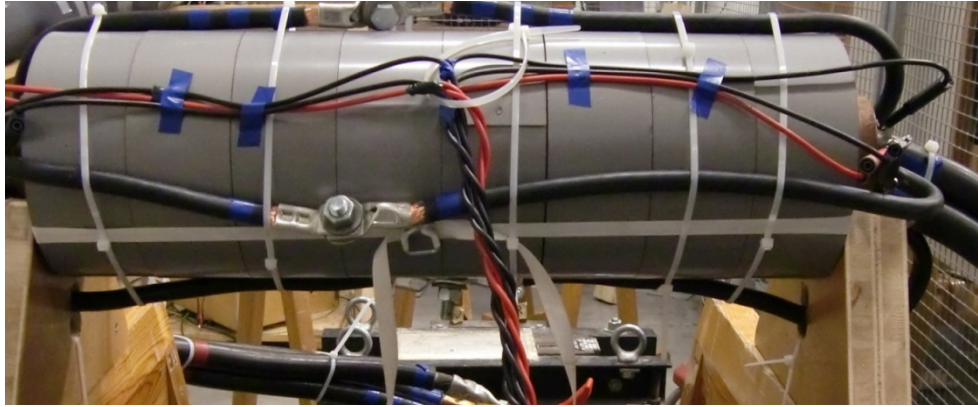


Figure 4-4: Illustration of twisted voltage measurement conductors, large transformer

4.7.3 DC-TESTS

The DC-tests were performed using Megger DLRO[®] 10X, digital low resistance ohmmeter, as seen in Figure 4-5. Since the measurement terminals are connected at the conductor cable shoe, transition resistance is included in the results.



Figure 4-5: DC test performed at the primary winding of the small transformer

4.8 LONG SECONDARY WINDING

4.8.1 LABORATORY SETUP

The instrument setup is analogous to the transformer only setups. Both short-circuit and open-circuit tests have been performed at both transformers. As stated before, the open-circuit results are presented together with the “transformer-only” short-circuits calculations since the secondary windings are stated to only influence the open-circuit results negligible. The cable-dimensions of both the primary and secondary windings are as pointed out in Table 4-1, except of the long conductor connected to the secondary winding. Speaking of measurement instruments, Fluke 175/177 and Fluke 43 have been used for both the small and large transformer. The current pincer 80i-500 was used during the small transformer measurements, whilst i1000S for the large transformer.

The secondary winding consists likewise here of four conductors connected in parallel. In the previous measurements, they were mounted evenly around the transformer, as illustrated in Figure 4-2. Here, they are mounted in a bundle using plastic strips. For the length L_4 from Figure 3-2, the two bundles are twisted around each other to minimize the system inductance.



Figure 4-6: Picture of small transformer with a long no-loop secondary winding

A picture of a long no-loop secondary cable is seen in Figure 4-6. Corresponding pictures of the half- and full-loop are found in Figure 13-4 and Figure 13-5, respectively. The two photos are taken from the other side of the transformer, illustrating the secondary cables more precisely.

4.8.2 LONG CONDUCTOR LENGTH

The long conductor lengths were approximately 12.15 meters and 11.60 meters for the small and large transformer, respectively. How the lengths are distributed, with reference to Figure 3-2 are presented in Table 4-3. These values are very inaccurate and only meant to give a rough estimate. The inaccuracy is mostly due to bends and turns which are difficult to avoid since the cable system is not lying at the ground. However, the purpose of this test is to find a trend more than accurate values of the loop-reactance.

Table 4-3: Long secondary winding lengths

	Small transformer			Large transformer		
	No loop	Half loop	Full loop	No loop	Half loop	Full loop
L1 [cm]	24	72	72	23	90	90
L2 [cm]	24	70	70	24	50	50
L3 [cm]	96	200	200	106	200	200
L4 [cm]	-	230	240	-	173	385
L5 [cm]	561	460	-	457	230	-

5 LABORATORY RESULTS

5.1 PART I: TRANSFORMER ONLY

5.1.1 INTRODUCTION

This part presents the laboratory work result from the «transformer only» prototypes, while the next treat the influence of connecting a long secondary conductor to the transformers' secondary winding. Typical measurement sets from each of the performed tests are displayed in Table 5-1 and Table 5-2. The indicated values are, as far as possible, written with equal number of digits as displayed on the measurement apparatuses. All measured values are listed in Table 13-1 to Table 13-6.

Based on these measurements, some central parameters are emphasized in this chapter. This included electrical parameters used in equivalent electric circuits together with B-H-curves and transformer core losses. Finally, a datasheet is created. Formulas used for the resistance, reactance and impedance calculations are based upon Eq. (2-15) to Eq. (2-17) and Eq. (2-20) to Eq. (2-22) from chapter 2.5.

Table 5-1: Typical measurements from the large transformer laboratory work

	V_{primary1} [V]	V_{primary2} [V]	V_{primary3} [V]	$V_{\text{primary avg.}}$ [V]	I_{primary} [V]	P_{primary} [W]
Short-Circuit	0.01261	0.01269	0.01238	0.01256	99.99	1.145
	0.02535	0.02546	0.02489	0.02523	200.45	4.616
	0.03818	0.03836	0.03753	0.03802	301.95	10.47
	0.05070	0.05094	0.04985	0.05050	400.9	18.47
	0.06372	0.06404	0.06267	0.06348	504.1	29.17
	0.07574	0.07613	0.07451	0.07546	598.3	41.16
	0.08870	0.08915	0.08726	0.08837	699.9	56.39
	0.10166	0.10219	0.10005	0.10130	801.4	74.3
	0.11451	0.11518	0.11295	0.11421	899.9	93.74
	0.12743	0.12817	0.12574	0.12711	1000.2	115.99
0.14067	0.14148	0.13884	0.14033	1100	140.88	
Open-circuit	1.002	1.002	1.000	1.00	1.904	1.46
	1.997	1.996	1.995	2.00	3.234	5.34
	2.996	2.996	2.994	3.00	4.413	11.5
	3.997	3.996	3.995	4.00	5.573	20.1
	4.998	4.997	4.995	5.00	6.86	31.0
	6.058	6.058	6.058	6.06	8.54	46
	7.01	7.00	6.99	7.00	10.76	64
	8.04	8.04	8.03	8.04	17.1	97
	9.03	9.02	9.01	9.02	64.0	1.7e02
	10.13	10.12	10.11	10.12	474	4e02

Concerning the large transformer’s primary winding, the measured voltage drop differences across each of the primary conductors were less than 1 per cent of almost every single measurement. When using the measured values in upcoming calculations, average voltage drop values are utilised.

Table 5-2: Typical measurements from the small transformer laboratory work

Short-circuit test			Open-circuit test		
V_{primary} [V]	I_{primary} [A]	P_{primary} [W]	V_{primary} [V]	I_{primary} [A]	P_{primary} [W]
0.0285	50.00	1.404	0.493	1.04	0.4
0.0572	100.37	5.664	1.009	1.79	1.4
0.0857	150.41	12.726	1.493	2.35	3.0
0.1140	199.74	22.467	1.996	2.90	5.0
0.1446	252.41	36.026	2.244	3.19	6.1
0.1731	301.36	51.491	2.505	3.54	7.6
			2.754	3.95	9.3
			3.006	4.46	11.2
			3.250	5.30	13.7
			3.506	7.23	17.2
			4.003	41.4	37.0
			4.502	163.7	106

5.1.2 SHORT-CIRCUIT TESTS

Figure 5-1 indicates the short-circuit impedance ($|Z_{eq}|$), reactance (X_{eq}) and resistance (R_{eq}) of both the two transformers. Two different measurement sets have been executed. For both transformers, $|Z_{eq}|$ is largest, followed by R_{eq} and X_{eq} . As observed, R_{eq} is 6.14 times larger than X_{eq} for the small transformer, while the equivalent value for the large transformer is 2.21.

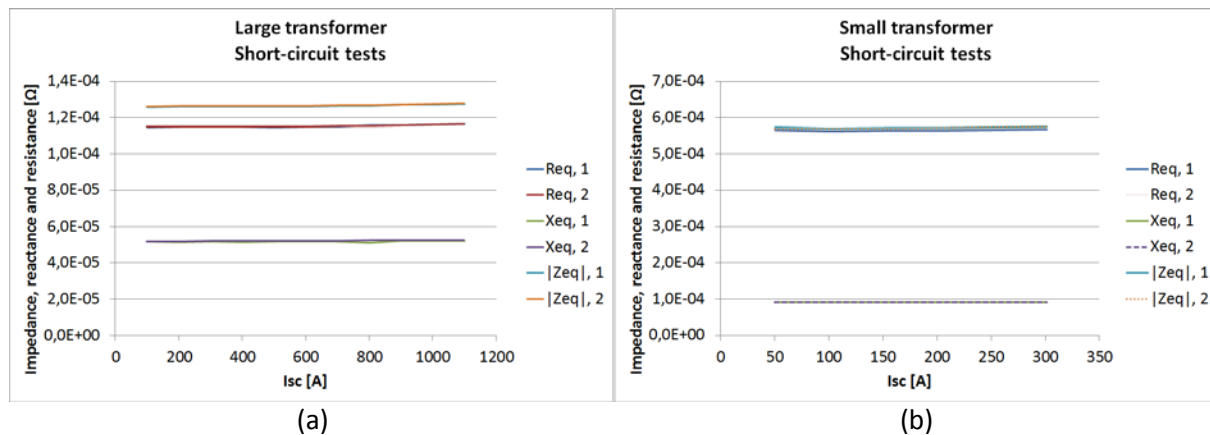


Figure 5-1: Short-circuit tests of the (a) small and (b) large transformer

Both measuring series of each transformer indicates that there are small deviations of the impedance as a function of current, within the measuring span. The resistance of the large transformer varies between 1.15e-4 Ω and 1.17e-4 Ω from the lowest to highest applied current. An insignificant higher deviation is found from the small transformer, where the analogous values are 5.62e4 Ω and 5.67e-4 Ω. This gives a variation of 0.9% and 1.3% of the small and large transformer, respectively.

Speaking of the reactance, the calculated deviations are in the same range as for the resistances. The smallest and largest values of the small transformer are $9.13\text{e-}05 \Omega$ and $9.23\text{e-}05 \Omega$ (1.1 %). Corresponding values of the large transformer are $5.16\text{e-}5 \Omega$ and $5.21\text{e-}5 \Omega$ (1.0%), excluding the small dip at $I_{sc}=800\text{A}$ for measurement set 1.

5.1.3 OPEN CIRCUIT TESTS

The open-circuit tests of both transformers are presented in Figure 5-2, Figure 5-3 and Figure 5-4, illustrating the iron core resistance (R_c), magnetizing reactance (X_m) and magnetizing impedance ($|Z_\phi|$), respectively.

The iron core resistance increases as a function of applied voltage until around 2.0 V for the small transformer and 5.0 V for the large transformer. Beyond this point, the resistance slope decreases somewhat at higher voltages before the slope becomes negative.

All individual measurement sets (1-6) results in approximately the same curve. A small deviation is seen in measurement set 1 of the small transformer, while a somewhat larger difference is found for the large transformer. If 5.0 V is applied across the large transformer during open-circuit, the highest and lowest resistance values are 0.83Ω and 0.80Ω respectively, ergo a 3.6% difference.

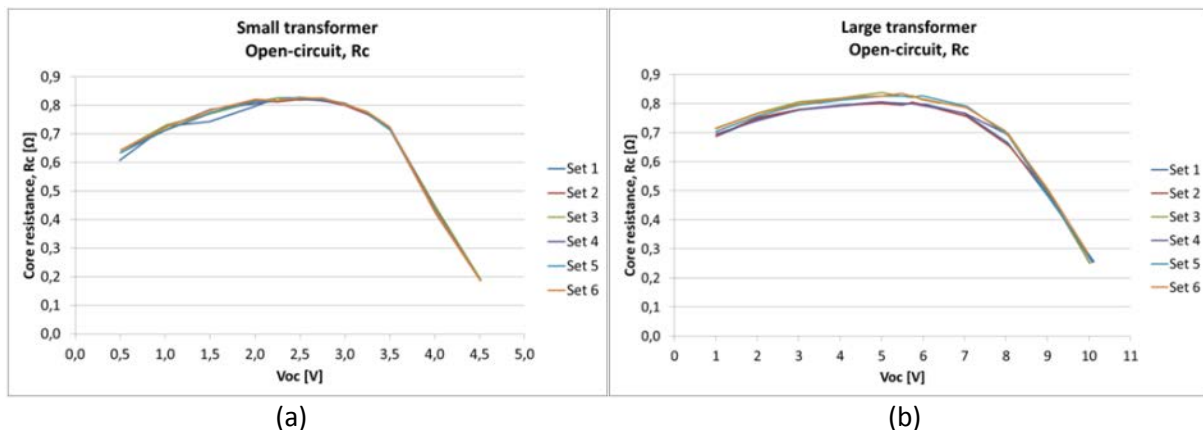


Figure 5-2: Core resistance from open-circuit test of the (a) small and (b) large transformer

The magnetizing reactance (Figure 5-3) has fairly the same shape as the measured iron core resistance; though with steeper gradients. Considering the small transformer, excluding measurement set 1, the magnetizing reactance increases linearly as a function of applied voltage until it reaches 2.0 V. The following volt unit, measurements differs a lot; some measurements indicate a reactance increase, while others indicate that the reactance levels out. From around 3.0 V, the resistance decreases rapidly.

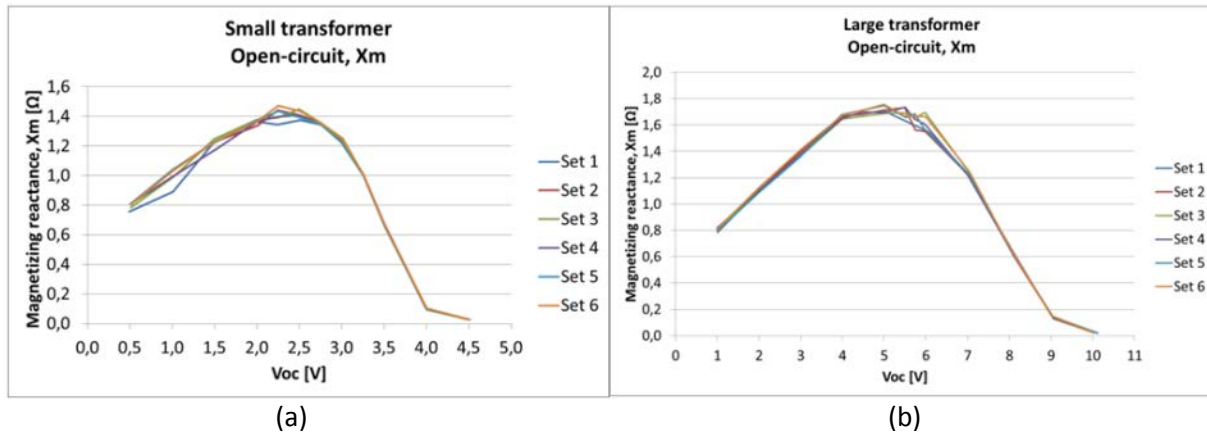


Figure 5-3: Magnetizing reactance from open-circuit test of the (a) small and (b) large transformer

A corresponding trend is also found from the large transformer, but the measurement sets are in general more similar. The exception is in the voltage range of 5.5-6.5 V. When the transformer core is highly saturated, the magnetizing reactance declines fast towards zero.

Figure 5-4 indicates the magnetizing impedance, $|Z_{\phi}|$ as a function of applied voltage. In contrast to the previous two figures, the magnetizing impedance deviates very little between the measurements. The reason is presented in the discussion chapter.

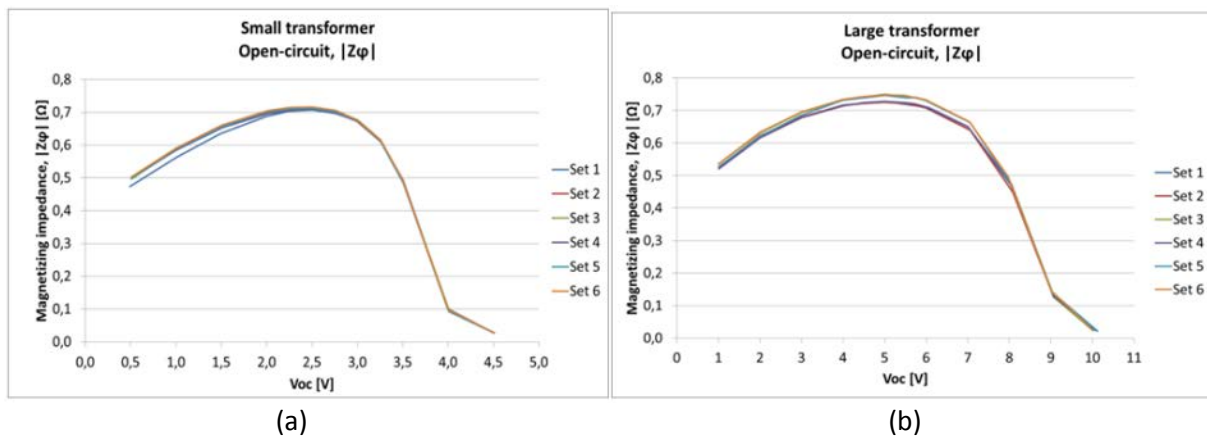


Figure 5-4: Magnetizing impedance from open-circuit test of the (a) small and (b) large transformer

5.1.3.1 VOLTAGE-CURRENT RELATIONSHIP

The applied open-circuit voltage as a function of the corresponding current is emphasized in Figure 5-5. Regarding the small transformer, the voltage/current relationship is approximately linear from the first measured voltage, 0.5 V, until around 3.0 V. At higher voltages, much larger short-circuit current is produced when increases the voltage by one unit.

A linear shape is observed for the large transformer until the applied open-circuit voltage reaches 6.5 V. The slope then decreases quite much. As seen, the current at $V_{oc}=10$ V is excluded from the sample, since the open-circuit current is the range of 400 A. It is though included as Figure 13-6.

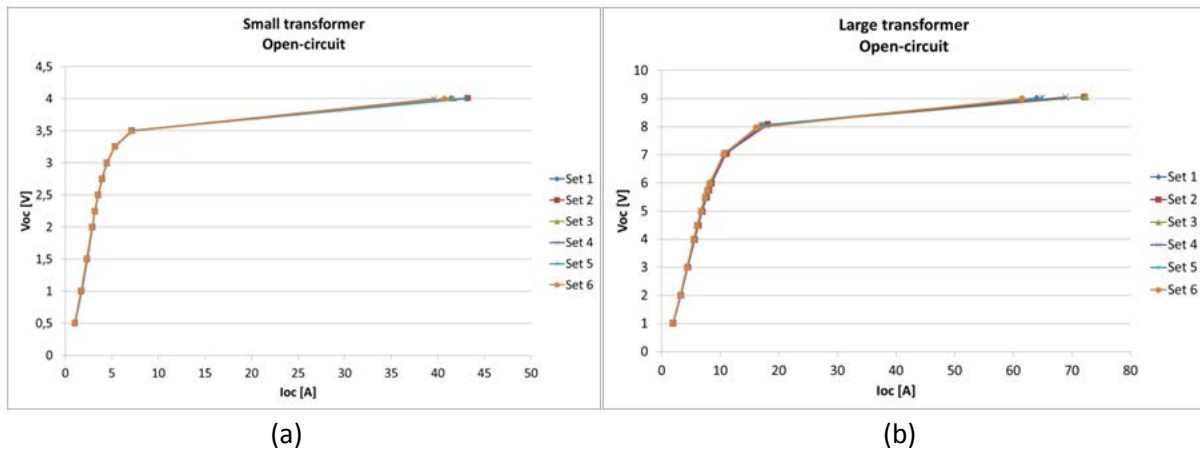


Figure 5-5: Open-circuit voltage as a function of appurtenant open-circuit current of the (a) small and (b) large transformer

5.1.3.2 CURRENT AS FUNCTION OF TIME

From the apparatus Fluke 43, the voltage- and current waveforms as a function of time were extracted. Combining the current/time-waveforms in one illustration gives Figure 5-6. Fluke 43 displays two values of each measuring point, one upper and one lower. The presented figure contains the average extracted value of one measuring set. In order to see how the waveform changes as voltage increases, the waveforms of the two largest voltage values are not included since their peak value of the open-circuit current are very large. All values are though attached in Figure 13-7. The equivalent voltage/time-waveforms are found in Figure 13-8. Their shape is more or less sinusoidal, but the largest voltage bends a little more around the zero-voltage crossings as seen from the figure. Similar current/time-waveform shapes are also found in Figure 2-11.

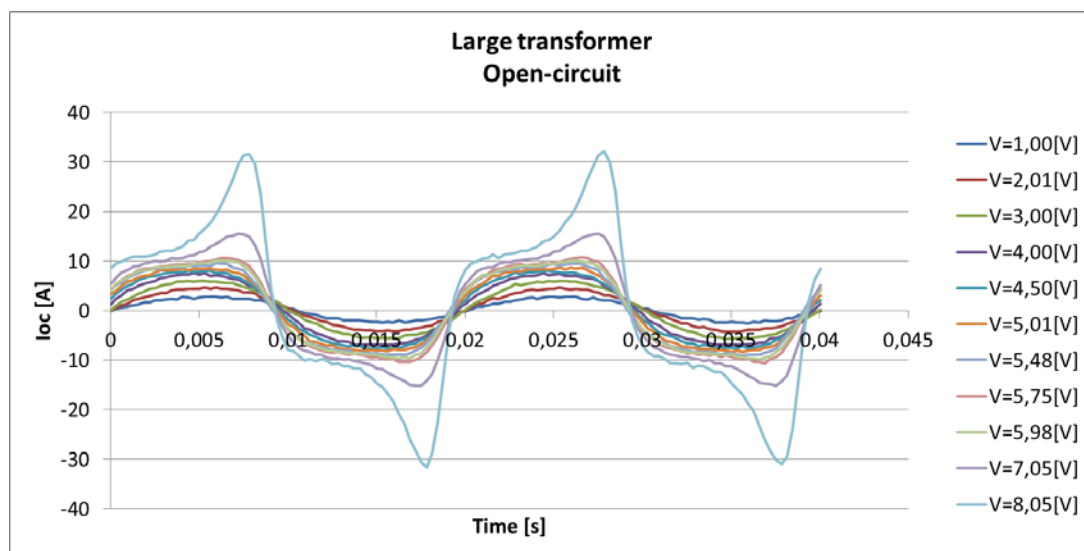


Figure 5-6: Current as function of time for large transformer

Analogous figures are also created for the small transformer. A small difference is that the current waveforms are much more wrinkled compared with the large transformer graph, as seen in Figure 13-9. The remaining open-circuit currents as a function of time (corresponding to Figure 13-7) are

found as Figure 13-11. Equivalent graphs to Figure 13-8 are found as Figure 13-10 for the small transformer.

5.1.3.3 RELATIVE PERMEABILITY

The relative permeability may be found from several formulas, depending on desired output values. Here, Figure 5-7 is created based on Eq. (5-1), where l is the mean flux path length. The equation is found by combining Eq. (2-8) and Eq. (2-29). As can be seen, the apparent relative permeability of the two transformers differs quite much. At flux density of 1.6 T, the relative permeability is approximately 24,118 and 22,282 for the small and large transformer core, respectively.

$$\mu_r = \frac{l}{\mu_0 \omega A} \cdot \frac{U_{rms}}{I_{rms}} \quad \text{Eq. (5-1)}$$

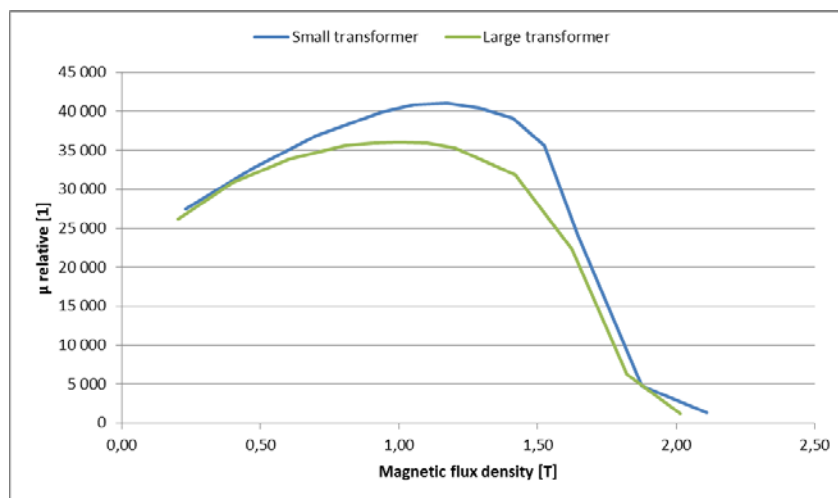


Figure 5-7: Relative permeability as a function of the magnetic flux density

As seen, the relative permeability is quite high. This is expected, as from chapter 2.4.1, due to the fact that this is a toroidal core without air gap in the magnetic flux path direction. This provides the maximum utilization of flux with the minimum of magnetic force

5.1.3.4 SPECIFIC LOSS AND MAGNETIC FIELD STRENGTH AS A FUNCTION OF THE FLUX DENSITY

By using the procedure called "support routine CONVERT" flux/current-curves are found. It is chosen to do the conversion using the program ATP-draw. V_{rms} and I_{rms} from the laboratory results are inserted, and the corresponding flux linkages and currents are extracted.

Subsequently, in order to convert this into a B-H-curve, the formulas from Eq. (5-2) and Eq. (5-3) are used. N , A and l are the number of turns, flux path area and average mean flux path length, respectively, as from Figure 2-17.

$$\hat{B} = \frac{\lambda}{A \cdot N} \quad \text{Eq. (5-2) [9]}$$

$$H = \frac{i}{\sqrt{2}} \cdot \frac{N}{l} \tag{5-3}$$

Figure 5-8 indicates the magnetic field strength, specific active loss and specific apparent loss as a function of magnetic flux density of both transformers. As can be seen, the two transformers follow approximately the same curve tendency.

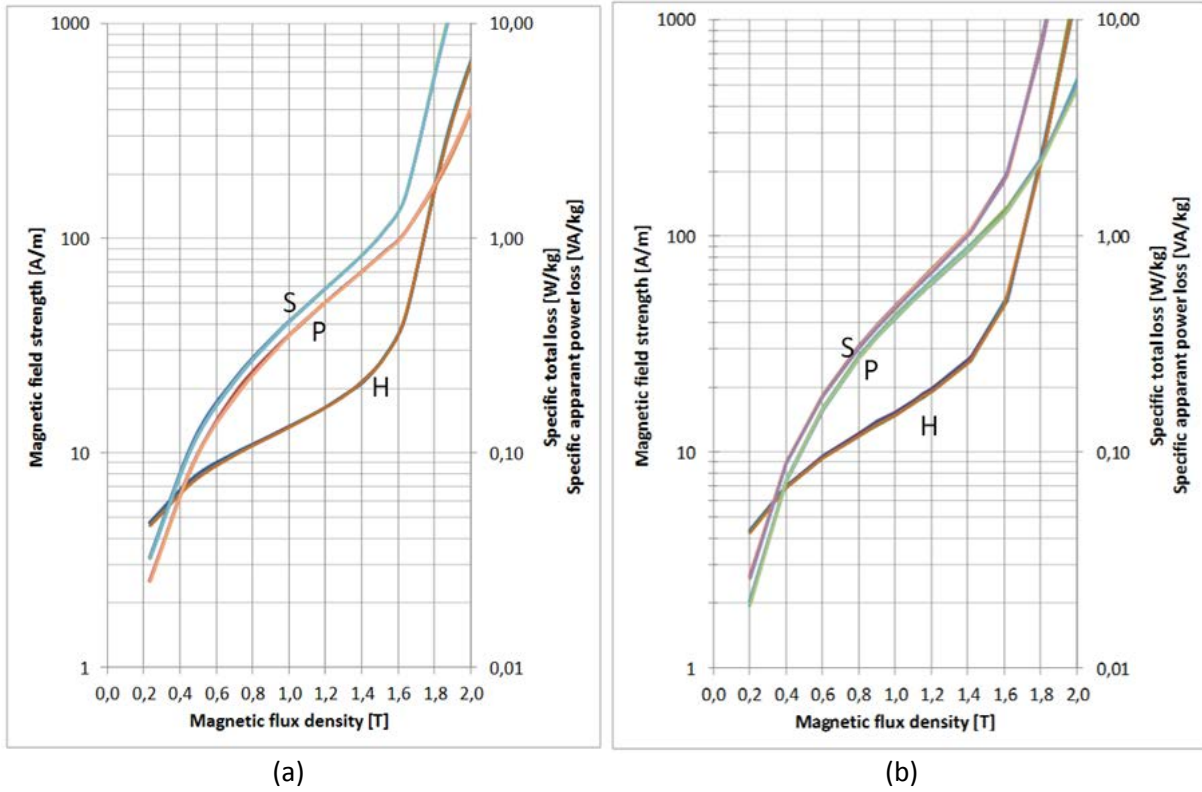


Figure 5-8: Magnetic field strength [H/m], specific active loss [W/kg] and specific apparent power loss [VA/kg] as function of magnetic flux density [T] of (a) small and (b) large transformer

Figure 5-9 illustrates the magnetic flux density as a function of the magnetic field strength of both transformers. From 0 till around 1.8 T, the produced magnetic field strength is quite similar. Subsequently, a large deviation is seen of the transformer core behaviour.

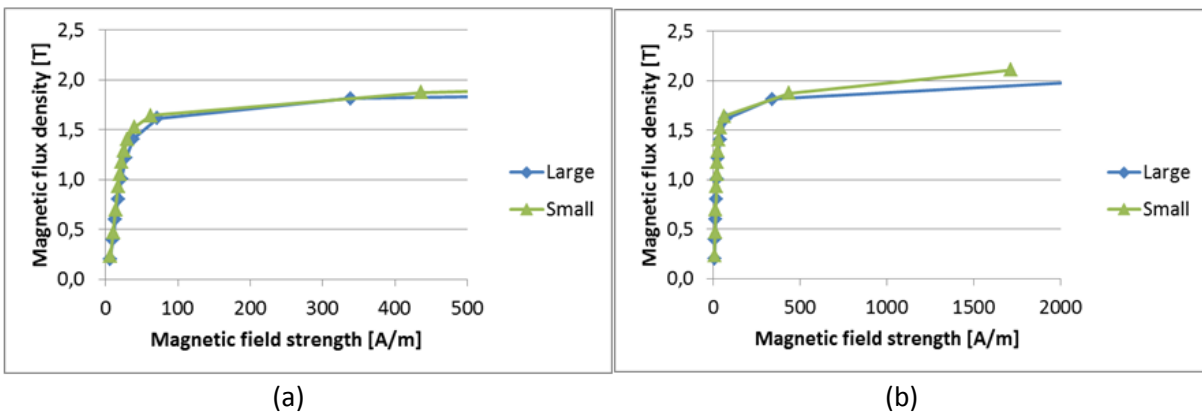


Figure 5-9: Magnetic flux density [B] as a function of magnetic field strength [H/m] of both transformers. (a): 0-500 A/m, (b) 0-2000 A/m.

5.1.4 DATASHEET

A datasheet of the two different transformers is recapitulated into Table 5-3. The leftmost values are during subsea operation conditions. The rightmost values are equivalent onshore values, assuming an ambient temperature of 30°C. When the rated current values are intermediate of the corresponding laboratory results, linear interpolation is utilised to find the correct short-circuit voltage, power loss and impedance.

Table 5-3: Datasheet of the two tested transformers

	Subsea		Onshore	
	Small transformer	Large transformer	Small transformer	Large transformer
S_n [VA]	918	7 200	748	5 880
I_n [A]	270	900	220	735
V_n [V]	3.4	8.0	3.4	8.0
f_n [Hz]	50	50	50	50
P_0 [W]	15.7	93.2	15.7	93.2
P_{sc} [W]	41.6	93.8	27.7	61.7
e_z [%]	4.55	1.43	3.70	1.43
e_R [%]	4.53	1.30	3.70	1.30
e_x [%]	0.44	0.59	0.072	0.50
$m_{iron\ core}$ [kg]	15.81	71.76	15.81	71.2
Winding material	Copper	Copper	Copper	Copper
Efficiency [%]	93.1	97.1	93.6	97.1

The efficiency is found based on following equation, assuming a power factor of 0.90:

$$\eta = \frac{P_{out}}{P_{in}} = \frac{P_{in} - P_{losses}}{P_{in}} = \frac{S_{in} \cdot pf - (P_{sc} + P_0)}{S_{in} \cdot pf} \cdot 100\% \quad \text{Eq. (5-4)}$$

5.2 PART II: LONG SECONDARY WINDING

5.2.1 INTRODUCTION

Multiple tests were carried out, but the one presented are selected with base in trustworthiness. All the results were approximately similar, but due to an undesirable large loop in the connection ends of some measurements, these results were discarded. A large loop in any part of the conductor system increases the system reactance.

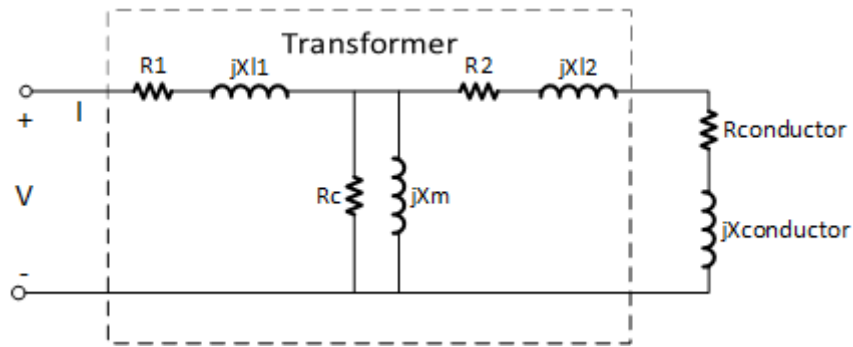


Figure 5-10: Equivalent circuit of the transformers having long secondary windings

A complete equivalent circuit of the system is sketched in Figure 5-10. The main goal is to find whenever $jX_{conductor}$ changes during different loop layouts as seen in Figure 3-2. With similar simplifications as in the background chapter, $R_{eq} = R_1 + R_2 + R_{conductor}$ and $X_{eq} = X_{l1} + X_{l2} + X_{conductor}$. Based on transformer parameters obtained prior in this chapter, the conductor only parameters could be found. The exact values are though not of interest, since the aim is to find whether the reactance changes or not.

5.2.2 EQUIVALENT SERIES REACTANCE

The equivalent series reactances for different loops are attached as Figure 5-11. As can be seen for both transformers sizes, the conductor placement is of large significance. The no-loop reactance of the small transformer is around 1 mΩ while the full loop it is around 3.75 mΩ. Corresponding values of the large transformer are 0.95 mΩ and 3.25 mΩ.

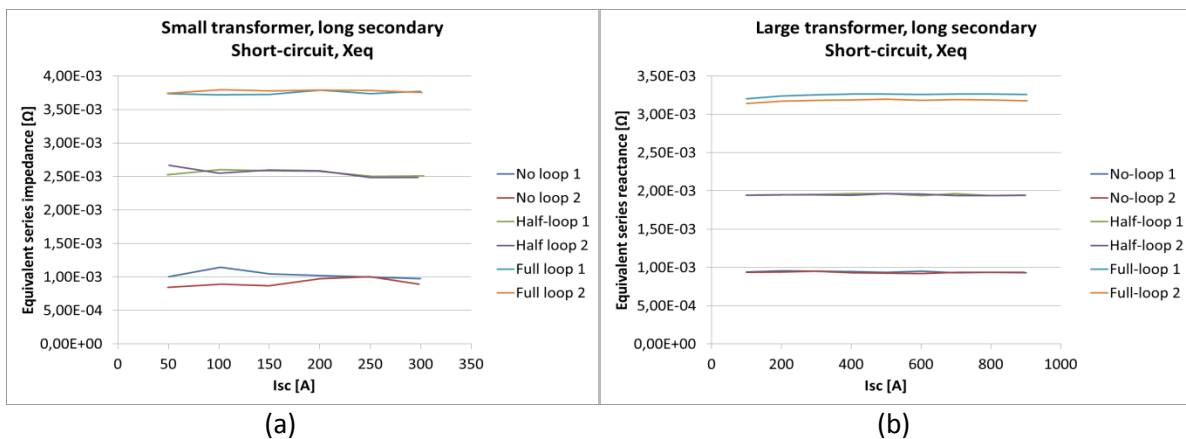


Figure 5-11: Short-circuit tests of the (a) small (left) and (b) large transformer, long secondary windings

5.2.3 EQUIVALENT SERIES RESISTANCE

The short-circuit resistance, R_{eq} , is sketched in Figure 5-12. As seen from the images, the resistance increases somewhat as applied current is increased for both the transformers. The increase is though most evidently for the large transformer measurements. Another tendency, which is more

unexpected, is that resistance increases in correlation with loop increase. This is also most conspicuous for the large transformer

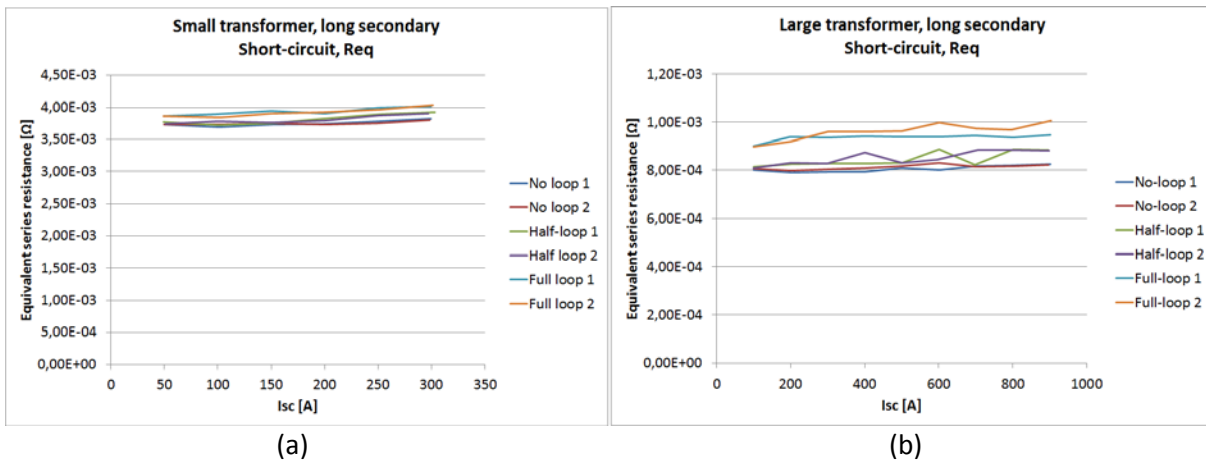


Figure 5-12: Short-circuit tests of the (a) small and (b) large transformer, long secondary windings

The lowest and highest resistance calculated from the small transformer measurements are approximate 3.7 mΩ and 4.0 mΩ, a difference of 7.5 %. The three corresponding values of the large transformer are 0.79 mΩ, 1.01 mΩ and 27.8 %. This is quite odd as the resistance was expected to stay rather constant, independent of applied current.

5.2.4 EQUIVALENT SERIES IMPEDANCE

Figure 5-13 shows the equivalent impedance. In difference to the above equivalent series resistance and reactance, the impedance is seen almost independent of applied current.

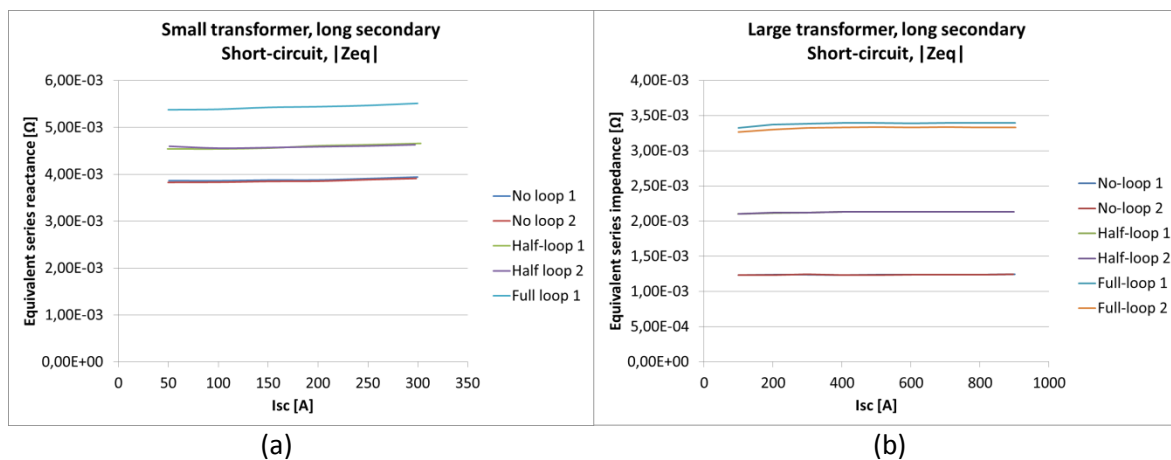


Figure 5-13: Short-circuit tests of the small (left) and large (right) transformer, long secondary windings

6 DISCUSSION

This part discusses results obtained in the laboratory work. First, instrument accuracy is set on agenda. Subsequently, formula simplifications from the equivalent electrical circuit are discussed. Thirdly, results from the transformer only part is discussed before dealing with the impact of a long secondary conductor connected to the transformers' secondary winding.

6.1 INSTRUMENT INACCURACY

The instruments' accuracy is of great importance since this expresses if measured quantities are actually true. As asserted in the results part there are variations, of different extent, in the estimated values extracted from the laboratory work. As measuring devices may have a comprehensive significance of the results' reliability, their accuracies are discussed thorough. All instruments and their area of application are displayed in Table 4-2.

6.1.1 CURRENT CLAMPS; FLUKE 80I-500 AND FLUKE I1000S

During the laboratory conditions, a basic accuracy of 2 % is given from Fluke 80i-500's datasheet. The corresponding value for Fluke 1000i is 2 % for conductor currents between 100 mA and 100 A, whilst 1 % up to 1000 A.

6.1.2 POWER QUALITY ANALYSER, FLUKE 43

Fluke 43 is the least accurate of the two power quality analysers. The accuracy of displayed fundamental power is $\pm (4\% + 4 \text{ counts})$. "4 counts" means that a displayed 0.4 W could mean 0.0 W or 0.8 W. Analogous, 0.400 W is in the range of 0.396 W – 0.404 W. In addition, the deviation in percentage is added.

When applying an open-circuit voltage of 9 V and 10 V across the large transformer, an active power loss of 0.17 kW and 0.4 kW, respectively, is generated. This is found from Table 13-4. Due to the accuracy deviation, these values might be considerably different, and significantly change the calculated resistance and reactance values. Since $Z_{\phi} = U/I$, the overall impedance would not be affected of large power inaccuracies. Regarding the open-circuit measurements, the most accurate values are found of applied voltage less and equal to 4.5 V, as three digits active power exactness is displayed.

A limitation of this instrument is that current and voltage is displayed in one menu, whilst the power is displayed from another. This means than an additional accuracy variance is added due to the period of time needed to change display output. For each display, it is possible to push a "pause"-button, but the instrument starts to run when changing display. The readings were executed when values of interest smoothed out, but some error must still be expected due to this problem.

One genuine example of the power variations from the apparatus is included, as Table 6-1. These measurement values are found when performing short-circuit testing of the large transformer, in which a long secondary conductor was connected. When performing measurements, the active

power displayed by the wattmeter fluctuate between the following values only, for one specific measurement set:

Table 6-1: Example of how measured power varies, despite constant voltage and current

Applied current [A]	300	400	500	600	700	800
Lower fluctuate value	83 W	147 W	232 W	0.33 kW	0.46 kW	0.59 kW
Upper fluctuate value	90 W	159 W	251 W	0.36 kW	0.50 kW	0.64 kW
Difference [%]	8.4	8.2	8.2	9.1	8.7	8.5

These fluctuations were seen even though the applied voltages and appurtenant currents were roughly constant at the same time instant. If only these values are considered, a variance of 8-9 per cent should be expected for corresponding measuring sets. The corresponding voltages and currents were displayed with four valid digits.

6.1.3 POWER QUALITY ANALYSER, NORMA 5000

Norma 5000 was utilised in the short-circuit measurements of the transformer only regarding both transformer sizes. Its basic accuracy is stated to 0.2 %, 0.1 % or 0.03 % depending on input modules, thus considerably better than Fluke 43. In addition, all required readings were displayed simultaneously avoiding the voltage or current to change when extracting power values.

6.2 VOLTAGE PROBE PLACEMENT, TWISTING AND EXTERNAL INFLUENCE

When two voltage probes are used to measure a voltage difference, the cables for the two probes should be gently twisted and firmly secured with a plastic spiral wrap. This minimizes induction of noise on the probe cables by the time rate of change of magnetic field, dB/dt , by minimizing the loop area between the probes and by giving a random orientation to the small area between the two cables [14]. From Figure 4-3, the cables are twisted as good as possibly. When they reach the iron core, they separate and are clamped at their respective termination point. Due to this inescapable separation, some induced voltage influence could be expected, but the significance is not quantified.

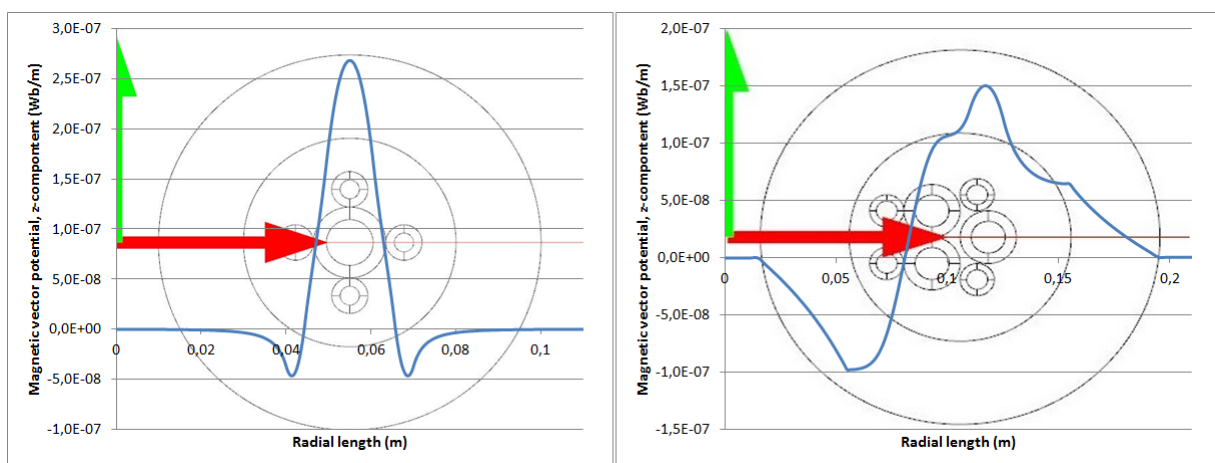


Figure 6-1: Magnetic vector potential, z-component of the transformers

The transformers' magnetic vector potentials are illustrated in Figure 6-1 by help of COMSOL-simulations. Only the conductors located inside the transformer are simulated. Appurtenant contour lines are found in Figure 13-13 and Figure 13-14. The aim is to see whenever the magnetic potential stretches beyond the transformer core. From the figures, almost no magnetic potential do reach outside the cores. This means that influences from the transformer is found to be small, based on the line graphs above.

6.3 FORMULA SIMPLIFICATIONS

Some simplifications are executed when finding the transformers' reactances and resistances. The two revealed simplifications of the transformer equivalents are examined here. Since the short-circuit tests of the transformer do not separate primary versus secondary winding values, the DC-test results are used for the resistance. Regarding the reactances, X_{l1} and X_{l2} are set equal. All values are collected at reference values.

6.3.1 SHORT-CIRCUIT FORMULA SIMPLIFICATIONS

Regarding the short-circuit-tests, simplifications made from Eq. (2-13) to Eq. (2-14) are examined. They are repeated as Eq. (6-1) and Eq. (6-2). By using the first formula and compare it with the result from the second, it is possible to find if the simplification is acceptable.

$$Z_{sc} = R_1 + jX_{l1} + \frac{Z_\varphi(R_2 + jX_{l2})}{Z_\varphi + R_2 + jX_{l2}} \tag{Eq. (6-1)}$$

$$Z_{sc} \approx R_1 + jX_{l1} + R_2 + jX_{l2} = R_{eq} + jX_{eq} \tag{Eq. (6-2)}$$

Table 6-2: Calculation of short-circuit simplifications

Name	Value		Unit
	Small transformer	Large transformer	
R_1	1.56e-04	1.98e-05	Ω
R_2	3.69e-04	9.21e-05	Ω
$X_{l1} = X_{l2}$	4.60e-05	2.60e-05	Ω
Z_φ	0.494	0.448	Ω
Z_{sc}	5.25e-04+j9.19e-05	1.12e-04+j5.20e-05	Ω
Z_{eq}	5.25e-04+j9.20e-05	1.12e-04+j5.20e-05	Ω

As seen from Table 6-2, the impedance of the exciting branch is much larger than that of the secondary leakage impedance, and the short-circuit impedance approximation is appropriate.

6.3.2 OPEN-CIRCUIT FORMULA SIMPLIFICATIONS

The simplifications for the open-circuit tests are Eq. (2-18) and Eq. (2-19), repeated in Eq. (6-3) and Eq. (6-4).

$$Z_{OC} = R_1 + jX_{l_1} + Z_\phi = R_1 + jX_{l_1} + \frac{R_c \cdot jX_m}{R_c + jX_m} \tag{Eq. (6-3) [9]}$$

$$Z_{OC} \approx Z_\phi = \frac{R_c \cdot jX_m}{R_c + jX_m} \tag{Eq. (6-4) [9]}$$

Table 6-3: Calculation of open-circuit simplifications

Name	Value	Unit	
	Small transformer	Large transformer	
R₁	1.56e-04	1.98e-05	Ω
X_{l1}	4.60e-05	2.60e-05	Ω
Z_φ	0.494	0.448	Ω

By just comparing the values in Table 6-3 to the equations, it is seen that the addition of R₁ and X_{l1} to Z_φ would only change the last-mentioned in the range of a thousand. Therefore, this simplification is also verified as good enough.

6.4 TRANSFORMER ONLY SHORT-CIRCUIT TESTS

6.4.1 EQUIVALENT SERIES RESISTANCE

Table 6-4 summarizes resistances of the primary and secondary winding based on theoretical values, DC-tests, and actual laboratory values. Based on the conductor lengths and cross section areas from Table 4-1, together with the physical properties of copper from Table 8-3 the theoretical part of Table 6-4 is found. The displayed numbers are average values from their respective measurement sets.

Table 6-4: Theoretical, DC-test and laboratory resistance of the two prototype transformers

		R _p [Ω]	R _s [Ω]	R _{eq} [Ω]
Small transformer	Theoretical	1,20E-04	3,78E-04	4,98E-04
	DC-test	1,56E-04	3,69E-04	5,25E-04
	Laboratory			5,65E-04
Large transformer	Theoretical	2,05E-05	8,77E-05	1,08E-04
	DC-test	1,98E-05	9,21E-05	1,12E-04
	Laboratory			1,15E-04

The values of the small transformer differ quite a lot. The equivalent resistance from the DC test is 5.42 % larger than the theoretical and 6.9 % smaller than the laboratory results concluded. On the other hand, all the values from the large transformer are quite similar. Even though the values

differs, it is expected that the laboratory values are largest, followed by DC-test and theoretical calculations. The following sub-chapters reveal some reasons for the values to be different.

6.4.1.1 CONDUCTOR LENGTH

It is difficult to measure the length of conductors since they are bulky. The significance of correct length is though very important at shorter stretches. If the 64 cm short primary conductor were 2 cm longer, the theoretical value would increase by 3 %. Corresponding measurement error could also have been done for the secondary conductors.

6.4.1.2 TRANSITION RESISTANCE

A reason for expecting higher resistance from the DC-tests compared with the theoretical is transition resistance. The terminals of the ohmmeter were connected to the cable shoes meaning that some transition resistance is present. During the transformer measurements, the voltage terminals were also connected to the cable shoes of the small transformer, or the screws concerning the large transformer. Due to the fact that the cable shoes were recently acquired, consisting of copper and were tighten firmly, transition resistance should not be considered main reasons for the measurement differences.

6.4.1.3 SKIN DEPTH

If the conductor radius exceeds the skin depth of copper, other formulas should be used in order to find theoretical resistance which better reflects the practical. Using values from Table 8-3 at 20°C, skin depth of copper is calculated to 9.5 mm, corresponding to an area of 284 mm² massive conductor. This means that the skin effect has only a minor impact on conductors in this laboratory work. Using COMSOL, the 50 Hz resistance of the large transformer's primary winding is 2.07e-5 Ω/m. An analogous DC-test in COMSOL gives a resistance of 2.05e-5 Ω/m. This means that skin depth should not impact the results in a very large degree, especially not for the small transformer. The results are in accordance with chapter 2.3.7, Skin effect in copper windings, since $d \leq 2\delta$.

6.4.1.4 TEMPERATURE DEPENDENCY

Since resistance increases linearly with temperature, it could be that the average conductor temperatures from the laboratory tests are somewhat higher than the DC-test. By studying the resistance measurements from Figure 5-1, it is seen that the resistances change insignificantly as function of applied current. Since the laboratory tests were executed in series, the resistance is also set to be independent of time, for these specific measurements. This means that a temperature increase alone cannot verify the measurement inaccuracies.

6.4.1.5 INSTRUMENT INACCURACY

The apparatus NORMA 5000 is used, and instrument inaccuracy is therefor considered to be small. Since the measurement results are outside the 1-2 % error given in the NORMA 5000 datasheet, other factors are believed to impact in a greater degree.

6.4.1.6 SUMMING-UP

From the previous mentioned reasons, it is difficult to point out one specific reason for larger deviation between the resistance values regarding the small transformer, compared to the large. As skin depth, instrument inaccuracy and temperature dependency are assumed to be minor; other contributors are expected to cause the main deviation. This could be conductor length measurement errors, or induced noise in the voltage probes.

6.4.2 EQUIVALENT SERIES REACTANCE

Since comparable transformer design is not found in available publications, it is difficult to relate the extracted reactance up to something. It is though possible to compare the reactance of the two tested transformers with each other. Table 5-3, repeated in Table 6-5, points out per unit resistance, reactance and impedance in per cent.

Table 6-5: Datasheet of per unit (%) resistance, reactance and impedance

	Subsea	
	Small transformer	Large transformer
e_z [%]	4.55	1.43
e_R [%]	4.53	1.30
e_x [%]	0.44	0.59
X/R ratio	0.10	0.45

As can be seen, per unit resistance is much smaller for the small transformer, compared with the large. In contrast, per unit reactance is somewhat larger. The relatively low per unit resistance for the large transformer is for example due to an oversized primary winding. In addition, the primary winding of both transformers are of equal length, longer than the transformer cores, meaning that the resistances are higher than they ideally should be. Both the relative and absolute additional length is worst for the small transformer as stated in Table 4-1. In addition, it is uncertain if the measured resistance for the small transformer should have been somewhat smaller, due to the deviations seen in Table 6-4.

The discoveries that reactance decrease and resistance increase as a function of transformer size are expected. This can also be seen from "Planleggingsbok for kraftnett" given in Table 13-7, where typical reference values of power transformers are reviled. Due to this, it is possible to say that these

two transformers follow an expected pattern, but the exact reactance values are not possible to verify from this.

6.5 TRANSFORMER ONLY OPEN-CIRCUIT TESTS

6.5.1 MAGNETIC FIELD STRENGTH AND LOSS AS FUNCTION OF MAGNETIC FLUX DENSITY

Vendor has reported that both transformer cores consist of the same grade, PowerCore® 140-30, meaning that the cores should be identical except for their physical dimensions. This means that both active and apparent losses per weight, in addition to the magnetic field strength, should be similar at the same magnetic flux density instant.

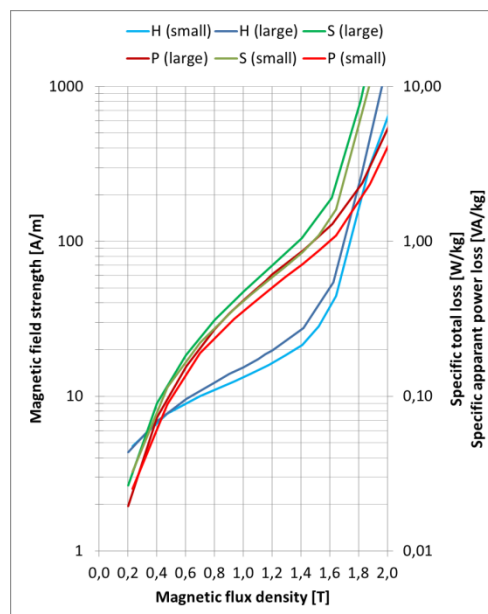


Figure 6-2: Comparison of magnetic field strength [H/m], specific total loss [W/kg] and specific apparent power loss [VA/kg] as function of magnetic flux density [T] of the two transformers

Figure 6-2 compares the two transformers of the mentioned parameters. As can be seen, each function of the two transformers follows a similar trend curve. Unfortunately, the lines do not lie upon each other.

Comparing Figure 6-2 and the manufacturer's datasheet, Figure 6-3 is created. It shows the magnetic field strength, active loss and apparent loss as a function of the magnetic flux density for the iron cores. The hand-drawn lines are from the laboratory tests while the remaining are manufacturer values.

How the manufacturer's transformer core specifications are created is uncertain. It is though assumed that their test results illustrate the iron core solely. This means for example that end effects obtained from this laboratory results are not included in their datasheet.

The very first to look into is that the manufacturer presents the magnetic polarisation J , instead of magnetic flux density B . Since $\hat{J} = \hat{B} - \mu_0 \hat{H} \approx 1.26 \cdot 10^{-6} \hat{H}$, the approximation is quite accurate due to the fact that H is less than 1000 in these specific cases.

Another instance which could also impact the deviations is that the laboratory results include the primary winding resistance, R_1 , and self-inductance, X_{1l} , as core impedance. As a consequence, both the current in and voltage drop across the transformer are different than if these values were excluded from the results. From Table 6-3 it was shown that the magnetization impedance is more than 3000 times larger than both the primary winding resistance and self-inductance at rated applied voltage. At larger applied voltages the primary winding resistance and self-inductance have some greater impact, but still not enough to vary the magnetizing impedance considerably.

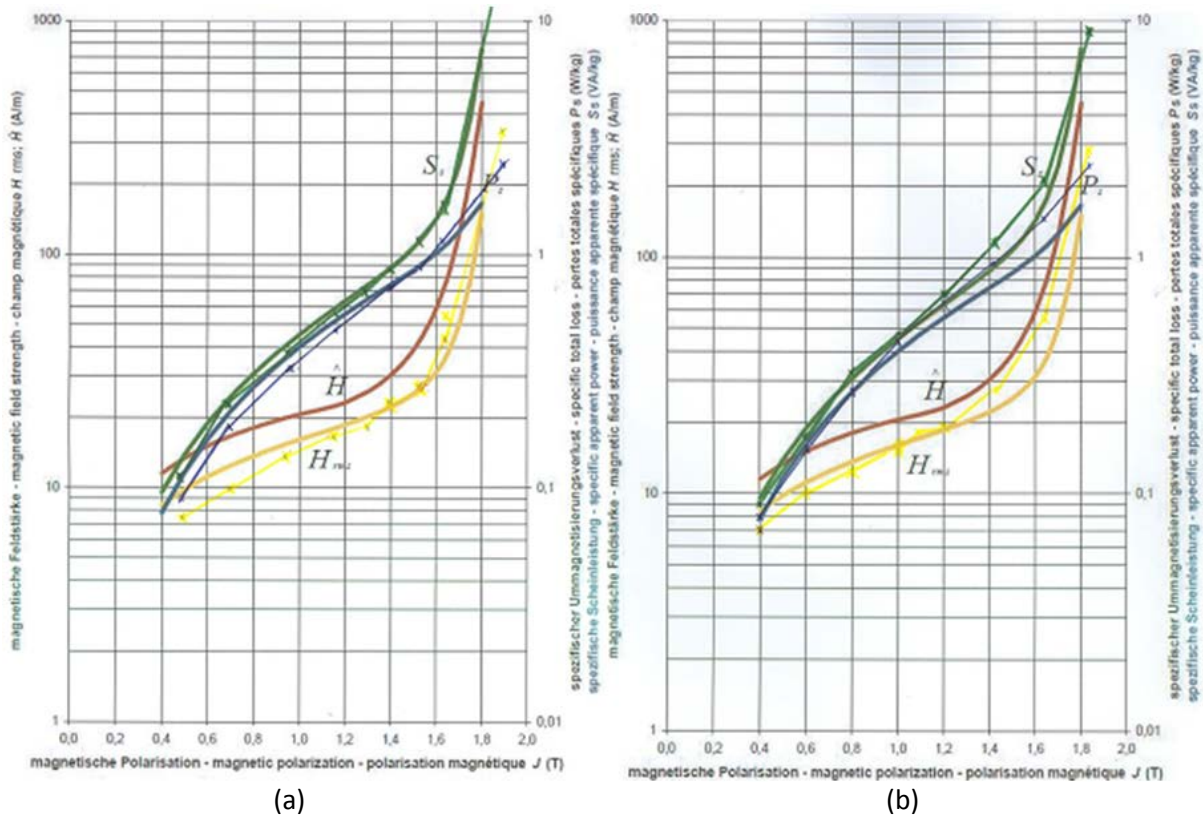


Figure 6-3: Magnetic field strength [H/m], specific total loss [W/kg] and specific apparent power loss [VA/kg] as function of magnetic flux density [T] of (a) small and (b) large transformer. Includes manufacture datasheet.

The densities of the small and large transformers are 7.5kg/dm^3 and 7.3kg/dm^3 , respectively. This indicates that the composition of the iron core materials have a nonlinear weight/volume relationship. A reason for this is probably different stacking factor, even though it is stated from manufacturer’s home page that the specific grain used in both transformers have a stacking factor of 96.5 %. As the transformer densities are different, some deviation of the power loss per weight could be expected. Though, when using equal density of the two transformers in the loss per weight calculations, the graphs are still quite different. In order to achieve equal loss per weight, the density of the large transformer must equal 8.6 kg/dm^3 .

It is still strange that the H-B curves obtained from the laboratory work, for both transformers, differs quite much from the datasheet. A reason for the deviation could be that the magnetic flux does not only occur in the iron core, but also on the outside of it. Another might be that the flux is not evenly distributed. Analytical formulas require both these two arguments to be fulfilled.

Figure 6-4 illustrates an open-circuit model of the small transformer. Figure 6-4b and c show the magnetic flux, $\phi = k \cdot B(r) \cdot r$. Here, a 50 Hz current is applied to the centre conductor with return path in the rightmost. The current is set to 0 for the small conductors inside the iron core. Figure 6-4b and c represents the magnetic flux as a function of radial direction out of origin. The only difference between the graphs is the logarithmic vertical axis of Figure 6-4c.

From Figure 6-4b it looks like all the magnetic flux appear in the iron core, but in reality some magnetic flux is also represented in the areas around, as from Figure 6-4c. This is however an insignificant small value. It is also seen that the magnetic flux is distributed evenly around the iron core. This means that the analytical formulas of both the mean flux path length and cross section area are quite accurate.

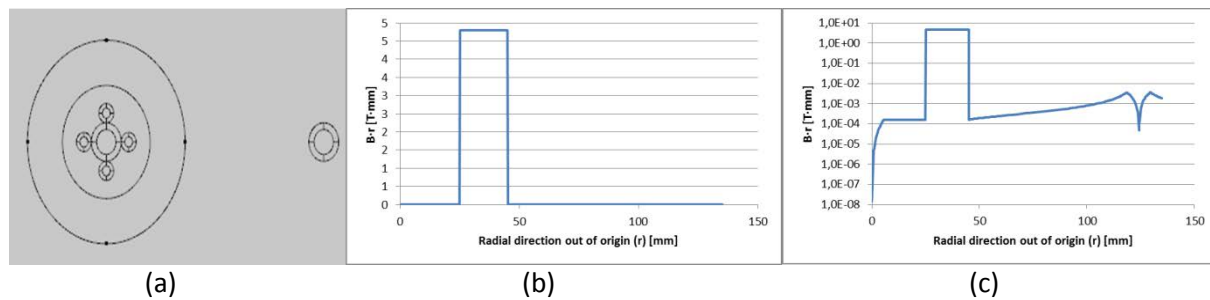


Figure 6-4: Flux density distribution of open-circuit small transformer, 50 Hz of (a) analysed model. (b): Magnetic flux density multiplied with radial direction out from origin, and (c) logarithmic scale.

The previous figure and equation does not take saturation into consideration. When applying higher voltage, the apparent mean flux path changes due to iron core saturation. The mean flux path is given by:

$$l = 2\pi \cdot \frac{r_i + r_y}{2} = \pi(r_i + r_y) \tag{Eq. (6-5)}$$

When increasing r_i with a factor δ due to saturation within this part, the average mean flux path increases; $l = \pi(r_i + \delta + r_y)$. An increased mean flux path leads subsequently to less apparent produced magnetic field strength (H) at constant flux density (B) as $H=i/l$. If this were to be plotted into Figure 6-3, the laboratory results (yellow painted line) would approach the manufacturer's corresponding line at higher flux densities. Regarding of how the manufacturer has created the H-B curve, this could be an explanation of the H-B-curve variation at higher flux densities.

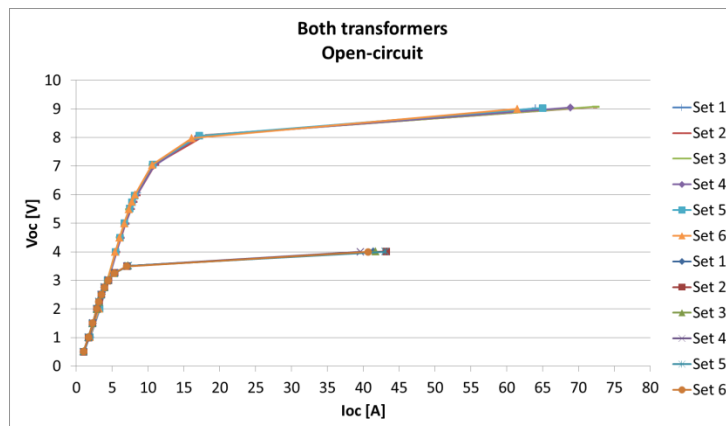


Figure 6-5: Open-circuit voltage as a function of its corresponding current for both transformers

As for the Support Routine CONVERT, which the B-H curve is based on, it is important that there are enough points (V_{rms}, I_{rms}) in order for the linear interpolation to be appropriate. At high applied voltage, there are very few measuring points, as seen from Figure 6-5. This could lead to deviation of the B-H curve, especially in the areas where few measurement points were carried out. If even more were included, the B-H curve could change significant.

In addition to the B-H-curves, the active and apparent power as a function of the magnetic flux density (B) also deviates. As described before, the equipment Fluke 43 has been used. This instrument has problems recording large power values.

6.5.2 IMPACT OF HAVING LONG SECONDARY CONDUCTORS CONNECTED TO THE SECONDARY WINDING DURING OPEN-CIRCUIT TESTS

It is mentioned that the open-circuit measurements are executed when long conductors are connected to the transformer’s secondary winding. If this actually has an extended impact on the measured values, a question mark should be set to the trustworthiness of the open-circuit results. The next paragraphs will try to demonstrate why it should not have any impact.

As from the circuit equivalent in Figure 6-6 it is seen that the secondary winding and appurtenant long conductor should not impact the current path at all since the branch is open-circuited. Even though, eddy currents could be setup due to the fact that there are large magnetic fields around the conductors placed inside the transformer.

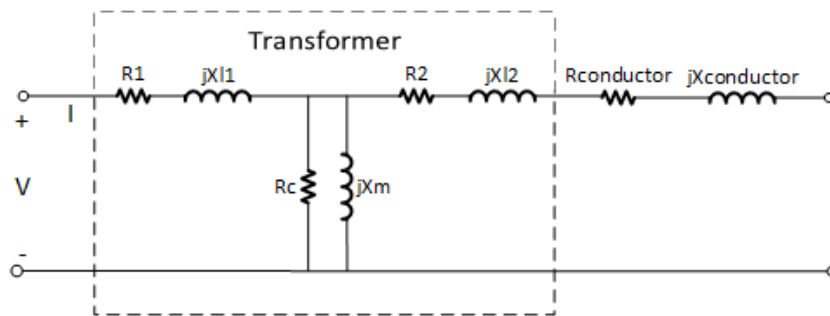


Figure 6-6: Electric open-circuit equivalent

When performing the open-circuit tests, the voltage across the primary terminal was measured. In addition, a voltmeter was connected to the open terminals at the end of the long secondary conductors. The extracted values from one specific measurement set of the large transformer are shown in Table 6-6. From this table it is seen that there is no voltage drop across the secondary side of the transformer.

Table 6-6: Measured primary and secondary voltage of the small transformer

$V_{primary}$	1.00	2.00	3.00	4.00	5.00	6.06	7.00	8.04	9.02	10.12
$V_{secondary}$	0.999	1.995	2.997	3.999	5.004	6.08	6.99	8.04	9.01	10.12

6.6 SHORT-CIRCUIT TESTS WHEN LONG CONDUCTOR ARE CONNECTED TO THE TRANSFORMERS' SECONDARY WINDING

6.6.1 INTRODUCTION

From the short-circuit results regarding the long conductor connected to the transformers' secondary winding, it was seen that the system reactance increased from no-loop to half-loop and half-loop to full-loop. In addition, the resistance increased during the corresponding measurements. The objective of this chapter is to see if these results can be connected with theory and COMSOL-simulations.

6.6.2 SERIES REACTANCE DEVIATION

Figure 5-11 contains the produced reactances of the small and large transformer, at no-loop, half-loop and full-loop. From what can be seen, the deviation of each measurement set is much larger for the small transformer compared with the large transformer. These deviations are probably caused due to difference in the measuring sequence of the two transformers.

Regarding the small transformer, a no-loop test was executed followed by the half-loop and finally the full-loop test. Next, this sequence was repeated. Since it is difficult to reproduce the conductors at the exact same spots, deviations of the similar measurement sets are expected. For the large transformer, the measurement tests were performed twice at each conductor location before rearranging. This leads to a smaller expected deviation of the results.

6.6.3 SERIES RESISTANCE DEVIATION

Figure 5-12 shows the series resistance as a function of applied current. As for both transformers, the resistance increases as applied current is increased. Due to the fact that resistive losses produce heat, leading to higher temperatures and accordingly larger resistance, a temperature increase could explain some of the resistance deviations. To summarize the results part, the highest measured resistance were 7.5 % and 21.8 % larger compared to the lowest values for the small and large transformer, respectively.

Since the tests are executed in series, the conductor temperatures are likely to increase. No thermometer was used, so the exact temperature of the conductors is not able to reproduce. During the tests, it was though possible to touch the conductor surfaces at terminations. When touching these areas, no unusual hot temperatures were noticed. Still, the temperature could have increased to for example 35 °C without special notice. Using values and formulas from Table 8-3 and Table 8-4, the following resistance increase could be expected:

$$\frac{R_{18^{\circ}\text{C}}}{R_{30^{\circ}\text{C}}} = \frac{1+0.004(35-20)}{1+0.004(18-20)} = 6.9\% \quad \text{Eq. (6-6) [9]}$$

This could explain the resistance increase of the small transformer, but not the large.

From the *transformer-only* short-circuit tests (Figure 5-1), executed with the best power analyse tool, the temperature increase was almost insignificant. A larger temperature increase could though be expected for the transformer-only tests, as a larger share of the conductors were placed together inside the transformer.

Based on this, it is assumed that a temperature increase is not the most decisive reason for the resistance increase. It has though most likely some impact, since the tests of the long secondary took longer time than the transformer-only, due to the different power quality analyser tools.

6.6.4 ANALYTICAL AND NUMERICAL ANALYSES OF THE SERIES REACTANCE AND RESISTANCE DEVIATION

In this sub-chapter, both numerical and COMSOL-simulations are carried out to find answers to how the long secondary conductor influences the system impedance. More specific, the strange resistance increase is looked into, in addition to the reactance increase; are the values as expected, or out of proportions?

In general, the conductor system consists of two four-conductor pairs which are placed closely (no-loop) and with a certain distance between them (full-loop). A no-loop configuration is seen in Figure 6-7a, and its two-conductor simplification in Figure 6-7b. A full-loop condition inside a laboratory workspace equivalent is illustrated in Figure 6-7c.

6.6.4.1 ANALYTICAL CALCULATIONS

The analytical theory is based upon Carson’s formulas from chapter 2.7. For simplicity reasons, the calculated reactances are based upon two equivalent single conductors as seen in Figure 6-7b. From Eq. (2-47), repeated in Eq. (6-7), the reactance of a single-phase loop with circular conductors is found:

$$X_{eq} = 2js\mu f \ln\left(\frac{D}{0.78r}\right) \tag{Eq. (6-7)}$$

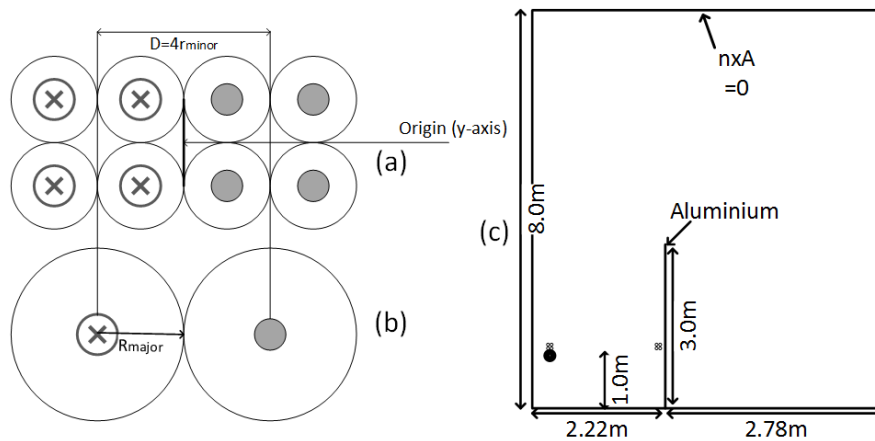


Figure 6-7: (a) Two four-conductors and (b) two equivalent single-conductors. (c): Simple sketch of laboratory workspace at full-loop

6.6.4.2 THE COMSOL-MODELS

Three COMSOL-models were created. The very first is similar to the analytical, in the way that it only consists of two single solid conductors, seen as Figure 6-8a. It is executed in order to make the models more trustworthy by comparing it with the analytical calculations. Secondly, a COMSOL-model of the two four-conductor pairs is created; see Figure 6-8b. Both these models are surrounded by air only, having a radius of 20 meters around origin. At the boundaries, $n \times A = 0$.

The third and last model consists of two four-conductor pairs inside the laboratory workspace illustrated in Figure 6-8c. A thin aluminium partition separates the workspace from the areas around. Note that an additional conductor is placed below the left four-conductor bundle. This conductor is from a former experiment which was not removed. The conductor has no purpose, but it might impact the results. The current is set to be 0 for this conductor and the aluminium wall.

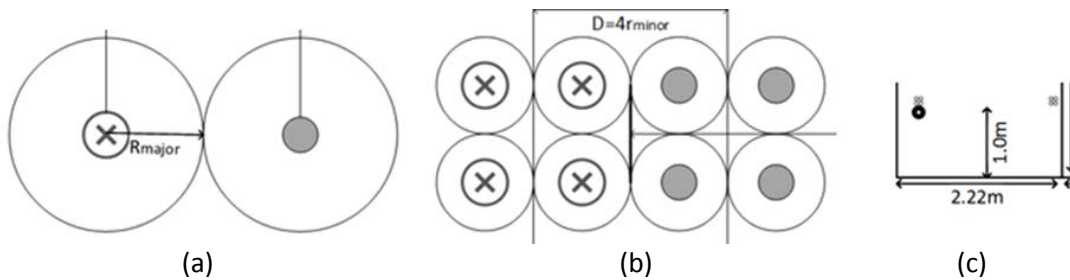


Figure 6-8: The three models simulated in COMSOL. (a): Two single conductors. (b): Two four-conductor pair. (c): Laboratory work approach.

6.6.4.3 PHYSICAL DIMENSIONS AND MATERIAL PROPERTIES OF THE ANALYTICAL AND NUMERICAL MODELS

All parameters used, except aluminium, are found in Table 8-3, at a constant temperature of 20 °C. The aluminium’s relative permeability and permittivity are set to 1, while its electrical conductivity is 3.774e7 S/m. Insulation is only used around conductors for the COMSOL-model representing the laboratory work, i.e. Figure 6-8c.

Table 6-7 reveals the physical dimensions of the conductors, together with the centre-to-centre distance, D , between the conductors at no-loop and full-loop conduction.

Table 6-7: Values of outer dimensions used in the COMSOL simulations and analytical calculations for long secondary winding

Description	Unit	Small transformer	Large transformer
A_{minor}	[mm ²]	16	70
r_{minor}	[mm]	2.2568	4.7203
$D_{no-loop}$	[mm]	9.027	18.88
$D_{full-loop}$	[mm]	1900	1900
R_{major}	[mm]	4.5135	9.4407

6.6.4.4 RESULTS FROM THE ANALYTICAL CALCULATION AND NUMERICAL MODELS

All results from the analytical calculation and numerical models are presented in Table 6-8. Regarding the laboratory results, the resistance and reactance from the transformer-only short-circuit tests are subtracted from their corresponding values found in the long secondary short-circuit test. This means

that the long secondary conductor is analysed solely. Note that the impedance is denoted in milliohms per meter, where “per meter” is pipeline length. Since each conductor bundle is of the same length as the pipeline length, the total conductor length is twice the pipeline length.

Table 6-8: Results of analytical calculations, COMSOL-simulations and measured reactance and resistance of long conductor connected to secondary winding

Large transformer					
	Analytical	COMSOL 2 conductors	COMSOL 8 conductors	COMSOL Laboratory approach	Laboratory values
$Z_{no-loop}$ [mΩ/m]	0.123+j0.118	0.137+j0.116	0.132+j0.106	0.130+j0.115	0.137+j0.178
$Z_{full-loop}$ [mΩ/m]	0.123+j0.698	0.130+j0.697	0.129+j0.685	0.184+0.421	0.163+j0.694

Small transformer					
	Analytical	COMSOL 2 conductors	COMSOL 8 conductors	COMSOL Laboratory approach	Laboratory values
$Z_{no-loop}$ [mΩ/m]	0.556+j0.118	0.559+j0.118	0.557+j0.107	0.556+0.123	0.575+j0.165
$Z_{full-loop}$ [mΩ/m]	0.556+j0.791	0.557+j0.790	0.557+j0.778	0.610+j0.495	0.606+j0.575

The first which can be considered is that the impedances of both no-loop and full-loop are found to be similar for the analytical model, and both simplified COMSOL-simulations. In addition, the no-loop resistance is found to be lower than the full-loop resistance. This is due to higher proximity effect when the conductors are placed adjacent to each other. Figure 6-9 shows the flux density of no-loop and full-loop condition.

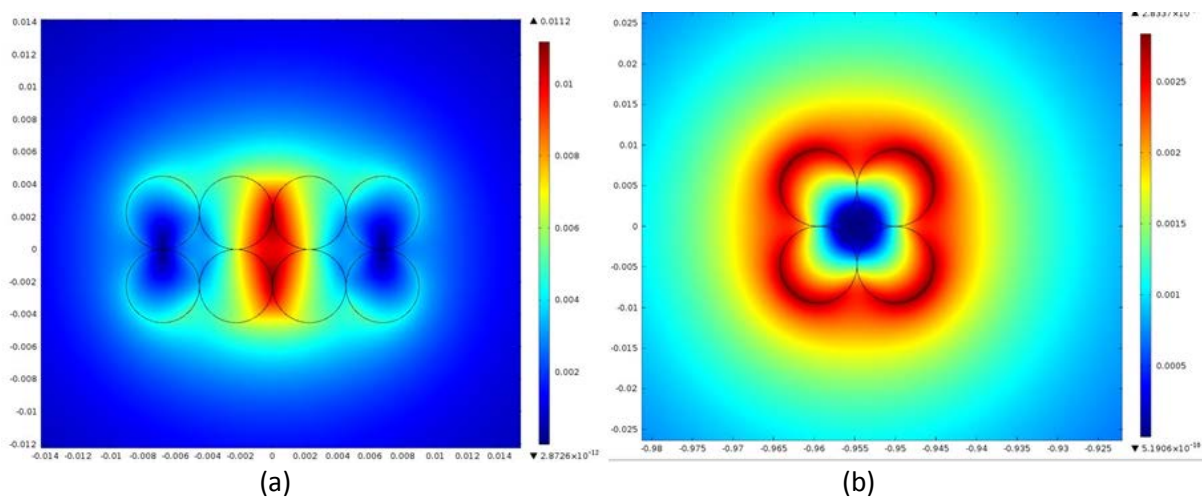


Figure 6-9: B-field of (a) no-loop condition and (b) full-loop condition of one four-conductor bundle

An interesting observation for the COMSOL laboratory approach is that the resistance *increases* as the conductor pairs are separated. This stands in contrast to the two first COMSOL-simulations. Two large differences between those simulations and the laboratory approach are the aluminium wall on one side and the large superfluous conductor on the other side. A graph representing the magnetic vector potential of the laboratory approach is attached in Figure 6-10. From this figure it is also possible to see that the aluminium plate and large conductor affects the magnetic field.

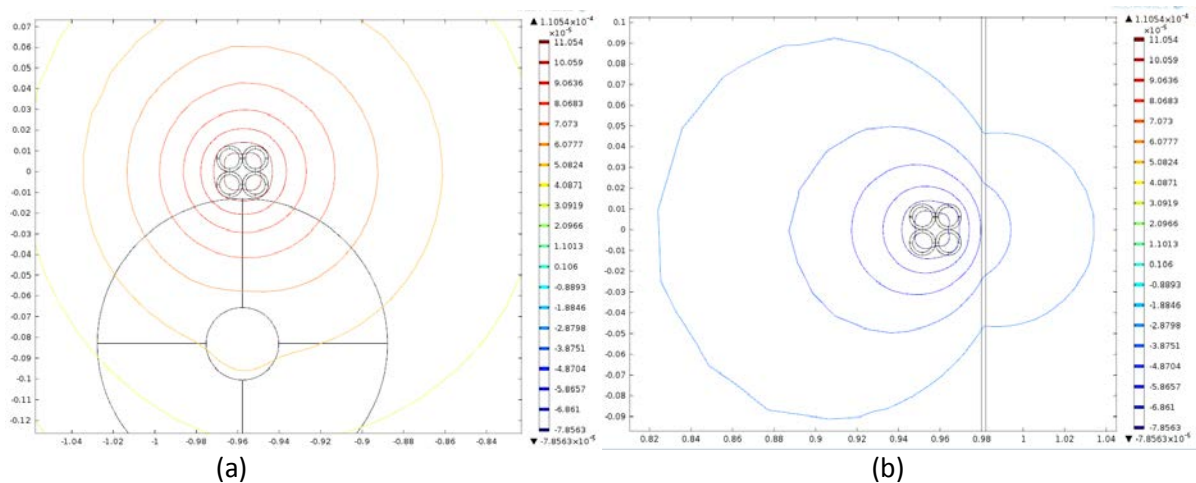


Figure 6-10: Magnetic vector potential contour of the COMSOL-simulation "laboratory work approach"

Since currents are induced to these surroundings, a larger resistance is expected for the full-loop case compared to the no-loop case. This could therefore explain why the resistance is noticeable higher in the full-loop measurements compared to the no-loop, from Figure 5-12. This does however not explain why the resistance increases as a function of applied current, which most probably is due to instrument inaccuracy.

7 ADDENDUM I: NUMERICAL AND ANALYTICAL APPROACH OF SERIES REACTANCE CALCULATIONS

By creating numerical and/or analytical equivalents, it is possible to perform rough series-reactance calculations of equivalent transformers without manufacturing them. Two simplified models are therefore created, one analytical and one numerical. The intention is to find out if it is possible, by help of some simplifications, to make reliable models of this transformer type. From the theory chapter 2.7 it was shown that the equivalent series reactance is given by the following equation:

$$X_{sc} = \frac{2W_{mag}}{I_{sc}^2} \cdot \omega \quad \text{Eq. (7-1)}$$

W_{mag} is the magnetic energy produced in the models. When energy is presented in upcoming tables, a current of one ampere is applied to the conductors.

7.1 ELUCIDATION

To start with, the small and large transformers were modelled as pictured in Figure 7-1. Here, the centre conductor(s) inside the iron core represents the piggy-back cable. The identical conductor(s) outside the transformer represents the piggy-back return path. The remaining eight conductors denote the secondary winding, wherein the outer four carries a total current of the same magnitude and direction as the piggy-back. The four inner conductors are opposite directed.

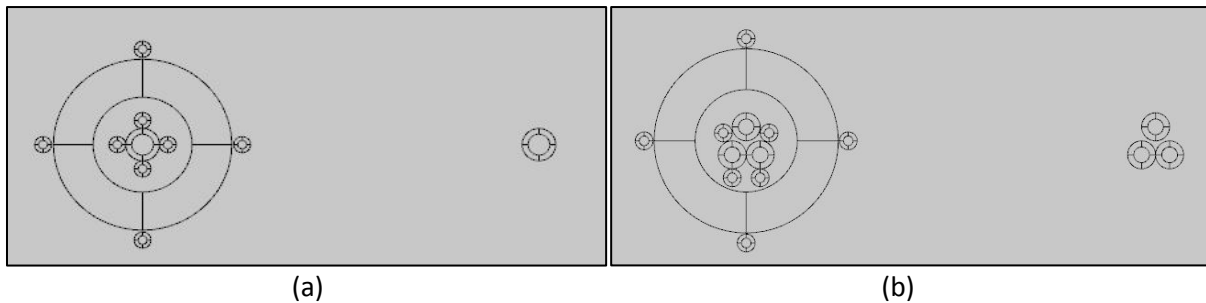


Figure 7-1: 2D-model of the small (a) and large (b) transformers

The largest problem of this approach is to decide a centre-to-centre distance between the piggy-back conductor and its corresponding return path. From simulations, it found that the distance has a major impact on the results. In addition, the boundary size around the transformer model influences greatly when modelling the return path.

Due to these considerations it is decided to simulate the conductors lying inside the iron core solely. The energies presented in upcoming tables do therefore only include energy concentrations from the iron cores, and everything inside. A circle consisting of air is set as boundary, satisfying the equation $nxA = 0$.

Most of the physical dimensions and material specific properties are as stated in Table 3-3, Table 4-1, and Table 8-3. The relative permeability, μ_r , of the iron core is set to 30.000 regarding the numerical calculations. The electrical conductivity is set to zero for both the iron core and air. All materials are assumed to be temperature independent.

7.2 NUMERICAL MODEL

The numerical equivalent transformer models are found as Figure 7-2. They are built similar to the laboratory tested prototypes. The insulation thicknesses outside the copper conductors are two and three mm for the primary and secondary windings, respectively, for the small transformer. The equivalent values of the large transformer are three and five mm.

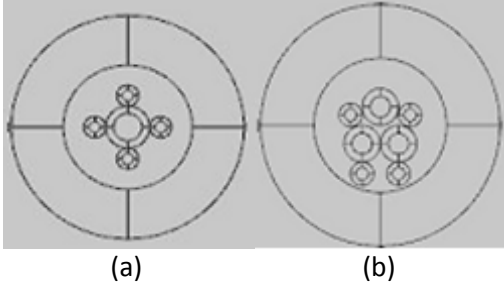


Figure 7-2: The actual simulated small (a) and large (b) transformers

Images of the magnetic vector potential of the two transformers are found in Figure 13-13 and Figure 13-14. The magnetic potential tells a lot about the models. When the conductors are placed uniformly, as for the small transformer, the leakage flux is smaller compared to the inconsistency large transformer. If six or eight secondary conductors were placed around the piggy-back cable, an even greater reduction in the leakage flux would be seen.

7.3 ANALYTIC MODEL

7.3.1 INTRODUCTION

Figure 7-3a shows the analytic model which is to be analysed. As stated, only magnetic energy produced inside (and including) the iron core is used further in this text. Still, equations for energy and magnetic flux strength as a function of the radial direction out from origin are developed for the entire figure.

Regarding the large transformer, one equivalent piggy-back cable is used. Its cross section area equals the sum of the original three. In addition, the secondary windings are placed uniformly around the piggy-back conductor as indicated in Figure 7-3b. A MATLAB-script calculating the energy and plotting magnetic field strength is attached as MATLAB 1.

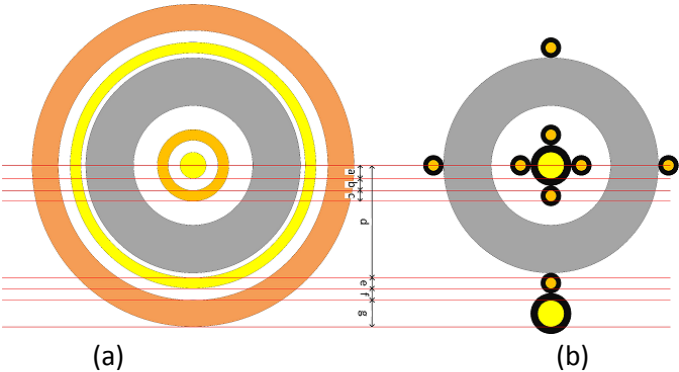


Figure 7-3: Concentric winding approach

7.3.2 FORMULAS – MAGNETIC FIELD STRENGTH AND MAGNETIC ENERGY AS FUNCTION OF RADIUS

The formulas representing the magnetic field strength [H/m] and magnetic stored energy [J/m] are found as Eq. (7-2) to Eq. (7-5). The formulas are developed in the appendix. They are all based on Figure 7-3a and the notation from Figure 7-4.

$$H(r) = \begin{cases} \begin{cases} I \cdot \frac{r}{2\pi a^2}, & r \in \langle 0, a \rangle \\ I \cdot \frac{1}{2\pi r}, & r \in \langle a, a + b \rangle \\ I \cdot \frac{(a + b + c - r)}{2\pi(a + b)c}, & r \in \langle a + b, a + b + c \rangle \end{cases} \\ \begin{cases} I \cdot \frac{r^2 - d^2}{2\pi r \cdot e(2d + e)}, & r \in \langle d, d + e \rangle \\ I \cdot \frac{1}{2\pi r}, & r \in \langle d + e, d + e + f \rangle \\ I \cdot \frac{(d + e + f + g - r)}{2\pi(d + e + f)g}, & r \in \langle d + e + f, d + e + f + g \rangle \end{cases} \end{cases} \quad \text{Eq. (7-2)}$$

$$W_{magnetic}(r) \begin{cases} \begin{cases} W_a, & r \in \langle 0, a \rangle \\ W_b, & r \in \langle a, a + b \rangle \\ W_c, & r \in \langle a + b, a + b + c \rangle \end{cases} \\ \begin{cases} W_e, & r \in \langle d, d + e \rangle \\ W_f, & r \in \langle d + e, d + e + f \rangle \\ W_g, & r \in \langle d + e + f, d + e + f + g \rangle \end{cases} \end{cases} \quad \text{Eq. (7-3)}$$

$$\begin{aligned} W_a &= \frac{\mu_0}{16\pi} I^2 \\ W_b &= \frac{1}{4\pi} \mu_0 I^2 \ln\left(\frac{a + b}{a}\right) \\ W_c &= \frac{1}{48\pi} \mu_0 I^2 \cdot \frac{c(c + 4(a + b))}{(a + b)^2} \\ W_e &= \mu_0 I^2 \frac{(2d^2 e^2 + 4de^3 + e^4 + 4d^4 \cdot \ln(d + e) - 4d^3(d \cdot \ln(d) + e))}{16\pi \cdot e^2(2d + e)^2} \\ W_f &= \frac{1}{4\pi} \mu_0 I^2 \cdot \ln\left(\frac{d + e + f}{d + e}\right) \\ W_g &= \frac{1}{48\pi} \mu_0 I^2 \cdot \frac{g(g + 4(d + e + f))}{(d + e + f)^2} \end{aligned} \quad \text{Eq. (7-4)}$$

$$W_{tot} = W_a + W_b + W_c + W_e + W_f + W_g \quad \text{Eq. (7-5)}$$

7.3.3 NOTATIONS AND CREDIBILITY

Figure 7-4 shows the magnetic field strength as a function of radial distance from origin, for the large transformer equivalent. W_a, W_b, \dots, W_f represent the produced energy in each segments stated in Figure 7-3a.

The analytical formulas are created assuming short-circuit operation and all magnetic materials to be saturated. Therefore, the material properties of the iron core equal the surrounding air [15].

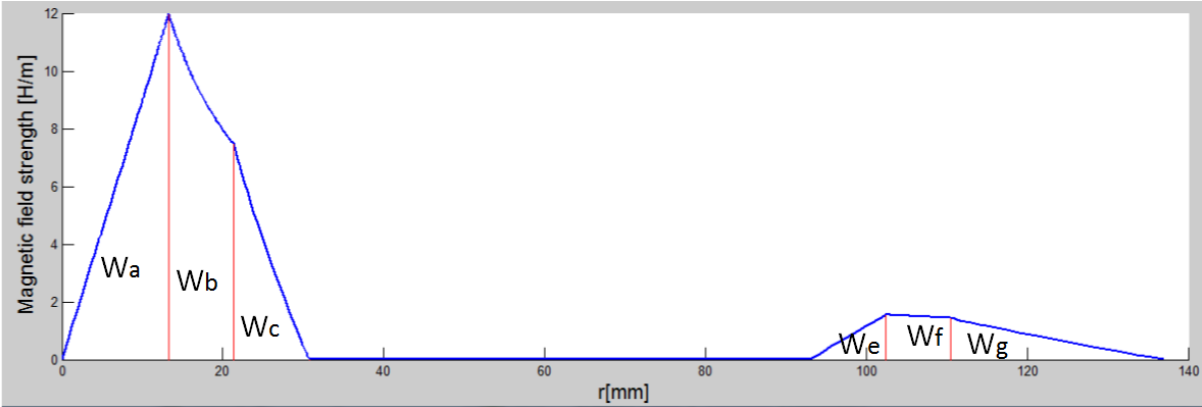


Figure 7-4: Magnetic field strength as a function of radius. The magnetic energy notation is included

Figure 7-5 illustrates the magnetic field strength as a function of radius for both a COMSOL-model representing Figure 7-3a, and the formulas developed from Eq. (7-2). As can be seen, the functions are identical, except for the segments c and g. To simplify the analytical formulas, it is assumed that the magnetic field strength decreases linearly in these sections. As can be seen, the simplification is quite good.

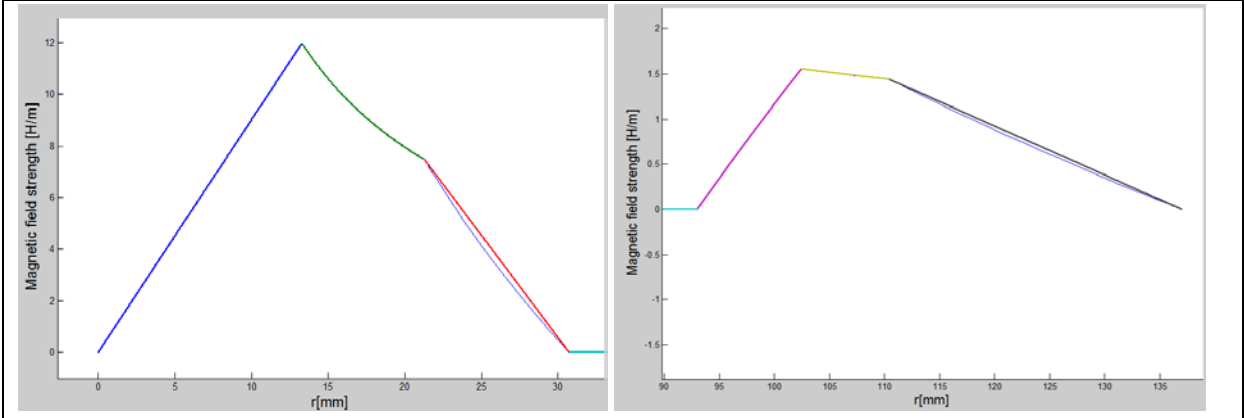


Figure 7-5: Magnetic field strength as a function of transformer radius.

Table 7-1 represents the stored energy for each segment based on the developed formulas and COMSOL-simulation of Figure 7-3a. As can be seen, the analytical formulas are trustworthy, and the linearization is a good approximation. In addition, W_a is verified in [16].

Table 7-1: Results from analytical and COMSOL-analysis of Figure 7-3a

	Small transformer		Large transformer	
	Analytical	Corresponding COMSOL-model	Analytical	Corresponding COMSOL-model
W_a [J/m]	2.500e-08	2.500e-08	2.500e-08	2.500e-08
W_b [J/m]	6.467e-08	6.467e-08	4.712e-08	4.712e-08
W_c [J/m]	1.587e-08	1.413e-08	1.642e-08	1.457e-08
W_e [J/m]	2.918e-09	2.918e-09	3.069e-09	3.069e-09
W_f [J/m]	9.264e-09	9.264e-09	7.519e-09	7.519e-09
W_g [J/m]	6.803e-09	6.460e-09	8.506e-09	7.984e-09
W_{tot} [J/m]	1.245e-07	1.225e-07	1.076e-07	1.053e-07

7.4 RESULTS FROM THE NUMERICAL AND ANALYTICAL MODELS

Table 7-2 summarizes the total magnetic energy produced in the iron core, conductors and the air between them for the analytical and numerical models. From the produced magnetic energy, the equivalent series reactances are found. Results from the laboratory work are also included in the table.

Table 7-2: Equivalent series reactance from analytical and numerical models together with laboratory work results

		$W_{magnetic}$ [J/m]	X_{eq} [Ω /m]	$X_{eq length}$ [Ω]
Small transformer	Analytical	1.055e-07	6.631e-05	3.183e-05
	Numerical	1.240e-07	7.793e-05	3.741e-05
	Laboratory			9.2e-05
Large transformer	Analytical	8.854e-08	5.563e-05	3.115e-05
	Numerical	8.392e-08	5.273e-05	2.953e-05
	Laboratory			5.2E-05

The laboratory results are 2.9 times greater than the analytical, regarding the small transformer, while the equivalent large transformer value is 1.7. This means that the simplifications are quite rough. Fortunately, all calculated reactances from the numerical and analytical models are smaller than the laboratory values. This means that the calculated values represent a *minimum* total series reactance which can be used in circuit analysis.

As seen, the analytical values are *smaller* than the numerical values by 15 % of the small transformer, while it is 5.5 % *larger* regarding the large transformer. An explanation of this could be that the approximation of the large transformer is more simplified compared with the small. From Figure 13-13 and Figure 13-14, significant differences are noted when plotting magnetic vector potential images.

By creating a COMSOL-model when the large transformer equals Figure 7-3b, W_{mag} becomes 1.06e-07. The analytical value is now 17 % smaller than the numerical values, and is in accordance with what was found from the small transformer.

8 ADDENDUM II: A FULL-SCALE MODEL

8.1 INTRODUCTION

In order to design and manufacture a full-scale transformer, required voltage drop across the t-off must be calculated. The total system is seen in Figure 8-1. A 14 inch main pipeline of arbitrary length is buried half way into the seabed and is heated with DEH. At a certain distance between the near- and rear end of the main pipeline, an eight inch pipeline is connected. This minor pipeline is to be heated either using DEH or IH.

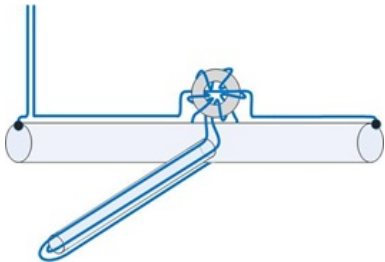


Figure 8-1: Sketch of a main pipeline heated using DEH, and a t-off heated by induction heating

The three different COMSOL-simulations executed are seen in Figure 8-2. Figure 8-2a shows a 14 inch pipeline buried half-way into the seabed. Figure 8-2b and c represent an eight inch pipeline heated with a two-paired conductor system and DEH, respectively. The colour codes are recapitulated in Table 8-1.

Table 8-1: Colour code for the DEH-models

Colour	Dark blue	Brown	Yellow	Red	Purple	Grey	Light blue
Description	Seawater	Seabed	Electric conductor	Conductor insulation	Pipeline insulation	Carbon steel	Pipeline content

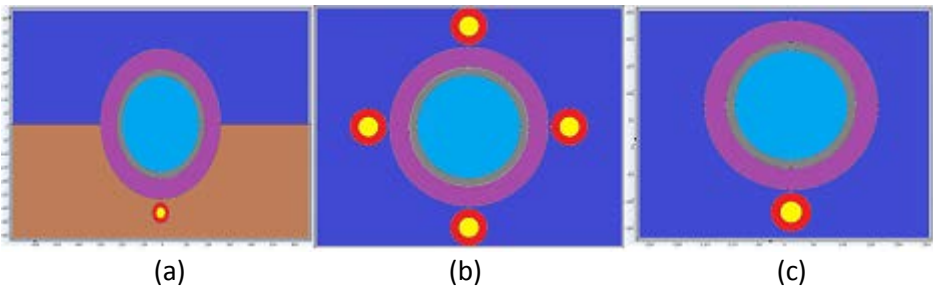


Figure 8-2: COMSOL model of a 14 inch pipeline headed by DEH (a), 8 inch pipeline, IH (b) and 8 inch pipeline, DEH (c)

The system is exposed to highest stress during heat-up period; heating the pipeline from 5°C to 25°C within 72 hours. Accordingly, required current and appurtenant voltage drop applicable to that operation state have to be found.

Model assumptions like water radius, temperature boundaries and mesh are as described in the project work.

8.2 PHYSICAL DIMENSIONS OF PIPELINES AND APPURTENANT ELECTRICAL CONDUCTORS

From Table 8-2, visualised in Figure 8-3, the physical dimensions of the analysed configurations are stated. ID represents the inner diameter of the pipeline. The Δ relates to the thickness, in radial direction, of the materials.

The steel is, as seen, divided into two pieces with identical electrical and thermal values. This separation has no practical utility value, except from simplifying the meshing.

Table 8-2: Physical dimensions of the 8 inch and 14 inch pipeline

Name	Unit	Values for 14 inch pipeline	Values for 8 inch
ID ⁽¹⁾	[inch]/[mm]	14/355.6	8/203.2
A _{copper}	[mm ²]	1500	1200
Δ _{steel}	[mm]	25	15.7
Δ _{steel2}	[mm]	2	2
Δ _{pipe isolation}	[mm]	75	39
D _{copper} ⁽²⁾	[mm]	43.7	35.7
D _{cable insulation}	[mm]	79.7	72.3
gap	[mm]	10	5

The gap is the distance between the outer pipeline insulation and conductor insulation. The ultimate is to minimize this distance in order to maximize the magnetic field density from the conductor. This is especially important in the case of induction heating since the heat is generated due to induced losses. It is though not possible to eliminate the gap because of different flexibility properties of the pipeline and conductor.

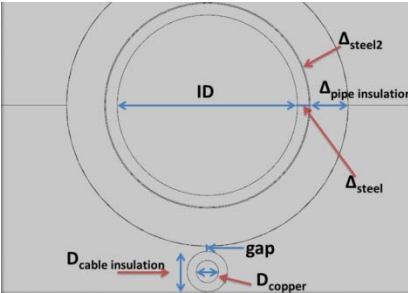


Figure 8-3: Structure of the model. Values are listed in Table 8-2

¹ 1 inch = 25.4 mm
² $D_{copper} = 2 \cdot \sqrt{A_{copper}/\pi}$

8.3 ELECTRICAL AND THERMAL MATERIAL VALUES

From Table 8-3 and Table 8-4, electrical and thermal parameters of the COMSOL-models are found. All values are considered constant, except the electrical conductivity of copper and steel which *decreases* as temperature rises.

Table 8-3: Electrical and thermal material parameters

Name	Electrical conductivity $\left[\frac{S}{m}\right]$	Relative permittivity [1]	Relative permeability [1]	Thermal conductivity $\left[\frac{W}{m \cdot K}\right]$	Heat Capacity $\left[\frac{J}{kg \cdot K}\right]$	Density $\left[\frac{kg}{m^3}\right]$
Copper	$\frac{5.62 \cdot 10^7}{1 + \alpha_{copper}(T - T_{20^\circ C})}$	1	1	385	0.353e7	1
Conductor insulation (XLPE)	0	2.3	1	0.286	0.189e7	1
Carbon steel	$\frac{4.61 \cdot 10^6}{1 + \alpha_{steel}(T - T_0 \text{ } ^\circ C)}$	1	400	50	0.353e7	1
Pipeline content	3.3	30	1	10	0.419e7	1
Pipeline Insulation (PP)	0	2.2	1	0.14	0.106e7	1
Sea Water	3.35 ³	80	1	0.57 ³	0.399e7 ³	1
Seabed	1	1	1	1.3	0.30e7	1

Table 8-4: Constants from the material parameters

Name	Value	Reference
α_{copper}	0.004	[17]
α_{steel}	0.003	
$T_{0^\circ C}$ [K]	277.15	
$T_{20^\circ C}$ [K]	297.15	

³ Linear interpolation from http://www.kayelaby.npl.co.uk/general_physics/2_7/2_7_9.html

8.4 ELECTRICAL AND THERMAL CALCULATIONS OF A T-OFF SYSTEM

Table 8-5 states required applied current in order to achieve 25°C in every part of the pipeline content, 72 hours subsequent to start-up. If the minor pipeline is to be heated by DEH, applied system current must be 1152 A. On the other hand, 1199 A is required when applying IH to heat the corresponding t-off.

Table 8-5: Required applied current to achieve 25°C in the pipeline content

	Main pipeline		T-off
	DEH	DEH	IH (Two conductor pairs)
$I_{0, rms}$ [A]	1152	1008	1199
$T_{pipeline\ content} _{t=72hours}$ [°C]	25.0	25.0	25.0
Q_{steel} [W/m]		63.3	62.4

Table 8-6 contains an overview of required applied current and corresponding system impedances of the t-offs, in order to heat them as described in previous paragraph. Note that the “per meter” notation refers to pipeline length.

Table 8-6: Overview of applied current and corresponding system impedances of the t-offs

Parameter	Unit	T-off: DEH		T-off: IH	
		Main pipeline	T-off	Main pipeline	T-off
$I_{0, rms}$ each conductor	A	1152	1152	1199	2398
$T _{t=72hours}$	°C	25.0	31.2	26.7	25.0
$Z_{system} _{t=0h}$	[Ω/m]	(7.8e-5+2.3e-4i)	9.23e-5+3.18e-4i	(7.8e-5+3.0e-4)	3.02e-5+2.33e-4i
$Z_{system} _{t=72h}$	[Ω/m]	(7.9e-5+3.0e-4)	9.30e-5+3.20e-4i	(9.9e-5+3.0e-4)	3.02e-5+2.33e-4i
$ Z_{system} _{t=72h} $	[Ω/m]		3.33e-4∠73.8°		2.349-4∠82.6°
V_{t-off}	[V/m]		0.384∠73.8°		0.563∠82.6°

A total current of 2398 A is required when heating the t-off using IH. This current is found assuming two parallel conductor pair to heat the t-off, each carrying a current of 1199 A. This is illustrated in Figure 8-5. Another graphical explanation of the IH system is attached in Figure 13-15.

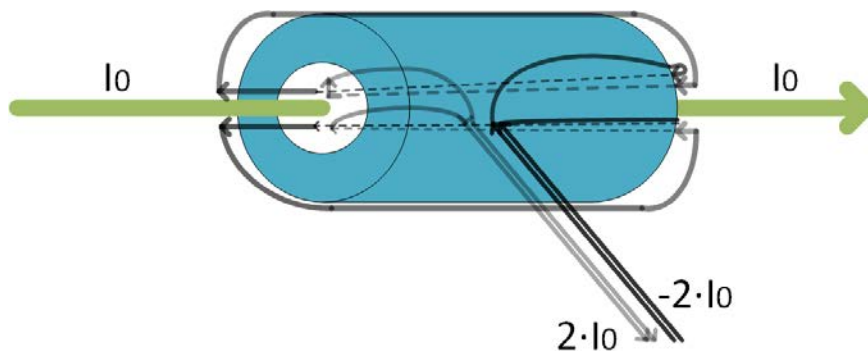


Figure 8-4: A parallel couplet two-pair secondary winding, each with two turns

8.5 PHYSICAL DIMENSIONS OF A FULL-SCALE TRANSFORMER

This sub-chapter uses the previous calculations to find required voltage and transformer dimensions to heat a 500 meter long pipeline. The cross section area is calculated assuming an average flux density peak of 1.6 T in the iron core.

As the mean flux path length is required in order to calculate the transformer dimensions, an inner transformer radius must be estimated. For the following calculations it is assumed that both the piggy-back cable and each of the secondary winding(s) have a cross section area of 1200 mm², representing a total conductor diameter (ID) of 72.3 mm. This is collected from Table 8-2.

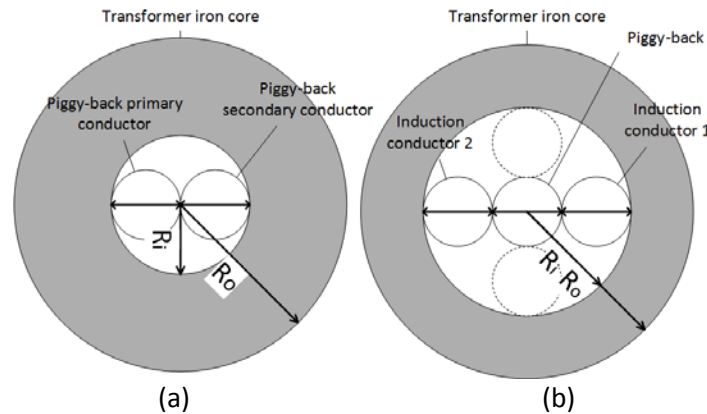


Figure 8-5: Transformer inside, where (a) is T-off heated using DEH and (b) T-off heated using IH

Figure 8-5 represents the minimum inner dimensions of the transformers where conductors including their insulation are drawn. The left transformer equivalent is used when heating the t-off using DEH, while the right represents an IH system. Theoretical minimum inner radius is therefore given by:

$$R_{i_{IH}} = ID \tag{Eq. (8-1)}$$

$$R_{i_{DEH}} = \frac{3}{2} \cdot ID \tag{Eq. (8-2)}$$

Required voltage, cross sectional area and minimum inner transformer core radius are given in Table 8-2. As can be seen, 50 % more voltage is needed in order to heat the jumper using IH.

Table 8-7: Required voltage, cross section area and inner transformer core radius

Description	T-off: DEH	T-off: IH
V _s [V]	192.0V∠73.8°	281.7V∠82.6°
A [m ²]	0.540	0.793
R _{i, minimum} [m]	0.0723	0.1085

Given the transformers' cross sectional area and inner radius, the outer iron core radius as a function of length is given by the following equation:

$$R_o = R_i + \frac{A}{l} \tag{Eq. (8-3)}$$

Table 8-8: Transformer dimensions of the different heating methods

T-off	Dimension	Length				
		1	2	3	4	5
DEH	R_o [m]	0.61	0.34	0.25	0.21	0.18
	V [m ³]	1.16	0.70	0.55	0.47	0.43
IH	R_o [m]	0.90	0.50	0.37	0.31	0.27
	V [m ³]	2.51	1.53	1.22	1.03	0.93

The first which can be seen from Table 8-8 is that the physical dimensions of the transformer are feasible. A two metre long transformer with an outer diameter of 68 cm could heat up a DEH-type t-off. Regarding an IH-type, a two metre long transformer gives an outer diameter of 100 cm, while a three metre long only requires a 74 cm outer diameter.

8.6 ELECTRICAL PARAMETERS AND PHYSICAL DIMENSIONS OF A DEFINED FULL-SCALE MODEL

In this chapter, the electrical parameters for the defined full-scale model are presented. The core specific values are collected from the laboratory results. Resistance per metre is from COMSOL-simulations including skin effect. All materials are temperature independent. These values are stated in Table 8-9.

Table 8-9: Values found from the prototype experiments

Symbol	ρ [kg/dm ³]	P_o [W/kg]	R [Ω /m]
Value	7.284 – 7.489	0.993-1.30	1.91e-5

The physical and electrical parameters are given in Table 8-10 and Table 8-11. Regarding the secondary winding, it is assumed that a ½ metre long conductor is required in order to bend it from the inside to the outside of the transformer. The reactances used are theoretically lowest found from COMSOL-simulations as described in chapter 1, meaning that only current is applied to the conductors inside the transformer core.

Table 8-10: Physical properties of the full-scale models

Parameters	DEH-system	IH-system
r_i [m]	0.0723	0.1085
r_o [m]	0.34	0.50
l [m]	2	2
$V_{\text{iron core}}$ [m]	0.70	1.53
$m_{\text{iron core}}$ [kkg]	5.10-5.24	11.11-11.45

Table 8-11: Electrical values of the full-scale models

Parameters	DEH-system	IH-system
l_{R1} [m]	2	2
l_{R2} [m]	5	18
R_1 [m Ω]	0.0382	0.0382
R_2 [m Ω]	0.0955	0.344
$X_{\text{eq,min}}$ [m Ω]	0.202	0.520

Based on previous calculations, Table 8-12 is created. The efficiency is calculated assuming that the illuminated apparent power is at the transformers' primary. A power factor of 0.90 is used when finding the efficiency.

Table 8-12: Datasheet of the full-scale models

Parameters	DEH-system	IH-system
S_n [kVA]	221.2	377.8
I_n [A]	1152	1198
V_n[V]	192.0	281.7
f_n [Hz]	50	50
n	1:1	1:2
P_o [kW]	5.06-6.82	11.1-14.9
P_{sc} [W]	177	549
Efficiency [%]	96-97%	95-96%

When studying the efficiency, power core loss and other values from the previous tables it is important to have in mind that these numbers are based upon many simplifications, as specified earlier. Correct values are found by building a full-scale model and execute laboratory work as carried out prior in this report. Dimensions of the transformer are though assumed to be quite correct if magnetic flux distributes uniformly across the iron core, independent of core dimensions.

9 CONCLUSIONS

Based on transformer design theory and the special application requirements, a ring core transformer consisting of multiple stabled toroidal cores build up from magnetic tape is found to be suitable. This construction design provides the maximum utilization of magnetic flux with the minimum of magnetic force. Two main reasons distinguish themselves regarding the application requirements. The first is absence of termination points. This enables the use of a piggy-back cable as primary winding, increasing the overall system reliability compared to a system consisting of joints. The other main design benefit is the possibility to connect appropriate winding ratio in an unproblematic manner. The expected winding ratios are 1:1, 1:2 or 1:4; depending on the t-off's heating system.

The rated currents of the two prototypes were found using the NEK-standard 400-5-52:2010, while the rated voltage estimates were calculated from equations based on fundamental magnetic theory. By use of regular transformer testing techniques, the actual voltage ratings were found equal to the a priori estimate. Other electrical properties of the prototypes were also extracted from these tests. No unusual electrical characteristics were found, compared with iron core theory and regular power transformers. An appurtenant datasheet is attached in Appendix A.

If the t-off is to be heated using IH, conductor placement subsequent to the transformer's secondary winding is of importance. By reducing displacement of these conductors, the overall impedance is dramatically reduced. This concern both the conductors' near and far end.

When creating numerical formulas and 2-D analytical models of the series reactance, the most beneficial and trustworthy is to calculate the theoretical minimum. This is executed by only considering the conductors within the transformer core. The analytical calculated series reactance is found to be approximately 15 % smaller than the numerical when four return path conductors are placed evenly, e.g. 90° displaced, around the piggy-back cable. At other conductor placements, the difference changes significantly. The analytical formulas are created assuming concentric windings inside the transformer core.

Using previous calculations and findings, rough calculations of a full-scale transformer is executed. 192 V is required to heat a 500 meter long and eight inch thick jumper system using DEH, while an IH-system requires 282 V. Using two metre long transformers, the iron core volume becomes 0.70 m³ and 1.53 m³, for the DEH and IH-system, respectively. This corresponds to a weight of approximately 5.2 and 11.2 metric tons. An appurtenant datasheet is attached in Appendix B.

All calculations as a whole indicates that this transformer type may be reasonable for both a DEH and IH heated t-off. For this analysis solely, a DEH system would be best as fewer conductors are required and the total system impedance is smaller. Small impedance subsequently leads to smaller required voltage across the transformer and thus transformer dimensions. Still, external factors must also be taken into consideration when choosing desired system.

10 FURTHER WORK

More additional research work should be performed before installing this kind of transformer designs. First, a full-scale model should be built and tested in order to achieve correct equivalent electrical parameters. A frequency analysis of the iron core is also of interest.

As for the FEM-analysis and/or numerical calculations, the simplifications executed in this thesis should be verified or dismissed, based on e.g. a full-scale model in correct environments. In addition, it would be of interest to develop formulas from which more precise series reactances could be calculated.

Electric current is utilized by the surround water during operation of a DEH-system. How this affects the transformer is of great interest. If the t-off is to be heated using DEH, the addition influence should be estimated. As the appurtenant pipelines consist of magnetic steel, they will, to some extent, also affect the transformer operation.

The transformer is to be set in a system surrounded by water, the water influence should be determined. Last, but not least, an installation analysis has to be carried out. This includes how to install it in a new pipeline system and discover if it is possible to install the transformer in an existing DEH-system

11 BIBLIOGRAPHY

- [1] A. Nysveen, H. Kulbotn, J. K. Lervik, A. H. Børnes, M. Høyser-Hansen and J. J. Bremnes, "Direct Electrical Heating of Subsea Pipelines - Technology Development and Operation Experience," *IEEE TRANSACTIONS ON INDUSTRI APPLICATIONS, VOL. 43, NO1*, pp. 118-129, January 2007.
- [2] EFI SINTEF GROUP, INTRODUCTION TO DIRECT HEATING OF SUBSEA PIPELINES, 1998.
- [3] A. Nysveen, H. Kulbotten, J. K. Lervik, A. H. Børnes, M. Høyser-Hansen and J. J. Bremnes, "Direct Electric Heating of Subsea Pipelines - Technology and Deveopment and Operating Experience," *IEEE TRANSACTIONS ON INDUSTRY APPLICATIONS, VOL. 43, NO. 1, JANUARY/FEBRUARY 2007*, pp. 118-129, JANUARY/FEBRUARY 2007.
- [4] Moham, Undeland and Robbins, *Power Electronics - Converters, Applications, and Design* (3rd Edition), Wiley, 2003.
- [5] R. E. Haimbaugh, "Theory of Heating by Induction," in *Practical Induction Heat Treating*, ASM International, 2001, pp. 5-11.
- [6] E. Tutorials. [Online]. Available: <http://www.electronics-tutorials.ws/electromagnetism/magnetic-hysteresis.html>. [Accessed 11 03 2013].
- [7] C. W. McLyman, *Transformer And Inductor Design Handbook*. Third Edition, Revised and Expanded, Idyllwild, California, USA: Kg Magnetics, Inc, 2004.
- [8] A. Nysveen, *Maritime and Offshore Power Systems*, Trondheim: Department of electric power engineering, 2011.
- [9] A. E. Fitzgerald, C. Kingsley, Jr. and S. D. Umans, "Electric Machinery," Singapore, McGRAW-HILL, 2003, pp. 57-104.
- [10] P. Dommel, *Electro-Magnetic-Transients-Program (EMTP) Theory Book*, Portland, Oregon: Branch of System Engineering - Bonneville Power Administration - Portland, Oregon - United States of America.
- [11] A. Nysveen, "High Voltage Equipment," in *Power Transformers*, Trondheim, Department of Electric Power Engineering, 2011.
- [12] L. Massimiliano, "Accurate evaluation of the ground impedance of real earthing systems," 2011/2012. [Online]. Available: <http://tesi.cab.unipd.it/39557/1/tesi.pdf>. [Accessed December 2012].
- [13] "ThyssenKrupp Electrical Steel," [Online]. Available: http://www.tkes.com/web2010/tkeswebcms.nsf/www/en_powercore_c.html. [Accessed April

2013].

- [14] R. B. Standler, "Protection of Electronic Circuits From Overvoltages," Mineola, New York 11501, Dover Publications, Inc., 2002, pp. 380, chapter 23.
- [15] E. D. Paula, J. C. Mendes and W. V. Cali, "Reactance Calculation of a Reactor with Non-Concentric Windings by Utilizing a Finite Element Method (FEM) based 3-D program," *2010 IEEE/PES Transmission and Distribution Conference and Exposition: Latin America*, pp. 610-615, 2010.
- [16] Z. Popovic and B. D. Popovic, "Introductory Electromagnetics," Prentice Hall, 2000, p. 284.
- [17] E. Ilstad, TET 4195 HIGH VOLTAGE EQUIPMENT - CABLE TECHNOLOGY, Trondheim: Department of Electric Power Engineering, 2009.
- [18] SINTEF, "PLANLEGGINGSBOK FOR KRAFTNETT, BIND III," in *Chapter 5 - TEKNISKE DATA FOR KOMPONENTER*, Trondheim, ', 1993, updated 2003, p. 26.
- [19] "Electrical Engineering," [Online]. Available: <http://www.electrical4u.com/open-and-short-circuit-test-on-transformer/>. [Accessed April 2013].

12 APPENDIX

12.1 APPENDIX A: PROTOTYPE DATASHEET AND DIMENSIONS

Table 12-1: Prototype datasheet

	Subsea		Onshore	
	Small transformer	Large transformer	Small transformer	Large transformer
S_n [VA]	918	7 200	748	5 880
I_n [A]	270	900	220	735
V_n [V]	3.4	8.0	3.4	8.0
f_n [Hz]	50	50	50	50
P_o [W]	15.7	93.2	15.7	93.2
P_{sc} [W]	41.6	93.8	27.7	61.7
e_z [%]	4.55	1.43	3.70	1.43
e_R [%]	4.53	1.30	3.70	1.30
e_x [%]	0.44	0.59	0.072	0.50
$m_{\text{iron core}}$ [kg]	15.81	71.76	15.81	71.2
Winding material	Copper	Copper	Copper	Copper
Efficiency [%]	93.1	97.1	93.6	97.1

Table 12-2: Prototype dimensions

Transformer type	Inner radius [mm]	Outer radius [mm]	Total height [mm]	Volume [dm ³]	Weight [kg]
Small	25	45	480	2.111	15.81
Large	50	90	560	9.852	71.76

12.2 APPENDIX B: FULL-SCALE MODEL DATASHEET AND DIMENSIONS

The full-scale models are supposed to supply a system, DEH or IH, to heat a 500 metre long t-off.

Table 12-3: Datasheet of the full-scale models

Parameters	DEH-system	IH-system
S_n [kVA]	221.2	377.8
I_n [A]	1152	1198
V_n [V]	192.0	281.7
f_n [Hz]	50	50
n	1:1	1:2 ⁴
P_o [kW]	5.06-6.82	11.1-14.9
P_{sc} [W]	177	549
Efficiency [%]	96-97%	95-96%

Table 12-4: Physical properties of the full-scale models

Parameters	DEH-system	IH-system
r_i [m]	0.0723	0.1085
r_o [m]	0.34	0.50
l [m]	2	2
$V_{iron\ core}$ [m]	0.70	1.53
$m_{iron\ core}$ [kg]	5.10-5.24	11.11-11.45

Table 12-5: Electrical values of the full-scale models

Parameters	DEH-system	IH-system
l_{R1} [m]	2	2
l_{R2} [m]	5	18
R_1 [m Ω]	0.0382	0.0382
R_2 [m Ω]	0.0955	0.344
$X_{eq,min}$ [m Ω]	0.202	0.520

⁴ The secondary winding is set to be two parallel conductors, each consisting of two turns. Each conductor carries a current of 1198 A.

12.3 APPENDIX C – ANALYTICAL FORMULA DEVELOPMENT

12.3.1 INTRODUCTION

The formulas developed are based in the simplifications from Figure 12-1. The magnetic field strength is sketched in Figure 12-2, where also the energy notation is included.

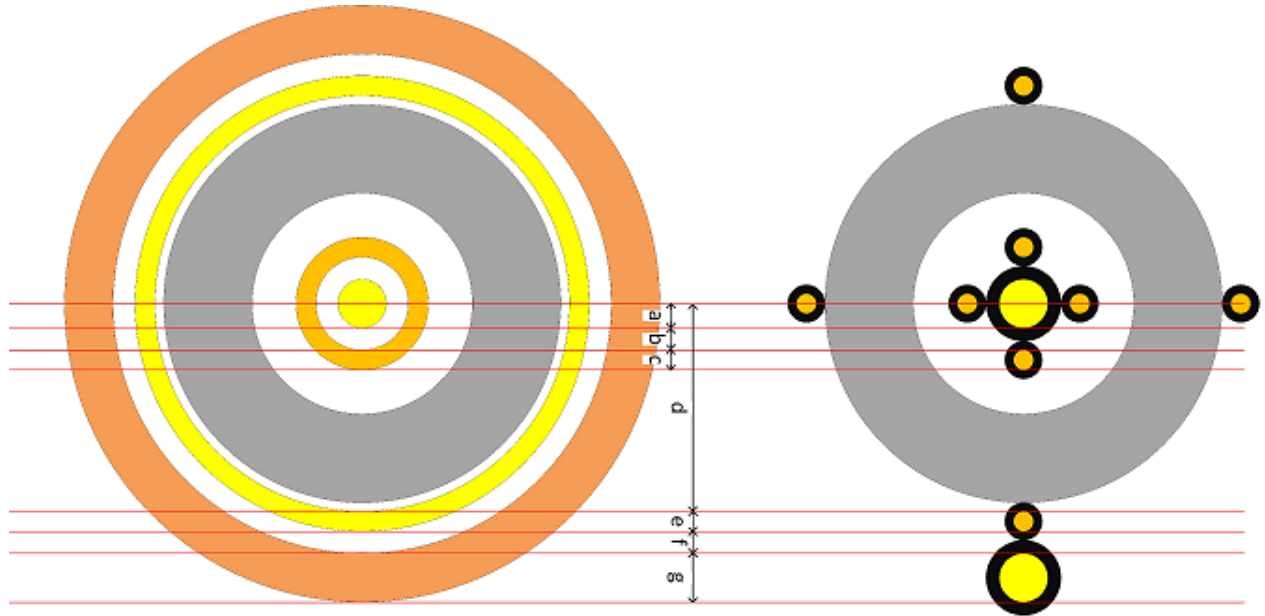


Figure 12-1: Concentric winding approach

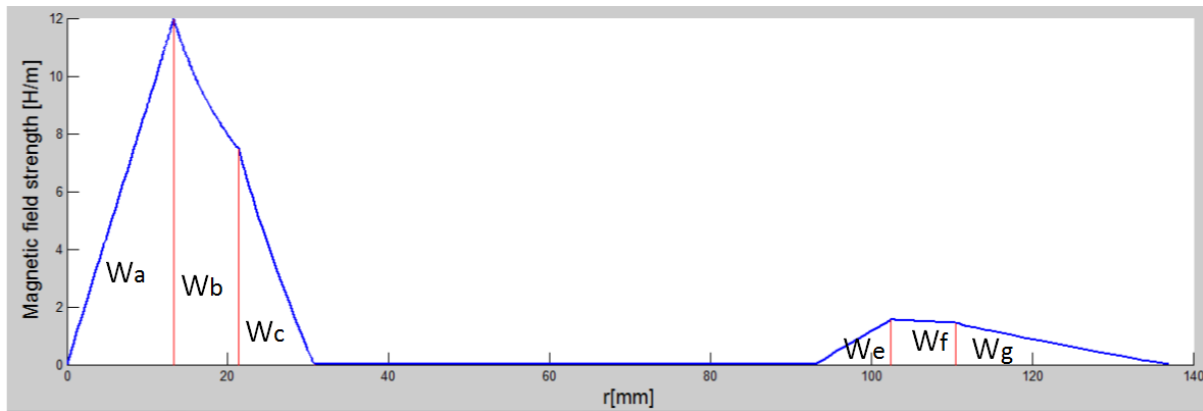


Figure 12-2: Magnetic field strength as a function of radius. Magnetic energies are included

The two basic equations used are:

$$W_{magnetic\ energy} = \frac{1}{2} \int_0^r B(r) \cdot H(r) 2\pi r dr \tag{Eq. (12-1)}$$

$$H \cdot l = I \tag{Eq. (12-2)}$$

12.3.2 MAGNETIC FIELD STRENGTH AS FUNCTION OF RADIAL DIRECTION OUT FROM ORIGIN

$$H(r) = \begin{cases} \begin{cases} I \cdot \frac{r}{2\pi a^2}, & r \in \langle 0, a \rangle \\ I \cdot \frac{1}{2\pi r}, & r \in \langle a, a+b \rangle \\ I \cdot \frac{(a+b+c-r)}{2\pi(a+b)c}, & r \in \langle a+b, a+b+c \rangle \end{cases} \\ \begin{cases} I \cdot \frac{r^2 - d^2}{2\pi r \cdot e(2d+e)}, & r \in \langle d, d+e \rangle \\ I \cdot \frac{1}{2\pi r}, & r \in \langle d+e, d+e+f \rangle \\ I \cdot \frac{(d+e+f+g-r)}{2\pi(d+e+f)g}, & r \in \langle d+e+f, d+e+f+g \rangle \end{cases} \end{cases} \quad \text{Eq. (12-3)}$$

12.3.3 MAGNETIC ENERGY AS FUNCTION OF RADIAL DIRECTION OUT FROM ORIGIN

$$W(r) \begin{cases} \begin{cases} W_a, & r \in \langle 0, a \rangle \\ W_b, & r \in \langle a, a+b \rangle \\ W_c, & r \in \langle a+b, a+b+c \rangle \end{cases} \\ \begin{cases} W_e, & r \in \langle d, d+e \rangle \\ W_f, & r \in \langle d+e, d+e+f \rangle \\ W_g, & r \in \langle d+e+f, d+e+f+g \rangle \end{cases} \end{cases} \quad \text{Eq. (12-4)}$$

$$W_a = \frac{\mu_0}{16\pi} I^2$$

$$W_b = \frac{1}{4\pi} \mu_0 I^2 \ln\left(\frac{a+b}{a}\right)$$

$$W_c = \frac{1}{48\pi} \mu_0 I^2 \cdot \frac{c(c+4(a+b))}{(a+b)^2}$$

$$W_e = \mu_0 I^2 \frac{(2d^2e^2 + 4de^3 + e^4 + 4d^4 \cdot \ln(d+e) - 4d^3(d \cdot \ln(d) + e))}{16\pi \cdot e^2(2d+e)^2} \quad \text{Eq. (12-5)}$$

$$W_f = \frac{1}{4\pi} \mu_0 I^2 \cdot \ln\left(\frac{d+e+f}{d+e}\right)$$

$$W_g = \frac{1}{48\pi} \mu_0 I^2 \cdot \frac{g(g+4(d+e+f))}{(d+e+f)^2}$$

$$W_{tot} = W_a + W_b + W_c + W_e + W_f + W_g \quad \text{Eq. (12-6)}$$

12.3.4 $r \in (0, a]$

First, the apparent current $I'(r)$ as a function of the applied current is required:

$$I = J \cdot \pi a^2 \quad \text{Eq. (12-7)}$$

$$I'(r) = J \cdot \pi r^2 \quad \text{Eq. (12-8)}$$

Combining the previous two equations gives:

$$I'(r) = I \cdot \frac{r^2}{a^2} \quad \text{Eq. (12-9)}$$

Using this equation further gives:

$$H(r) \cdot l = I'(r) \quad \text{Eq. (12-10)}$$

$$H(r) \cdot 2\pi r = I \cdot \frac{r^2}{a^2} \quad \text{Eq. (12-11)}$$

$$H(r) = I \cdot \frac{r}{2\pi a^2} \quad \text{Eq. (12-12)}$$

And the energy becomes

$$W_a = \int_0^a \frac{1}{2} \mu_0 \cdot H(r)^2 \cdot 2\pi r \, dr \quad \text{Eq. (12-13)}$$

$$W_a = \int_0^a \frac{1}{2} \mu_0 \cdot \left(\frac{r}{2\pi a^2} \right)^2 \cdot 2\pi r \, dr \quad \text{Eq. (12-14)}$$

$$W_a = \frac{1}{4\pi} \mu_0 I^2 \int_0^a r^3 \, dr \quad \text{Eq. (12-15)}$$

$$W_a = \frac{\mu_0}{16\pi} I^2 \quad \text{Eq. (12-16)}$$

W_a is verified in [16].

12.3.5 $r \in [a, a + b]$

The magnetic field strength decreases at $1/r$, giving:

$$H(r) \cdot 2\pi r = I \quad \text{Eq. (12-17)}$$

$$H(r) = \frac{I}{2\pi r} \quad \text{Eq. (12-18)}$$

The magnetic energy is found:

$$W_b = \int_a^{a+b} \frac{1}{2} \cdot \mu_0 H(r)^2 \cdot 2\pi r \, dr \quad \text{Eq. (12-19)}$$

$$W_b = \int_a^{a+b} \frac{1}{2} \mu_0 \left(\frac{I}{2\pi r} \right)^2 \cdot 2\pi r \, dr \quad \text{Eq. (12-20)}$$

$$W_b = \frac{1}{4\pi} \mu_0 I^2 \int_a^{a+b} \frac{1}{r} \, dr \quad \text{Eq. (12-21)}$$

$$W_b = \frac{1}{4\pi} \mu_0 I^2 \ln \left(\frac{a+b}{a} \right) \quad \text{Eq. (12-22)}$$

12.3.6 $r \in \langle a + b, a + b + c \rangle$

The magnetic field strength is approximated to decrease linearly:

$$H(r) = -A \cdot r + b \quad \text{Eq. (12-23)}$$

$$H(r) = -\frac{H_b}{c}r + H_{x1} \quad \text{Eq. (12-24)}$$

H_x is the point where $H(r)$ intersects the y-axis

$$H_b = H(r = (a + b)) = \frac{I}{2\pi(a + b)} \quad \text{Eq. (12-25)}$$

$$H(r) = -\frac{I}{2\pi(a + b)}r + \frac{I}{2\pi} \cdot \frac{a + b + c}{(a + b)c} \quad \text{Eq. (12-26)}$$

$$H(r) = \frac{I}{2\pi(a + b)c}(a + b + c - r) \quad \text{Eq. (12-27)}$$

The magnetic energy is given by

$$W_c = \int_{a+b}^{a+b+c} \frac{1}{2} \cdot \mu_0 H(r)^2 \cdot 2\pi r \, dr \quad \text{Eq. (12-28)}$$

$$W_c = \int_{a+b}^{a+b+c} \frac{1}{2} \cdot \mu_0 I^2 \left[\frac{a + b + c - r}{2\pi(a + b)c} \right]^2 \cdot 2\pi r \, dr \quad \text{Eq. (12-29)}$$

$$W_c = \frac{1}{4\pi} \cdot \frac{\mu_0 I^2}{(a + b)c} \int_{a+b}^{a+b+c} (a + b + c - r)^2 r \, dr \quad \text{Eq. (12-30)}$$

$$W_c = \frac{1}{48\pi} \mu_0 I^2 \cdot \frac{c(c + 4(a + b))}{(a + b)^2} \quad \text{Eq. (12-31)}$$

12.3.7 $r \in \langle d, d + e \rangle$

Also here, the apparent current $I'(r)$ as a function of the applied current must be found:

$$I = J \cdot \pi((d + e)^2 - d^2) = J \cdot \pi e(2d + e) \quad \text{Eq. (12-32)}$$

$$I'(r) = J \cdot \pi(r^2 - d^2) \quad \text{Eq. (12-33)}$$

$$I'(r) = I \cdot \frac{r^2 - d^2}{e(2d + e)} \quad \text{Eq. (12-34)}$$

The magnetic field strength is given by:

$$H(r) \cdot 2\pi r = I'(r) \quad \text{Eq. (12-35)}$$

$$H(r) = I \cdot \frac{r^2 - d^2}{2\pi r \cdot e(2d + e)} \quad \text{Eq. (12-36)}$$

The magnetic energy:

$$W_e = \int_d^{d+e} \frac{1}{2} \cdot \mu_0 H(r)^2 \cdot 2\pi r \, dr \quad \text{Eq. (12-37)}$$

$$W_e = \int_d^{d+e} \frac{1}{2} \mu_0 I^2 \left[\frac{r^2 - d^2}{2\pi r \cdot e(2d + e)} \right]^2 2\pi r \, dr \quad \text{Eq. (12-38)}$$

$$W_e = \frac{1}{4\pi} \cdot \frac{\mu_0 I^2}{e^2 (2d + e)^2} \int_d^{d+e} \frac{(r^2 - d^2)}{r} \, dr \quad \text{Eq. (12-39)}$$

$$W_e = \frac{\mu_0 I^2 \cdot (2d^2 e^2 + 4de^3 + e^4 + 4d^4 \cdot \ln(d + e) - 4d^3(d \cdot \ln(d) + e))}{16 \cdot \pi e^2 (2d + e)^2} \quad \text{Eq. (12-40)}$$

12.3.8 $r \in [d + e, d + e + f]$

The magnetic field strength is given as:

$$H(r) \cdot 2\pi r = I \quad \text{Eq. (12-41)}$$

$$H(r) = \frac{I}{2\pi r} \quad \text{Eq. (12-42)}$$

$$H_f = H(r = d + e + f) = \frac{I}{2\pi(d + e + f)} \quad \text{Eq. (12-43)}$$

The magnetic energy:

$$W_f = \int_{d+e}^{d+e+f} \frac{1}{2} \mu_0 H(r)^2 2\pi r \, dr \quad \text{Eq. (12-44)}$$

$$W_f = \int_{d+e}^{d+e+f} \frac{1}{2} \mu_0 \left(\frac{I}{2\pi r} \right)^2 2\pi r \, dr \quad \text{Eq. (12-45)}$$

$$W_f = \frac{1}{4\pi} \mu_0 I^2 \int_{d+e}^{d+e+f} \frac{1}{r} \, dr \quad \text{Eq. (12-46)}$$

$$W_f = \frac{1}{4\pi} \mu_0 I^2 \cdot \ln \left(\frac{d + e + f}{d + e} \right) \quad \text{Eq. (12-47)}$$

$$W_f = \mu_0 I^2 \frac{(2d^2e^2 + 4de^3 + e^4 + 4d^4 \cdot \ln(d + e) - 4d^3(d \cdot \ln(d) + e))}{16\pi \cdot e^2(2d + e)^2} \quad \text{Eq. (12-48)}$$

12.3.9 $r \in [d + e + f, d + e + f + g]$

The magnetic field strength is approximated to decrease linearly:

$$H(r) = -A \cdot r + b \quad \text{Eq. (12-49)}$$

$$H(r) = -\frac{H_f}{g}r + H_{x2} \quad \text{Eq. (12-50)}$$

H_{x2} is the point where $H(r)$ intersects y-axis

$$H(r) = -\frac{I}{2\pi(d + e + f)g}r + \frac{I}{2\pi} \cdot \frac{d + e + f + g}{(d + e + f)g} \quad \text{Eq. (12-51)}$$

$$H(r) = \frac{I}{2\pi(d + e + f)g}(d + e + f + g - r) \quad \text{Eq. (12-52)}$$

The magnetic energy is given by

$$W_g = \int_{d+e+f}^{d+e+f+g} \frac{1}{2} \cdot \mu_0 H(r)^2 \cdot 2\pi r \, dr \quad \text{Eq. (12-53)}$$

$$W_g = \int_{d+e+f}^{d+e+f+g} \frac{1}{2} \cdot \mu_0 I^2 \left[\frac{d + e + f + g - r}{2\pi(d + e + f)g} \right]^2 \cdot 2\pi r \, dr \quad \text{Eq. (12-54)}$$

$$W_g = \frac{1}{4\pi} \cdot \frac{\mu_0 I^2}{(d + e + f)^2 g^2} \int_{d+e+f}^{d+e+f+g} (d + e + f + g - r)^2 r \, dr \quad \text{Eq. (12-55)}$$

$$W_g = \frac{1}{48\pi} \mu_0 I^2 \cdot \frac{g(g + 4(d + e + f))}{(d + e + f)^2} \quad \text{Eq. (12-56)}$$

13 ATTACHMENTS

13.1 TABLES

Table 13-1: Short-circuit test results of small transformer

	V primary [V]	I primary [A]	P primary [W]
Set 1	0,02889	50,40	1,437
	0,05752	100,99	5,734
	0,08649	151,37	12,9
	0,11361	198,5	22,262
	0,14359	250,8	35,537
	0,17331	301,68	51,606
Set 2	0,02845	50,00	1,404
	0,05717	100,37	5,664
	0,08572	150,41	12,726
	0,11397	199,7	22,467
	0,14461	252,4	36,026
	0,17311	301,36	51,491

Table 13-2: Short-circuit test results of large transformer

	V primary1 [V]	V primary2 [V]	V primary3 [V]	V primary avg. [V]	I primary [A]	P primary [W]
Set 1	0,01261	0,01269	0,01238	0,01256	99,99	1,145
	0,02535	0,02546	0,02489	0,025233333	200,45	4,616
	0,03818	0,03836	0,03753	0,038023333	301,95	10,47
	0,0507	0,05094	0,04985	0,050496667	400,9	18,47
	0,06372	0,06404	0,06267	0,063476667	504,1	29,17
	0,07574	0,07613	0,07451	0,07546	598,3	41,16
	0,0887	0,08915	0,08726	0,08837	699,9	56,39
	0,10166	0,10219	0,10005	0,1013	801,4	74,3
	0,11451	0,11518	0,11295	0,114213333	899,9	93,74
	0,12743	0,12817	0,12574	0,127113333	1000,2	115,99
0,14067	0,14148	0,13884	0,14033	1100	140,88	
Set 2	0,0125	0,01254	0,01225	0,01243	98,67	1,118
	0,02562	0,02567	0,02516	0,025483333	201,95	4,692
	0,03793	0,03802	0,03727	0,03774	298,88	10,3
	0,05071	0,05083	0,04985	0,050463333	399,6	18,37
	0,06368	0,06384	0,06263	0,063383333	501,6	28,96
	0,07614	0,07635	0,07492	0,075803333	599,4	41,37
	0,08897	0,08921	0,08756	0,08858	699,9	56,46
	0,10186	0,10215	0,10028	0,10143	800,2	73,92
	0,11473	0,11505	0,11296	0,114246667	899,6	93,63
	0,1278	0,12814	0,12586	0,127266667	999,6	115,95
0,14115	0,14151	0,13902	0,14056	1099,7	140,96	

Table 13-3: Open-circuit test results of small transformer

	V primary [V]	I primary [A]	P primary [W]		V primary [V]	I primary [A]	P primary [W]
Set 1	0,493	1,04	0,4	Set 2	0,504	1,01	0,4
	1,009	1,79	1,4		0,999	1,7	1,4
	1,493	2,35	3,0		1,496	2,29	2,9
	1,996	2,90	5,0		2,001	2,87	4,9
	2,244	3,19	6,1		2,245	3,17	6,2
	2,505	3,54	7,6		2,500	3,52	7,6
	2,754	3,95	9,3		2,756	3,94	9,3
	3,006	4,46	11,2		2,996	4,46	11,2
	3,250	5,30	13,7		3,257	5,34	13,8
	3,506	7,23	17,2		3,5	7,09	17,0
	4,003	41,4	37		4,011	43,2	38
	4,502	163,7	106		4,51	167,6	109
Set 3	0,507	1,02	0,4	Set 4	0,504	1,01	0,4
	1,012	1,72	1,4		1,006	1,72	1,4
	1,495	2,28	2,9		1,510	2,31	2,9
	1,996	2,85	4,9		2,008	2,89	5,0
	2,244	3,16	6,1		2,252	3,19	6,2
	2,495	3,50	7,6		2,500	3,52	7,6
	2,751	3,91	9,2		2,759	3,95	9,3
	3,010	4,46	11,3		3,011	4,48	11,3
	3,253	5,28	13,6		3,259	5,32	13,7
	3,504	7,18	17,1		3,500	7,09	16,9
	4,008	41,7	36		3,994	39,6	36
	4,512	167,1	108		4,501	164,3	106
Set 5	0,504	1,01	0,4	Set 6	0,508	1,01	0,4
	1,000	1,70	1,4		1,006	1,70	1,4
	1,499	2,29	2,9		1,507	2,28	2,9
	1,998	2,85	4,9		2,006	2,85	4,9
	2,251	3,17	6,2		2,252	3,15	6,2
	2,493	3,50	7,5		2,505	3,50	7,6
	2,749	3,92	9,2		2,757	3,91	9,2
	2,995	4,44	11,1		3,002	4,44	11,2
	3,254	5,32	13,7		3,253	5,28	13,6
	3,505	7,24	17,2		3,493	7,04	16,8
	4,004	43,1	37,0		4,000	40,7	37,0
	4,508	168,3	109,0		4,510	167,7	109,0

Table 13-4: Open-circuit test results of large transformer

	V primary1 [V]	V primary2 [V]	V primary3 [V]	V primary avg. [V]	I primary [A]	P primary [W]
Set 1	1,002	1,002	1	1,00	1,904	1,46
	1,997	1,996	1,995	2,00	3,234	5,34
	2,996	2,996	2,994	3,00	4,413	11,5
	3,997	3,996	3,995	4,00	5,573	20,1
	-	-	-	-	-	-
	4,998	4,997	4,995	5,00	6,86	31,0
	-	-	-	-	-	-
	6,058	6,058	6,058	6,06	8,54	46
	-	-	-	-	-	-
	7,01	7,00	6,99	7,00	10,76	64
	8,04	8,04	8,03	8,04	17,1	97
	9,03	9,02	9,01	9,02	64,0	1,7E+02
	10,13	10,12	10,11	10,12	474	4E+02
Set 2	1,01	1,009	1,009	1,01	1,916	1,48
	2	1,999	1,997	2,00	3,215	5,31
	3,007	3,007	3,005	3,01	4,416	11,6
	3,994	3,992	3,99	3,99	5,576	20,1
	4,496	4,495	4,492	4,49	6,230	25,3
	4,991	4,99	4,988	4,99	6,88	31,1
	5,495	5,493	5,494	5,49	7,610	38,0
	5,746	5,746	5,746	5,75	8,03	41
	5,989	5,986	5,985	5,99	8,45	45
	7,07	7,06	7,05	7,06	11,03	66
	8,09	8,09	8,08	8,09	18,05	100
	9,07	9,06	9,06	9,06	72,1	1,7E+02
	10,03	10,02	10,01	10,02	407	4E+02
Set 3	1,001	1	1	1,00	1,87	1,4
	2,007	2,006	2,005	2,01	3,18	5,25
	3,005	3,004	3,002	3,00	4,33	11,2
	3,998	3,997	3,995	4,00	5,45	19,5
	4,501	4,498	4,499	4,50	6,04	24,5
	5,014	5,014	5,013	5,01	6,68	30,0
	5,482	5,481	5,482	5,48	7,35	36,0
	5,753	5,753	5,752	5,75	7,77	40
	5,981	5,981	5,979	5,98	8,16	44
	7,05	7,05	7,04	7,05	10,6	63
	8,06	8,05	8,05	8,05	17,04	93
	9,09	9,08	9,07	9,08	72,4	1,7E+02
	10,008	10,008	10,007	10,01	439	4,00E+02
Set 4	1,005	1,004	1,003	1,00	1,93	1,45
	2,003	2,002	2	2,00	3,25	5,4

	3,006	3,006	3,003	3,01	4,43	11,6
	4,002	4,002	3,999	4,00	5,60	20,2
	4,493	4,492	4,491	4,49	6,20	25,2
	4,991	4,988	4,988	4,99	6,86	30,9
	5,502	5,501	5,501	5,50	7,600	38,0
	5,731	5,728	5,728	5,73	7,96	41
	5,976	5,973	5,974	5,97	8,4	45
	7,01	7,01	7	7,01	10,79	64
	8,04	8,04	8,03	8,04	16,96	93
	9,06	9,05	9,04	9,05	68,9	1,7E+02
	10,09	10,08	10,08	10,08	441	4E+02
Set 5	1,011	1,01	1,01	1,01	1,916	1,45
	2,004	2,003	2,002	2,00	3,223	5,3
	2,998	2,997	2,995	3,00	4,369	11,3
	3,99	3,989	3,987	3,99	5,46	19,6
	4,498	4,498	4,495	4,50	6,07	24,6
	5,002	5,001	4,9994	5,00	6,70	30,3
	5,522	5,52	5,518	5,52	7,43	37,0
	5,736	5,735	5,734	5,74	7,76	40
	5,965	5,963	5,964	5,96	8,15	43
	7,06	7,06	7,05	7,06	10,64	63
	8,06	8,06	8,05	8,06	17,14	94
	9,04	9,03	9,03	9,03	65,0	1,7E+02
	10,11	10,1	10,09	10,10	445	4E+02
Set 6	1,004	1,003	1,003	1,00	1,87	1,41
	2,008	2,007	2,006	2,01	3,169	5,26
	2,992	2,991	2,989	2,99	4,304	11,2
	3,993	3,992	3,992	3,99	5,44	19,5
	4,495	4,494	4,494	4,49	6,05	24,5
	4,988	4,999	4,998	5,00	6,68	30,2
	5,484	5,483	5,481	5,48	7,340	36,0
	5,746	5,743	5,745	5,74	7,77	40
	5,991	5,991	5,99	5,99	8,18	44
	7,05	7,04	7,03	7,04	10,58	63
	7,98	7,98	7,97	7,98	16,12	90
	9,01	9	8,99	9,00	61,5	1,6E+02
	9,99	9,99	9,98	9,99	374	4E+02

Table 13-5: Short-circuit test results of small transformer, long secondary winding

	V primary [V]	I primary [A]	P primary [W]		V primary [V]	I primary [A]	P primary [W]
No loop 1	0,195	50,45	9,5	No loop 2	0,190	49,65	9,2
	0,392	101,5	38		0,392	102,3	39
	0,585	150,9	85		0,576	149,7	84
	0,774	199,6	149		0,773	200,6	150
	0,983	251,5	239		0,970	249,7	234
	1,181	299,7	343		1,167	298,4	339
Half loop 1	0,223	49,10	9,1	Half loop 2	0,234	50,90	9,7
	0,459	101,1	38		0,457	100,3	38
	0,686	150,5	85		0,683	149,5	84
	0,913	198,2	150		0,919	200,3	152
	1,166	251,8	247		1,153	250,4	243
	1,411	302,9	360		1,376	297,2	345
Full loop 1	0,268	49,85	9,6	Full loop 2	0,264	49,05	9,3
	0,532	98,8	38		0,551	102	40
	0,815	150,2	89		0,816	150,1	88
	1,091	200,5	157		1,088	199,5	156
	1,368	250,2	250		1,379	251,5	251
	1,652	299,7	361		1,660	301,3	366

Table 13-6: Short-circuit test results of large transformer, long secondary winding

	V primary1 [V]	V primary2 [V]	V primary3 [V]	V primary avg. [V]	I primary [A]	P primary [W]
No-loop 1	0,1227	0,1234	0,1237	0,123	99,9	8
	0,248	0,2496	0,2503	0,249	201,4	32
	0,3687	0,371	0,372	0,371	299,4	71
	0,4911	0,4942	0,495,6	0,493	399,0	126
	0,6139	0,6181	0,6202	0,617	498,8	201
	0,744	0,748	0,750	0,747	602	2,9E+02
	0,863	0,868	0,870	0,867	700	4,0E+02
	0,985	0,991	0,993	0,990	797	5,2E+02
	1,115	1,122	1,125	1,121	901	6,7E+02
No-loop 2	0,1224	0,1231	0,1234	0,123	99,7	8
	0,2457	0,2472	0,2478	0,247	200,1	32
	0,3674	0,3697	0,3797	0,372	299,2	72
	0,4942	0,4973	0,4987	0,497	402,6	131
	0,6117	0,6157	0,6176	0,615	498,5	203
	0,742	0,746	0,748	0,745	601	3,0E+02
	0,865	0,87	0,872	0,869	701	4,0E+02
	0,996	1,001	1,004	1,000	806	5,3E+02
	1,110	1,116	1,118	1,115	896	6,6E+02
Half-loop 1	0,2088	0,2088	0,2091	0,209	99,2	8
	0,4224	0,4227	0,4234	0,423	199,9	33
	0,6363	0,6368	0,641	0,638	300,9	75
	0,851	0,85	0,852	0,851	399,4	132
	1,067	1,066	1,068	1,067	500,4	208
	1,28	1,28	1,282	1,281	601	3,2E+02
	1,484	1,484	1,486	1,485	697	4,0E+02
	1,707	1,707	1,71	1,708	801	5,7E+02
	1,91	1,911	1,913	1,911	896	7,1E+02
Half-loop 2	0,2091	0,2096	0,2098	0,210	99,5	8
	0,4218	0,4226	0,4234	0,423	199,5	33
	0,6316	0,6333	0,6343	0,633	298,8	74
	0,853	0,854	0,855	0,854	400,5	140
	1,068	1,07	1,071	1,070	501,5	209
	1,268	1,271	1,272	1,270	596	3,0E+02
	1,5	1,503	1,505	1,503	705	4,4E+02
	1,694	1,698	1,7	1,697	796	5,6E+02
	1,912	1,916	1,919	1,916	898	7,1E+02
Full-loop	0,3318	0,3324	0,3325	0,332	99,9	9

1	0,669	0,67	0,67	0,670	198,5	37
	1,014	1,015	1,015	1,015	299,6	84
	1,358	1,36	1,361	1,360	400,3	151
	1,691	1,693	1,694	1,693	498,0	233
	2,04	2,043	2,044	2,042	602	3,4E+02
	2,37	2,372	2,374	2,372	698	4,6E+02
	2,719	2,722	2,723	2,721	801	6,0E+02
	3,058	3,063	3,064	3,062	902	7,7E+02
Full-loop	0,3266	0,327	0,3272	0,327	100,1	9
2	0,6597	0,664	0,664	0,663	200,5	37
	0,998	0,999	0,999	0,999	300,3	87
	1,329	1,33	1,33	1,330	399,3	153
	1,67	1,672	1,672	1,671	500,6	241
	2,002	2,004	2,005	2,004	601	3,6E+02
	2,341	2,344	2,345	2,343	702	4,8E+02
	2,653	2,655	2,656	2,655	797	6,2E+02
	3,008	3,012	3,012	3,011	903	8,2E+02

Table 13-7: Datasheet of per unit (%) resistance, reactance and impedance for power transformers [18]

S [kVA]	P_k	e_k	e_R	e_x
31,5	520	2,5	1,65	1,88
50	740	3,6	1,48	3,28
100	1200	3,6	1,20	3,39
200	1950	3,8	0,98	3,67
315	2900	4,3	0,92	4,20
500	3900	4,6	0,78	4,53
630	4750	4,9	0,75	4,84
800	6300	4,9	0,79	4,84
1000	8900	5,3	0,89	5,22
1250	9700	5,7	0,78	5,65
1600	13100	6,2	0,82	6,15

13.2 PHOTOS

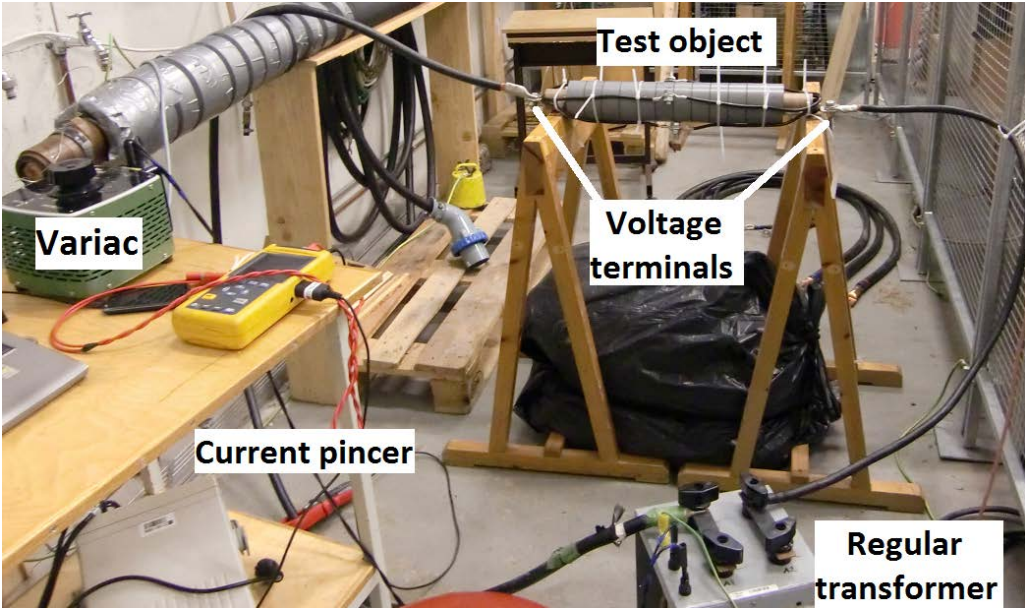


Figure 13-1: Photograph of small transformer, short-circuit test. Fluke NORMA 5000 was used, even though it's not included in the image.



Figure 13-2: Primary and secondary conductors when removing the transformer core



Figure 13-3: Large transformer; side view of the short-circuit assembly



Figure 13-4: Picture of small transformer with a long half-loop secondary winding



Figure 13-5: Picture of small transformer with a long full-loop secondary winding

13.3 GRAPHS

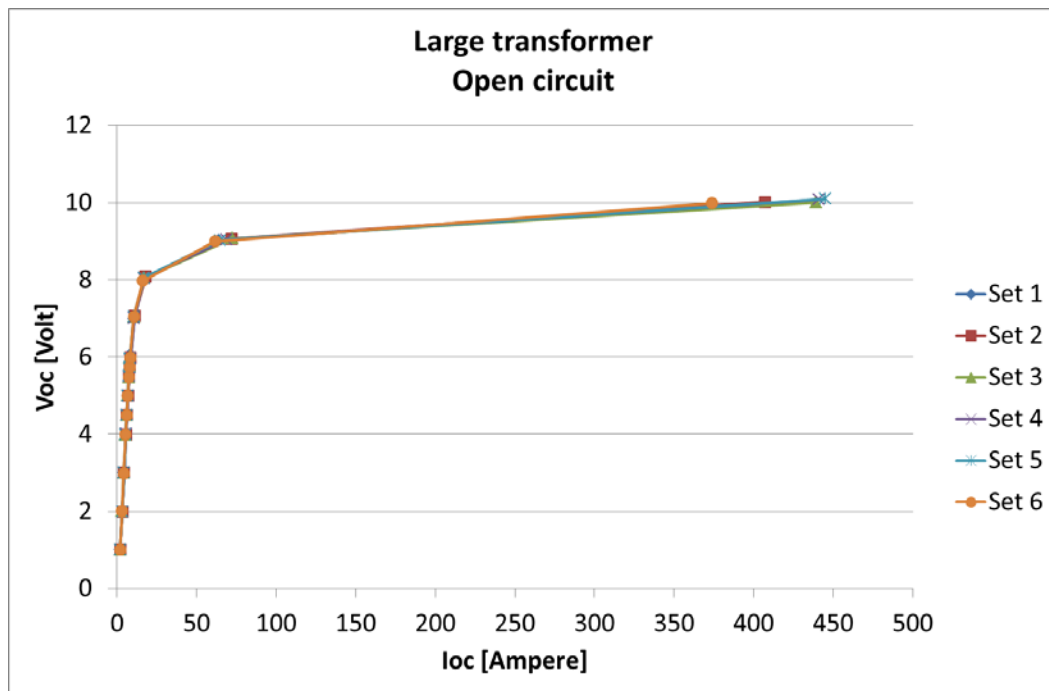


Figure 13-6: Open circuit voltage as a function of open circuit current of the large transformer

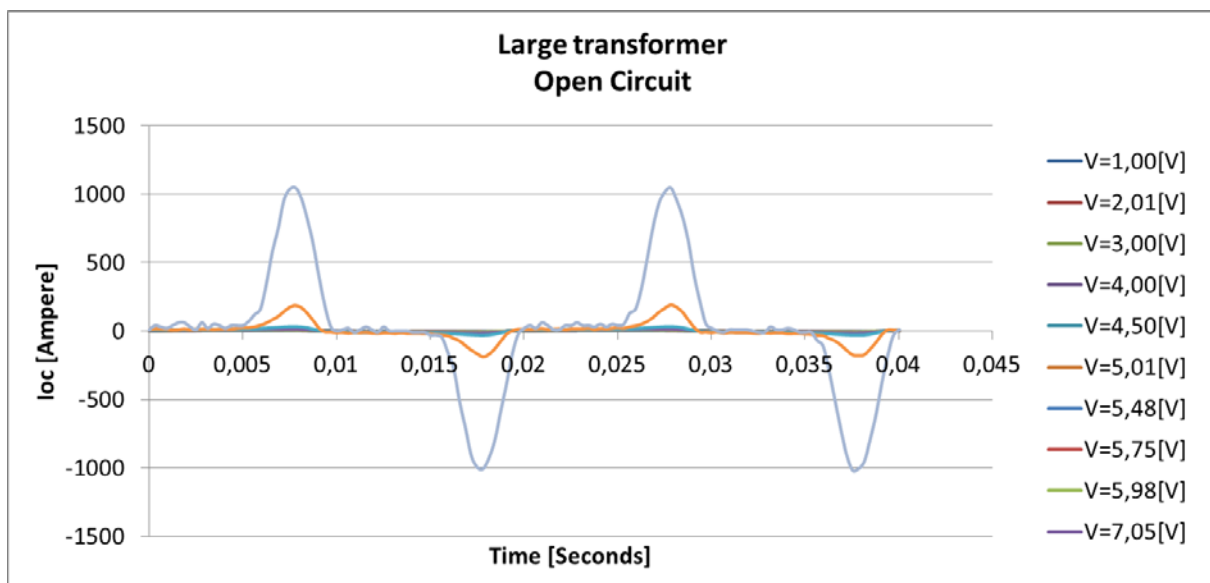


Figure 13-7: Current as function of time for large transformer

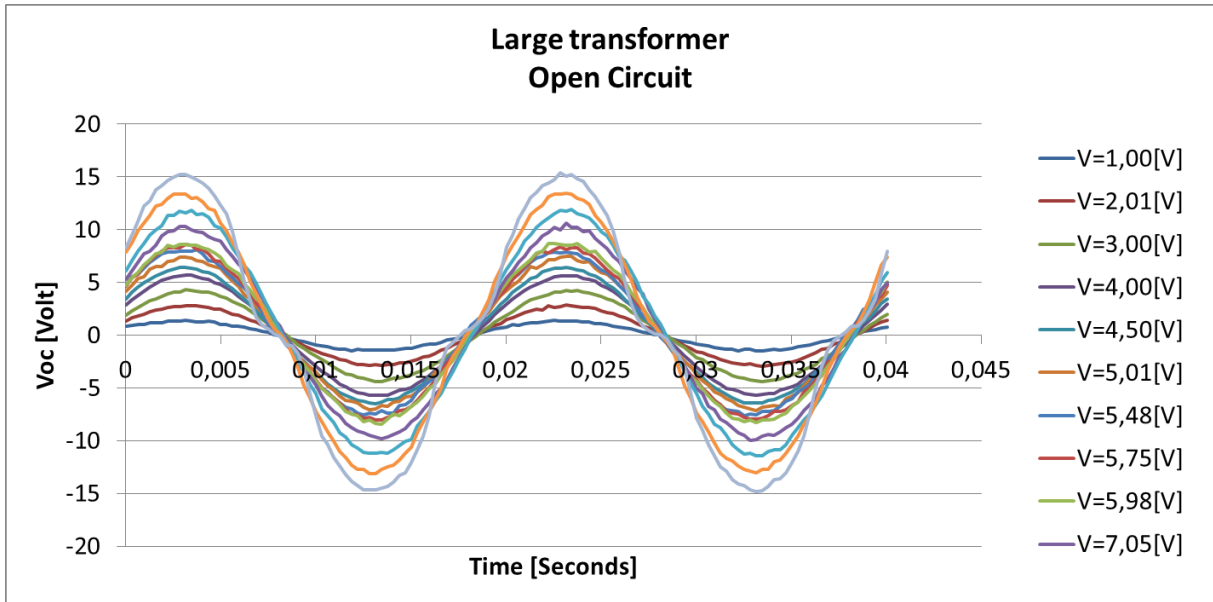


Figure 13-8 Voltage as function of time for large transformer

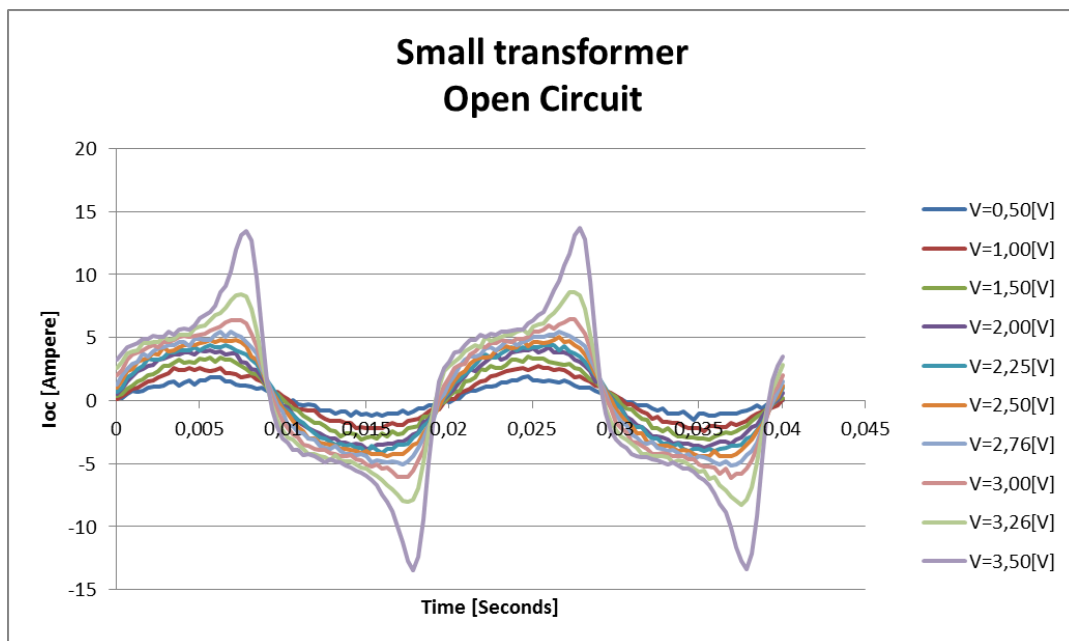


Figure 13-9: Current as function of time for small transformer

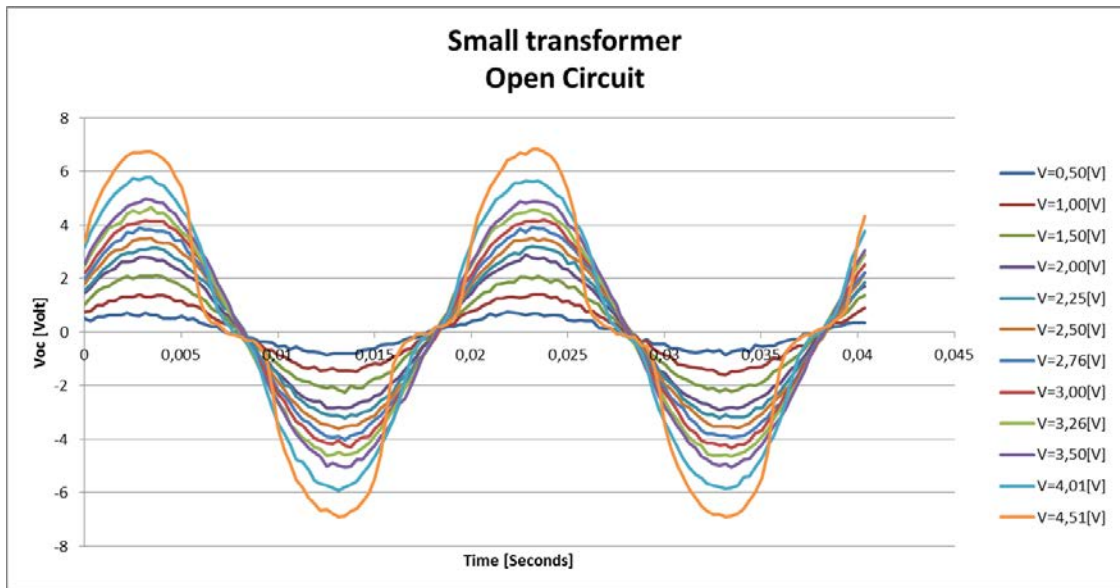


Figure 13-10 Voltage as function of time for small transformer

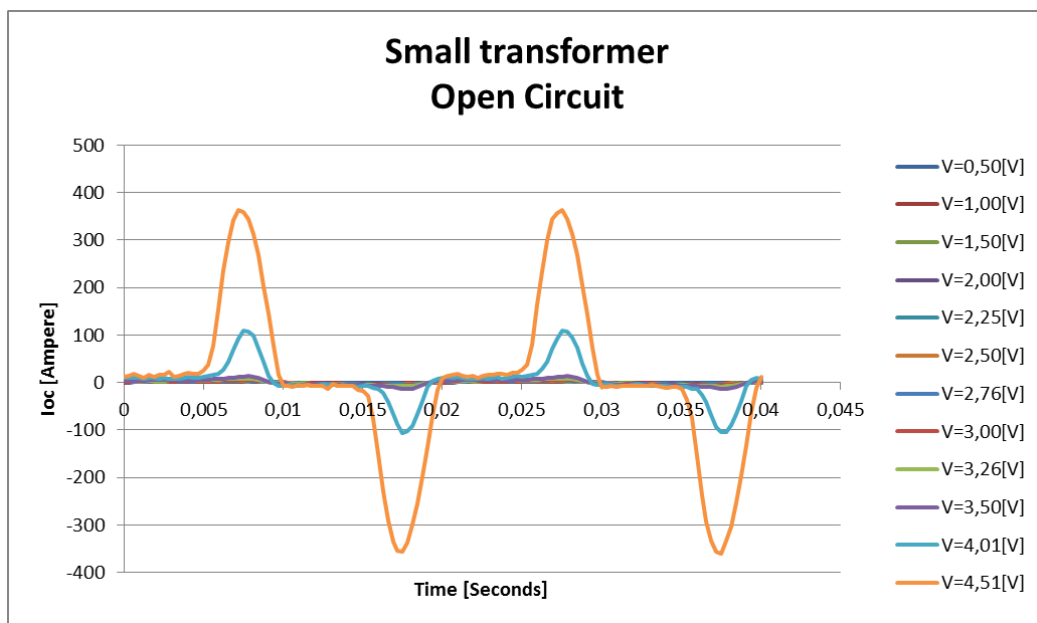


Figure 13-11: Current as function of time for small transformer, including the largest currents

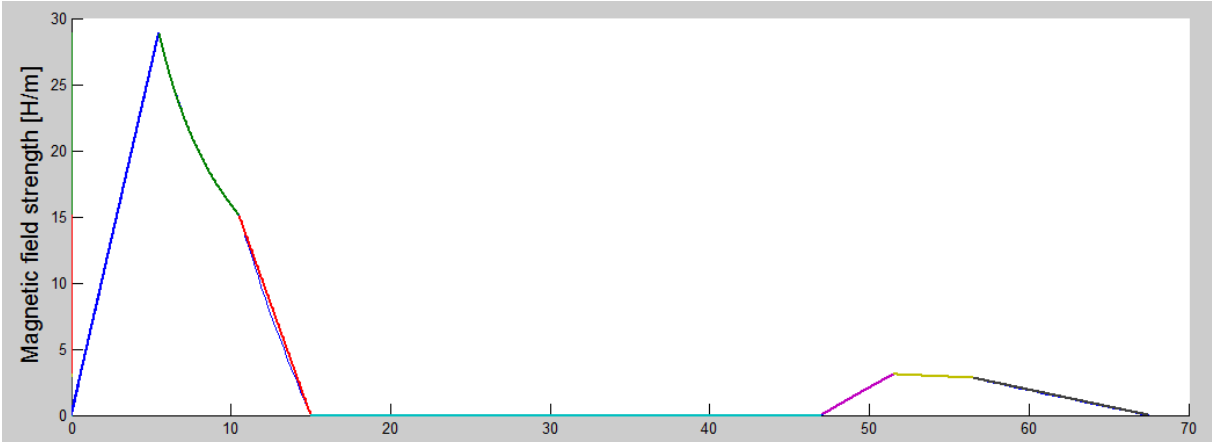


Figure 13-12: Magnetic field strength as a function of transformer radius, illustrate both the numerical and analytical results. Small transformer equivalent.

13.4 ILLUSTRATIONS

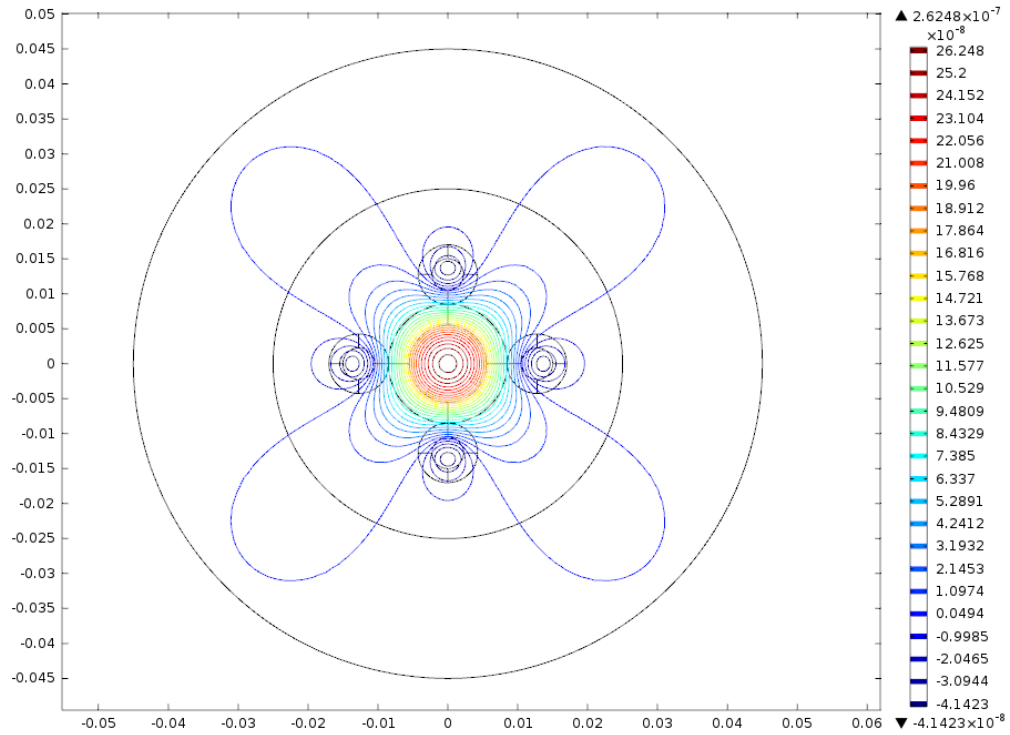


Figure 13-13: Magnetic vector potential. 2D-model of the simplified small transformer equivalent

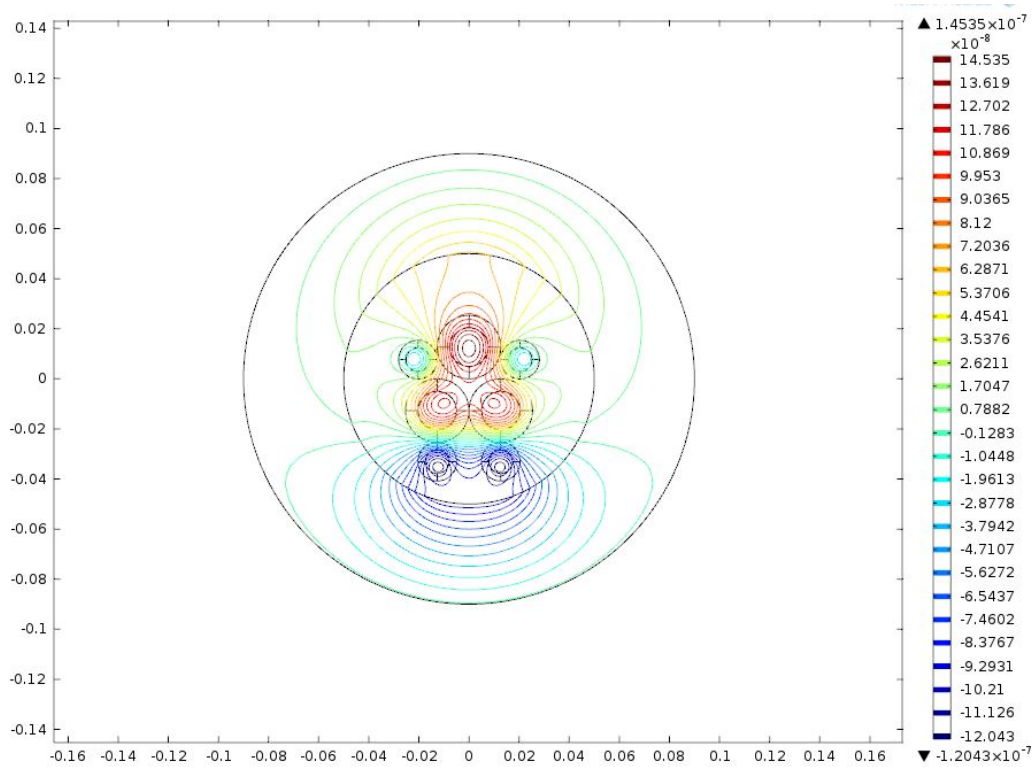


Figure 13-14: Magnetic vector potential. 2D-model of the simplified large transformer equivalent

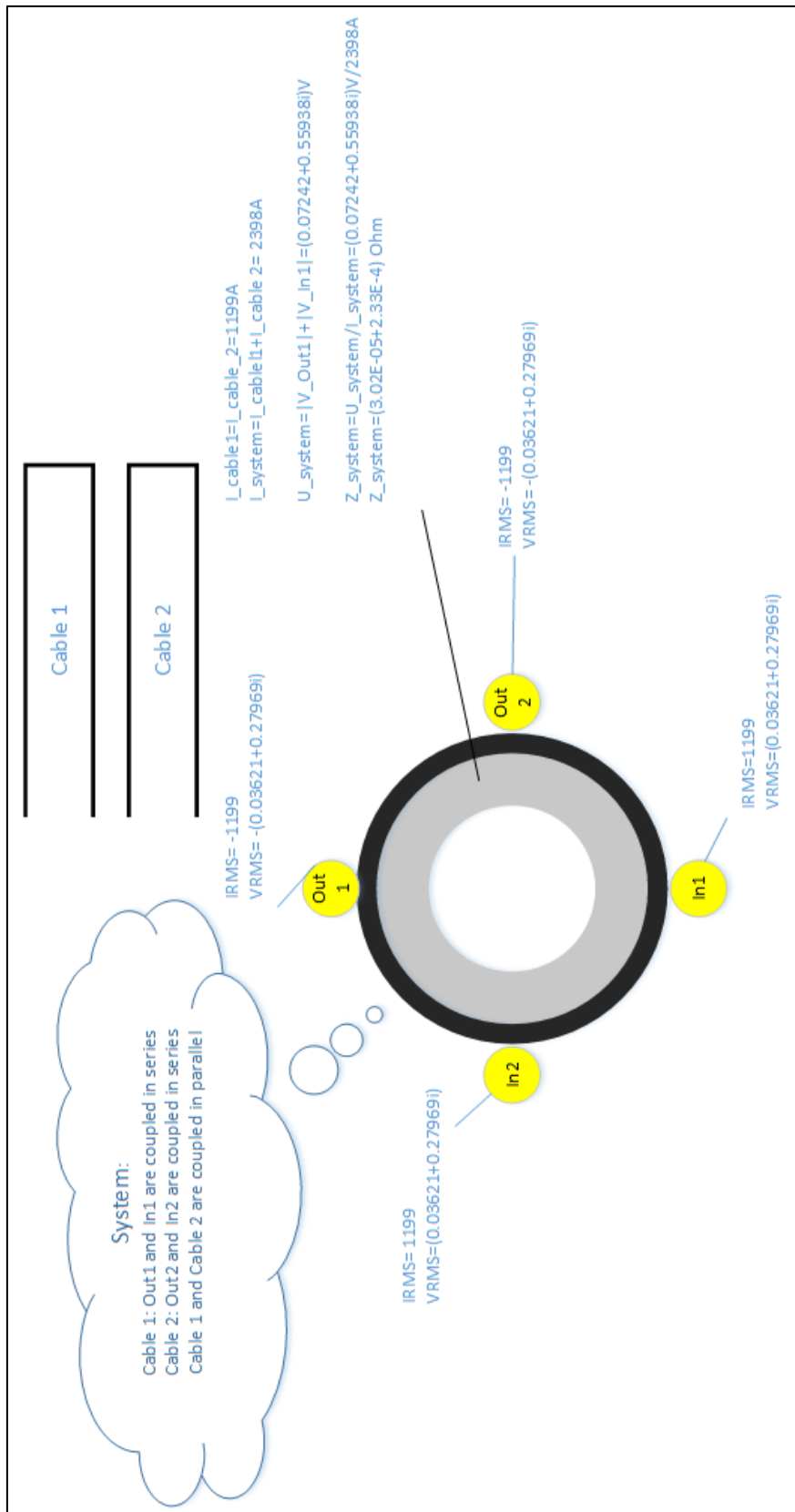


Figure 13-15: Detailed illustration of the t-off IH system

13.5 MATLAB-SCRIPTS

MATLAB 1: Script of the analytical transformer model. Calculates energy and plots H-field

```

clc
clear all

LARGE=0;
%0:small
%1:large

if LARGE==1
    R_core_outer=90;%mm
    A_major=3*185;%mm^2
    A_minor=70;%mm^2
    insulation_minor=3;%mm
    insulation_major=5;%mm
    l=1;%

    comsol=importdata('Comsol_H_Large.mat');
    comsol_x=comsol(:,1);
    comsol_y=comsol(:,2);

else
    R_core_outer=45;%mm
    A_major=95;%mm^2
    A_minor=16;%mm^2
    insulation_minor=2;%mm
    insulation_major=3;%mm
    l=1;%

    comsol=importdata('Comsol_H_Small.mat');
    comsol_x=comsol(:,1);
    comsol_y=comsol(:,2);

end

a=sqrt(A_major/pi)/1000;%m
b=(insulation_minor+insulation_major)/1000;%m
c=2*sqrt(A_minor/pi)/1000;%m
d=(R_core_outer+insulation_minor)/1000;%m
e=c;
f=b;
g=2*a;

res=5e-7;
x1=0:res:a;
x2=a:res:(a+b);
x3=(a+b):res:(a+b+c);
x4=(a+b+c):res:d;
x5=d:res:(d+e);
x6=(d+e):res:(d+e+f);
x7=(d+e+f):res:(d+e+f+g);

y1=l.*x1/(2*pi*a^2);
y2=l./(2*pi.*x2);
y3=l*(a+b+c-x3)/(2*pi*(a+b)*c);
y4=x4*0;
y5=l.*(x5.*x5-d^2)./(2*pi.*x5.*e*(2*d+e));
y6=l./(2*pi.*x6);

```

```

y7=l.*(d+e+f+g-x7)./(2*pi*(d+e+f)*g);

F1=[x1;y1]';
F2=[x2;y2]';
F3=[x3;y3]';
F4=[x4;y4]';
F5=[x5;y5]';
F6=[x6;y6]';
F7=[x7;y7]';

teikne=1;
if teikne==1

    hold on
    plot(comsol_x*1000,comsol_y,'LineWidth',1);
    %plot(x1,y1,x2,y2,x3,y3,x4,y4,x5,y5,x6,y6,x7,y7, 'LineWidth', 2);
    plot(x1*1000,y1,x2*1000,y2,x3*1000,y3,x4*1000,y4,x5*1000,y5,x6*1000,y6,x7*1000,y7, 'LineWidth', 2);
    %plot(x1*1000,y1,x2*1000,y2,x3*1000,y3);

    FontSize=15;
    xlabel('r[mm]','FontSize',FontSize);
    ylabel('Magnetic field strength [H/m]','FontSize',FontSize);
end

lines=0;
if lines==1
    line([a*1000 a*1000], [0,y1(size(y1,2))], 'Color','r')
    line([(a+b)*1000 (a+b)*1000], [0,y2(size(y2,2))], 'Color','r')
    line([(a+b+c)*1000 (a+b+c)*1000], [0,y3(size(y3,2))], 'Color','r')
    line([(d+e)*1000 (d+e)*1000], [0,y5(size(y5,2))], 'Color','r')
    line([(d+e+f)*1000 (d+e+f)*1000], [0,y6(size(y6,2))], 'Color','r')
end

my0=4*pi*10^-7; %H/m

Wa=1/16*my0/pi*I^2;
Wb=1/(4*pi)*my0*I^2*log((a+b)/a);
Wc=1/48*my0*I^2*c*(c+4*a+4*b)/(pi*(a+b)^2);
We=my0*I^2/(16*pi*e^2*(2*d+e)^2*(2*d^2*e^2+4*d*e^3+e^4+4*d^4*log(d+e)-4*d^3*(d*log(d)+e)));
Wf=1/(4*pi)*my0*I^2*log((d+e+f)/(d+e));
Wg=1/(48*pi)*my0*I^2*g*(g+4*(d+e+f))/(d+e+f)^2;

W_all=[Wa;Wb;Wc;We;Wf;Wg];
%W_tot=Wa+Wb+Wc+We+Wf+Wg;
W_tot=Wa+Wb+Wc

L=2*W_tot/I^2;
X=L*100*pi; %(Ohm/m)

if LARGE==1
    X*0.56
else
    X*0.48
end

```